A-2 MODELING PURPOSE AND MOTIVATION

A-2.1 Purpose

The primary purposes of developing new INTEC conceptual and numerical models are to predict future concentrations of contaminants of concern (COCs) resulting from historical INTEC releases and to allow evaluation of proposed remedial actions for those COCs. The specific COCs considered here were identified in the OU 3-14 RI/FS Work Plan (DOE 2004a). The flow model parameterization is largely based on an updated geologic and hydrologic description of the subsurface relative to the previous OU 3-13 Remedial Investigation/Baseline Risk Assessment (RI/BRA) model (DOE-ID 1997). The updates are based on data collected during the 1997-2004 time frame. This model is similar to that used during the OU 3-13 RI/BRA investigation in that it considers transient three-dimensional infiltration and transport through the vadose zone, and saturated flow and transport in the aquifer. Much of the data reviewed in that document along with additional data collected during the ongoing OU 3-13 remedial activities and OU 3-14 RI/FS is used as the basis of this analysis, with primary differences occurring in the treatment of individual sedimentary interbeds, the hydraulic parameters assigned to them, and in the contaminant source releases for OU 3-14. The specific differences between the OU 3-13 and the OU 3-14 model is discussed in Section A-2.2. The simulation results will be used to

- Evaluate impacts to aquifer water quality from historical leaks and spills in the tank farm and INTEC.
- Predict concentrations in the Snake River Plain Aquifer for use in the risk assessment.
- Evaluate impacts to aquifer water quality from the non-tank-farm OU 3-13 RI/BRA (DOE-ID 1997) contamination sources along with the OU 3-14 sources. If necessary, adjust OU 3-13 sources to reflect contaminants removed during the remedial work or new information.
- Evaluate proposed remedial actions during the feasibility study phase of the OU 3-14 RI/FS.

A-2.2 Motivation

Development of an updated INTEC conceptual and numerical model was needed because data gathered during the OU 3-13 Group-4 (perched water) and Group-5 (Snake River Plain Aquifer) remedial actions and INEEL CERCLA Disposal Facility (ICDF) groundwater investigations are inconsistent with the OU 3-13 RI/BRA conceptual and numerical models (DOE-ID 1997). The OU 3-13 conceptual model grouped the many INTEC interbeds into four “effective” interbeds. This grouping simplified the vadose zone model and allowed efficient numerical simulation of the OU-13 contaminant fate and transport problem. However, the “effective” interbed structure was much more continuous than the observed structure and the simulated perched water moved a large horizontal distance. The model predicted percolation pond water would recharge the perched water beneath the tank farm. However, the INTEC vadose zone tracer test and geochemical analysis presented in DOE-ID (2003a) indicate this may not be occurring. The RI/BRA model also placed the large tank farm releases (Sites CPP-31 and CPP-28) directly into the basalt beneath the alluvium. The “effective” interbeds and placing the large tank farm releases below the alluvium may have significantly misrepresented the risk to the aquifer posed by contaminants at the tank farm. The specific differences between the OU 3-13 and OU 3-14 models are:

- OU 3-14 vadose zone model correctly simulates interbed placement and the OU 3-13 model used “effective” interbeds.
- OU 3-14 vadose zone model uses smaller grid discretization (100- x 100-m horizontal grid block vs. 200- x 200-m grid blocks).

- OU 3-14 vadose zone model was parameterized with INTEC properties versus OU 3-13 model's parameterization from SDA properties (sediment hydraulic properties and the infiltration rate).

- More data was available to parameterize and calibrate the OU 3-14 model (stratigraphy, water level and concentration data).

- OU 3-14 aquifer model correctly simulates effective aquifer thickness and aquifer surface. The aquifer depth was variable and estimated from temperature logs of deep wells (25 m to 375 m thick). The OU 3-13 model used a uniform 76-m thickness.

- OU 3-14 aquifer model uses smaller grid discretization (100- x 100-m horizontal grid block vs. 200- x 200-m grid blocks near INTEC and 2-m vertical grid block near water table and HI interbed vs. 20 m).

A-3 SUMMARY OF VADOSE ZONE DATA

Accidental releases of contaminant-bearing liquids during fuel reprocessing activities at INTEC have resulted in a long history of subsurface monitoring and characterization. Numerous historical DOE remedial investigations, DOE remediation activities, and United States Geological Survey (USGS) investigations have contributed to the subsurface transport characteristics at INTEC. In addition, the INTEC subsurface is probably the most instrumented and monitored location at the INL Site. The INTEC subsurface has been the subject of several different modeling studies, most of which were focused on integrating geologic, hydrologic, and transport data into predictive simulations. As a result of these various activities, there is a wide range of qualitative, quantitative, and interpretive information available for parameterizing this updated large-scale INTEC vadose zone flow and transport model.

A-3.1 Vadose Zone Geology and Lithology

USGS and DOE have drilled numerous wells within the vicinity of the INTEC to investigate the movement of water and contaminants. USGS has described the stratigraphy of basalt-flow groups and sedimentary interbeds in the upper 700 ft of material extending from land surface, through the vadose zone and into the aquifer. Information sources include geophysical logs, lithologic logs, and well cores. These geological cross-sections, basalt flow groups, interbed elevation maps, interbed thickness maps, and lithologic data were presented by Anderson (1991). More recent drilling activities were described in the Phase I Monitoring Well and Tracer Study Report (DOE-ID 2003a), in the ICDF drilling reports (INEEL 2003a; Cahn and Ansley 2004). The work described included drilling and installation of monitoring systems ranging from alluvium boreholes to perched water and aquifer monitoring wells. Perched water and soil samples extracted from well cores during drilling were analyzed for chemical and hydrological properties (DOE-ID 2003a). In total, USGS and DOE investigations have provided 125 wells around INTEC with 75 of those completed in the vadose zone and 49 penetrating into the SRPA.

A detailed study of the borehole data from most of these wells was completed during the preparation of the OU 3-13, Group 4, Monitoring Well and Tracer Study (DOE-ID 2003a). The study evaluated basalt/interbed core, geochemical, paleomagnetic, K-Ar age date, and petrographic data. Results of the study indicated that several distinct lithologic layers exist beneath INTEC that can be used as marker units. The marker units included the following:

- Surficial alluvium - is the uppermost sediment unit that extends from land surface. It exists across the facility, is on the order of 40 ft thick, and is underlain by fractured basalt.
- Upper basalt flows - are the numerous basalt flows between the 30- to 115-ft depth ranges from one to four flow units. Up to four units exist beneath the northern portion of INTEC while a single flow unit exists beneath the southern portion of the facility.
- 110-ft interbed - is generally encountered between 100 to 120 ft below land surface and ranges from 3 to 25 ft thick. It is an important marker unit due to its presence in nearly all of the wells penetrating deep enough to encounter it. The thickest portions of the unit rest under the northeast corner of INTEC.
- High K_2O basalt flow - is characterized by a high natural gamma count due to higher potassium content. The flow is found between 110 to 150 ft below land surface and is absent from the east and southeast extremes of INTEC. The unit lies stratigraphically below the 110-ft interbed when it is present.
- 140-ft interbed - does not appear to be as continuous as the 110-ft interbed. These predictions may reflect reality but there is uncertainty due to more limited data in the area.
- Middle massive basalt - is one of the thickest, most massive basalt flows found in the INTEC vadose

zone. Typical thickness for the unit is around 100 ft. The base of the unit appears to be relatively flat-lying while the upper surface has a south-to-southwest slope. The unit is encountered between 220 to 280 ft below land surface.

- Interbed below the middle massive basalt flow (BM interbed) - is as continuous as the 110-ft interbed and more continuous than the 140-ft interbed based on a geostatistical analysis. It ranges in thickness between 0 to 40 ft and exists below the middle massive basalt flow. This name is unique to this document and does not follow the common nomenclature of residing between a B and M basalt flow.
- 380-ft interbed - is a relatively continuous flat layer that varies in thickness from 6 to 27 ft. Depth to the interbed ranges from 320 to 420 ft below land surface. The interbed appears to be continuous and relatively thick beneath the INTEC tank farm and thin to the south.
- Low K_2O basalt flow - was identified in USGS-121 and USGS-123 at 415 ft below land surface. It has a low percentage by weight of K_2O. A similar reading from a basalt was found at 384 ft below land surface in well ICPP-COR-A-023.

In addition to the data provided by Anderson (1991) and DOE-ID (2003a), well logging information was also obtained from the INL's Hydrogeologic Data Repository (HDR) to construct the complete lithologic database of the INTEC subsurface. Interpretation of the lithologic data for the purposes of simulation was provided in Appendix C and is reviewed in Section A-5.1.4.1.

A-3.2 Vadose Zone Hydrological Data

Hydrologic data available for the INTEC vadose zone include soil moisture characteristics, particle size distribution, porosity, effective porosity, bulk density, and moisture content. These data are available from a variety of sources including Appendix F of the OU 3-13 RI/BRA (DOE-ID 1997) and the OU 3-13, Group 4, remedial activities (DOE-ID 2003a). The former document reviews the results of perched water tests, and the latter reviews the analysis of core samples collected during drilling of perched water wells at the INTEC. The OU 3-13, Group 4, remedial work collected a total of 37 surficial alluvium and interbed samples during Phase I drilling. The laboratory analysis developed soil moisture characteristic curves and determined material particle size distribution, porosity, effective porosity, bulk density, and initial moisture content. These data are presented in the next three subsections for the alluvium, basalt, and interbed, respectively.

A-3.2.1 Surficial Alluvium

The INTEC alluvium ranges in thickness from 22 to 61 ft near INTEC and varies in texture from inorganic clays and silts to well-sorted gravel, but it is primarily poorly graded gravel and sand mixtures. Hydraulic properties for 17 samples of alluvium were obtained during the OU 3-13, Group 4, remedial activities using laboratory core analysis and are presented in Table A-3-1.

Table A-3-1. INTEC alluvium unsaturated hydraulic properties from DOE-ID (2003a).

Well Name	Depth	Unified Soil Class	Dry Bulk Density	Saturated Hydraulic Conductivity	van Genuchten Parameters		Volumetric Moisture Content		
(ICPP-SCI-P-)	(ft)		(g/cm^3)	(cm/sec)	Alpha (1/cm)	N	In Situ	Residual	Saturated
216	33-34	GW-GM	1.8	4.80E-02	1.9868	1.2407	0.066	0.026	0.2555
216	34-35	GM	1.3	1.10E-01	1.2729	1.1024	0.21	1.00E-04	0.4198

Well Name	Depth	Unified Soil Class	Dry Bulk Density	Saturated Hydraulic Conductivity	van Genuchten Parameters		Volumetric Moisture Content		
(ICPP-SCI-P-)	(ft)		(g/cm^3)	(cm/sec)	Alpha (1/cm)	N	In Situ	Residual	Saturated
226	10-10.5	GW-GM	2.01	6.90E-02	0.3126	1.2521	0.117	0.0256	0.2864
226	19-20	GP	2.16	7.40E-03	0.1123	1.5444	0.097	0.0516	0.2247
226	45-46	SM-SC	1.79	6.60E-07	0.0163	1.1881	0.223	1.00E-04	0.401
226	51-52	ML-CL	1.95	6.70E-08	0.0002	1.3428	0.379	1.00E-04	0.3851
248	10-10.5	GP	1.78	3.80E-02	0.1723	1.4687	0.048	0.0326	0.3321
248	18-18.5	GP-GM	1.68	4.70E-02	0.0467	2.0252	0.053	0.0602	0.3696
250	15-15.5	GW	1.7	8.00E-02	0.0124	2.3011	0.062	0.0316	0.2354
250	26-26.5	GP	1.67	1.00E-01	0.2086	1.3291	0.095	0.0144	0.3745
250	31-31.5	GP-GM	1.61	1.60E-02	0.3134	1.2618	0.11	0.0192	0.3923
251	19-19.5	GP	2	3.00E-02	0.0197	4.2289	0.081	0.0622	0.3142
251	19-19.5	GW	1.9	2.70E-02	0.123	1.327	0.102	0.0265	0.3477
251	30.5-31	GP-GM	1.82	1.70E-02	1.5208	1.1435	0.103	1.00E-04	0.2677
252	20-23	GP	1.89	5.60E-02	0.7955	1.2084	0.087	1.00E-04	0.321
252	26-27	GW	1.99	4.40E-02	0.0861	1.914	0.085	0.0642	0.2518
252	41-42.5	GP-GM	1.88	6.10E-02	0.159	1.5421	0.087	0.0432	0.2939

A-3.2.2 Vadose Zone Basalt

The geology of the Eastern Snake River Plain is the result of plains-style, low-shield volcanoes. The basalt flows are episodic, and during quiescent periods, sediments are deposited over the basalt. The basalt flows typically have five layered elements consisting of a fractured and fissured base surface followed by a sequence of a rubble zone, lower vesicular zone, massive center, and upper vesicular zone (Knutson et al. 1990).

Direct measurements of unsaturated hydraulic characteristics are unavailable for the highly heterogeneous basalts. However, saturated hydraulic conductivity is available for the perched water tests conducted at INTEC. These results are reproduced in Table A-3-2 from Appendix F of the OU 3-13 RI/BRA (DOE-ID 1997).

Table A-3-2. Basalt hydraulic conductivity from perched water tests from DOE-ID (1997).

Well	Depth (ft bls)	Test Type	Material	Hydraulic Conductivity (cm/sec)
CPP 33-2	97.8-105.8	Pumping/recovery	Basalt	1.80E-03
CPP 33-3	111.2-121.8	Pumping/recovery	Basalt	9.50E-04

Well	Depth (ft bls)	Test Type	Material	Hydraulic Conductivity (cm/sec)
CPP 33-4	103.7-118.2	Pumping/recovery	Basalt	2.40E-03
CPP 33-4	103.7-118.2	Pumping/recovery	Basalt	3.40E-03
CPP 55-6	105.2-113.1	Pumping/recovery	Basalt	4.20E-04

A-3.2.3 Interbeds

The sedimentary interbeds at INTEC consist of fluvial, lacustrine, and eolian deposits of clay, silt, sand, and gravel, which have accumulated during quiescent periods between basalt flows (Anderson 1991). There are between 15 to 20 sedimentary interbeds beneath INTEC, depending on location. However, as reviewed in Section A-3.1, the OU 3-13, Group 4, Monitoring Well and Tracer Study (MWTS) report (DOE-ID 2003a) suggests there are only four significant interbeds. These are the (1) 110-ft interbed, which is 3 to 25 ft thick and encountered 100 to 120 ft below land surface; (2) 140-ft interbed, which is discontinuous; (3) the interbed below the middle massive basalt unit (BM interbed); and (4) the 380-ft interbed, which is 6 to 27 ft thick and is encountered 320 to 420 ft below land surface.

Appendix F of the OU 3-13 RI/BRA (DOE-ID 1997) included the results of the perched water tests conducted in interbed zones and laboratory analysis of core samples. The OU 3-13, Group 4, remedial work included laboratory analysis of 20 interbed core samples. These data and the data from the OU 3-13 RI/BRA are presented in Tables A-3-3 and A-3-4, respectively.

Table A-3-3. INTEC interbed unsaturated hydraulic properties from DOE-ID (2003a).

Well Name	Depth	Unified Soil Class	Dry Bulk Density	Saturated Hydraulic Conductivity	van Genuchten Parameters		Moisture Content		
(ICPP-SCI-P-)	(ft)		(g/cm^3)	(cm/sec)	Alpha (1/cm)	N	Iin Situ	Residual	Saturated
248	87-87.5	ML-MC	1.39	1.00E-06	0.0006	1.2776	0.456	0	0.4799
248	167.6-168.3	ML	1.43	4.60E-05	0.0045	1.2501	0.333	0	0.4533
248	167.6-168.3	ML	1.29	4.70E-04	0.0158	1.1925	0.358	0	0.44
249	376-377.5	SM	1.53	2.50E-06	0.0008	1.3951	0.445	0	0.394
249	381.8-382.8	SM	1.8	8.00E-04	0.0851	1.1797	0.261	0	0.3138
249	387.1-388.2	ML	1.32	9.90E-04	0.0509	1.1683	0.285	0	0.5238
249	387.1-387.2	ML	1.53	7.50E-07	0.0007	1.2883	0.383	0	0.434
249	164.2-164.7	ML	1.37	7.80E-04	0.0003	1.3161	0.331	0	0.3921
250	110.8-111.45	SM	1.08	3.30E-02	0.105	1.2886	0.266	0.0685	0.6024
250	122.2-122.9	ML	1.46	3.10E-04	0.0021	1.4487	0.422	0.0447	0.4758
250	132.7-133.1	ML	1.51	2.40E-04	0.0023	1.2575	0.399	0	0.4724
250	168-173.3	SM	1.19	4.40E-03	0.0972	1.1932	0.339	0	0.517

Well Name	Depth	Unified Soil Class	Dry Bulk Density	Saturated Hydraulic Conductivity	van Genuchten Parameters		Moisture Content		
(ICPP-SCI-P-)	(ft)		(g/cm^3)	(cm/sec)	Alpha (1/cm)	N	Iin Situ	Residual	Saturated
250	170-170.9	SM	1.23	8.20E-04	0.0266	1.2199	0.339	0	0.5109
250	384-385.1	SM	0.92	1.50E-02	1.6681	1.1352	0.207	0	0.5625
250	384-384.4	ML	1.33	4.60E-07	0.0001	2.1085	0.338	0.0764	0.4442
251	103-103.8	SM	1	2.80E-02	0.2005	1.1726	0.268	0	0.6049
251	108.3-109.5	ML	1.31	4.20E-03	0.0076	1.1638	0.366	0	0.4847
251	114-114.7	CL	1.4	2.50E-07	0.0001	1.3795	0.464	0	0.4934
252	144.6-152.2	SM	1.13	8.10E-03	0.1212	1.1666	0.275	0	0.5116
252	154.5-156.2	ML	1.51	8.20E-07	0.0003	1.3471	0.322	0	0.4226

Table A-3-4. Interbed hydraulic conductivity from perched water and core tests from DOE-ID (1997).

Well	Material	Hydraulic Conductivity (cm/sec)	Depth (ft bls)	Test Type
MW-2	Sandy clay interbed	3.7E-3	107.9-112.0	Aquifer slug
MW-4	Silty sand and gravel interbed	3.86E-5	104.6-110.6	Aquifer slug
MW-6	Silty sand, fine grained interbed	1.3E-3	140.0-151.0	Aquifer slug
MW-3	Silty clay	8.9E-5	117.0-119.3	Laboratory core
MW-4	Silty sand and gravel	1.6E-5	108.0-109.3	Laboratory core
MW-7	Silt with fine gravel	1.3E-3	113.5-114.5	Laboratory core
MW-8	Clay with silt	1.1E-5	122.3-123.7	Laboratory core
MW-10	Sandy silt	1.0E-5	110.3-111.0	Laboratory core
MW-11	Silty sand	1.2E-5	113.7-115.3	Laboratory core
MW-4	Silt	3.2E-5	105.1-105.6	Laboratory core
MW-4	Silt	6.7E-5	105.6-106.8	Laboratory core
MW-6	Clay	3.0E-7	110.0-111.0	Laboratory core
MW-9	Clay with silt	2.1E-3	111.6-112.5	Laboratory core
MW-11	Clay	5.2E-8	135.4-136.0	Laboratory core
MW-3	Silty clay	8.3E-4	138.0-139.0	Laboratory core
MW-6	Silty clay	2.2E-3	142.0-143.0	Laboratory core

Well	Material	Hydraulic Conductivity (cm/sec)	Depth (ft bls)	Test Type
MW-9	Silt with clay	3.4E-4	148.7-149.4	Laboratory core
MW-1	Sand with silt	3.3E-4	231.7-232.3	Laboratory core

A-3.3 Vadose Zone Infiltration from Precipitation

Infiltration is the process by which surface water enters the soil. After surface water has infiltrated into the soil, it is redistributed in response to gravity and capillary forces. The redistribution process ultimately partitions the infiltrated water into (1) surface losses to evaporation and transpiration, (2) drainage that eventually becomes aquifer recharge, and (3) storage that remains in the vadose zone. Infiltrating water moves down through the contaminated soils, mobilizing contaminants, and eventually transports them to the aquifer. The storage or residual moisture is important because it determines the amount of water in contact with soil, which affects the sorption characteristics. Determination of net infiltration is primarily accomplished by analyzing field data using numerical models. One of the analyses available was performed near INL's Subsurface Disposal Area (SDA), and was used in the OU 3-13 RI/BRA, and the more relevant and recent study was conducted at the INTEC and is described in detail in Appendix B.

Infiltration values used in the OU 3-13 RI/BRA (DOE-ID 1997) were based on a USGS study (Cecil et al. 1992) for undisturbed and vegetated conditions and were based on field data representative of disturbed soils collected in the SDA (Martian 1995). Undisturbed conditions were assumed to exist outside the INTEC fence line where a value of 1 cm/year (Cecil et al. 1992) was applied. Disturbed conditions were assumed inside the INTEC fence line where 10 cm/year (Martian 1995) were applied. The 10-cm/year rate was based on moisture content and soil tension data collected over several years and at several SDA locations. Evaporation, infiltration, and storage parameters were estimated through model calibration. The infiltration behavior varied widely between monitoring locations with the primary mechanism for recharge identified as infiltration following the spring snowmelt. The fast snowmelt during periods of low evapotranspiration allowed a large percentage of the annual precipitation to become recharge even though the total potential evapotranspiration at the SDA is several times the annual precipitation. These recharge rates may not be appropriate for the tank farm because recharge resulting from precipitation is strongly dependent on soil type, topography, and surface vegetation type, which differ between the tank farm and the SDA.

Infiltration in the tank farm was investigated during 1993 and 1994. The investigation measured soil moisture content using a neutron moisture probe at 20 locations near and within the tank farm during December 1993 and early spring 1994 (INEL 1995). This time period included dry and wet periods, with data collected approximately monthly (dates provided in Table A-3-5). Although these data are more representative of INTEC than the SDA values, we note that (1) the recorded 6.3 in. of precipitation during 1994 was less than the long-term average INTEC precipitation of 8.3 in. per year and (2) irregular and infrequent sampling made it difficult to uniquely determine infiltration parameters. Additional uncertainty is introduced in the neutron probe calibration which used a standard calibration curve for Schedule 80 stainless-steel casing and moisture in a "standard block". The calibration was verified by comparing neutron probe-measured soil moisture data at two locations to laboratory-measured soil moisture from the same location. The overall ratio between probe- and laboratory-measured moisture content was 1:0.92. While introducing some uncertainty, this calibration was thought to be adequate for the tank farm soil and was used for all measurements.

In addition to these 20 sample locations, the 1993-1994 tank farm investigation also included two small-scale infiltration tests designed to determine the extent of lateral versus vertical migration. A secondary objective was to determine the sampling frequency required to observe wetting front propagation through the vadose zone. The first test used an infiltration basin emplaced around neutron probe monitoring well A-67. The basin inner radius was 7 ft from the well, the outer radius was 15.8 ft from the well, and the basin was filled to a 3.8 in. depth. The neutron probe was monitored for 72 hours. Water was never seen in the well and it was concluded that water moved vertically through the alluvium with very little lateral movement. A similar test

was conducted using a 10-ft-radius infiltration pond placed around well A-68. The basin was also filled to a 3.8 in. depth and was monitored for 72 hours. The wetting front reached the basalt interface within 40 hours. The rapid movement of the wetting front through the alluvium indicated that monitoring intervals of at least twice daily would be needed to observe wetting front movement following a period of significant precipitation.

In Appendix B, the soil moisture data and numerical calibration for 14 locations within and near the tank farm are presented. These data include samples beneath and adjacent to the membrane liner overlying the tank farm. The calibration was performed in a manner analogous to the Martian (1995) SDA infiltration study. Soil hydraulic properties were estimated by matching variable-depth and transient moisture content measurements at each location. Initial values during the calibration were taken from the OU 3-13, Group 4, characterization work (DOE-ID 2003a). The calibrated infiltration models were then used to simulate infiltration into the tank farm soil and underlying basalt for the entire historical operational period of INTEC (1953-2003). The simulations suggest that approximately 18-cm/year pass through the tank farm soil. This is a very large percentage (86%) of the approximately 21-cm/year annual total precipitation. As with the SDA data, the INTEC recharge is highly seasonal with much of the recharge resulting from spring snowmelt and rainfall. The simulated aquifer recharge at wells located beneath the liner was spatially variable with some locations experiencing higher or lower recharge rates than locations away from the liner. However, the average recharge rate for all locations beneath the membrane was nearly the same as the average rate for locations outside of the lined area. It appears as though the liner covering the tank farm redistributes infiltration and that it does not significantly change the overall recharge rate.

A very high net infiltration percentage of precipitation is not consistent with observed annual drainage percentages seen at the Hanford Field Lysimeter Test Facility (Gee et al. 1993). The highest observed drainage out of a gravel surface lysimeter was as 83% of the precipitation/irrigation treatment. Drainage percentages would be expected to be higher at the INL Site because the Site generally has a lower potential evapotranspiration rate than the Hanford Site and the INL Site's soil remains frozen for longer periods of time during winter months. Frozen soil will greatly reduce soil moisture evaporation during the winter.

More frequent monitoring of the tank farm soil moisture during the 1994 monitoring period would have improved confidence in the model calibration because many more infiltration events would have been captured in the monitoring. However, the uncertainty in the predictions is acceptable because of the following reasons: (1) a numerical model was used to estimate the total net infiltration rate, (2) the model used the compete historical weather record for the INTEC (1953-2003), and (3) the model accurately mimicked the events seen in the data. The net infiltration rate cannot be estimated from the observed data alone, because a large fraction of the infiltration events were not seen in the infrequent monitoring.

Table A-3-5. Tank farm infiltration monitoring data summary.

Well	Total Monitored Depth (ft)	Monitoring Dates
A-60	32	12/8/93, 1/28/94, 2/28/94, 4/11/94, 5/11/94
A-61	34	12/8/93
A-62	36	12/8/93, 1/28/94, 3/1/94, 4/11/94, 5/11/94
A-63	36	3/1/94, 4/11/94, 5/11/94
A-64	35	12/8/93, 1/28/94, 3/1/94, 4/11/94, 5/11/94
A-65	30	12/7/93, 1/28/94, 3/1/94, 4/11/94, 5/11/94
A-66	35	12/7/93
A-67	37	12/7/93, 1/28/94, 3/1/94, 3/31/94, 5/11/94
A-68	30	12/7/93, 1/28/94, 3/1/94, 3/31/94, 5/11/94

Well	Total Monitored Depth (ft)	Monitoring Dates
81-02	28	12/8/93, 1/28/94, 2/28/94, 4/11/94
81-04	15	2/28/94, 4/11/94, 5/11/94
81-05	13	2/28/94, 4/11/94, 5/11/94
81-06	27	4/11/94, 5/11/94
81-09	22	4/11/94, 5/11/94
81-10	28	12/8/93, 1/28/94, 2/28/94, 4/11/94, 5/11/94
81-15	11	12/8/93, 1/28/94, 2/28/94, 4/11/94
81-17	17	12/8/93, 1/28/94, 2/28/94, 4/11/94, 5/11/94
81-19	23	4/11/94, 5/11/94
81-20	28	4/11/94, 5/11/94
81-21	11	12/8/93, 1/28/94, 4/11/94, 5/11/94

A-3.4 Perched Water Depth and Soil Moisture/Tension

There are several discontinuous perched water zones beneath INTEC associated with the alluvium/basalt interface, the shallow primary interbeds at 110 ft and 140 ft, the below massive basalt (BM) interbed at 220-280 ft, and the deep interbed at 380 ft. Perched water appears to also be associated with low-permeability basalt and numerous other thin and discontinuous interbeds. For the purposes of discussion, the perched zones have been grouped into shallow, deep, and middle zones:

- The shallow perched water occurs in the northern and southern regions of INTEC, while the central area of the INTEC does not appear to have significant shallow perched water (DOE-ID 2003a). The northern shallow perched water can be divided into two principal zones associated with the 110-ft and 140-ft interbeds, respectively. Shallow perched water has been identified beneath two separate areas of southern INTEC. A small perched water body has been identified in the vicinity of Building CPP-603, and a larger perched water body has developed from the discharge of wastewater to the former percolation ponds. The larger perched water body began rapidly draining when use of the percolation ponds was discontinued in August 2002.
- The deep perched water appears to be primarily associated with the 380-ft interbed. The top of this interbed occurs beneath the western portion of INTEC at depths ranging from 375 to 426 ft below land surface (bls). Water has been encountered in the northern deep zones at approximately 322, 407, and 383 ft bls. The sources of recharge to the western portion of the northern deep perched water are unknown, although the Big Lost River and facility water leaks are likely contributors.
- An intermediate perched water zone appears at approximately 250 ft below land surface south of INTEC near the ICDF, and recharge was most likely from the former percolation pond. Recent data indicate that it has also been draining since the percolation ponds were discontinued (Cahn and Ansley 2004).

The sources of the perched water include recharge from the BLR, infiltration from the former percolation ponds, precipitation, and other anthropogenic water.

Historically, the perched water has been monitored by USGS and by DOE. Many of the wells were installed prior to the OU 3-13 RI/FS or during the OU 3-13 RI/FS. As a result of the OU 3-13 ROD

(DOE-ID 1999) institutional controls were implemented in 2002. These institutional controls include reducing the surface infiltration and monitoring resultant soil moisture and COC concentrations. The primary reduction in surface infiltration occurred when the percolation ponds were moved approximately 2 miles west of the INTEC facility on August 26, 2002. Prior to removal, the percolation ponds discharged in excess of 1 M gal of wastewater per day and accounted for approximately 70% of the known water recharging the aquifer near INTEC.

To record the transient effects resulting from moving the ponds and to reduce the overall uncertainty, the OU 3-13, Group 4, activities (DOE-ID 2003a) added several well sets around the Big Lost River, sewage treatment lagoons, and percolation ponds. These additional wells included piezometers to monitor perched water elevations, suction lysimeters to collect samples from the unsaturated zone, tensiometers to measure matric potential, and temperature sensors. Soil moisture sensors were installed in some initial wells, but were excluded from subsequent wells because of instrument failures. The Group 4 remedial wells included the following sets:

- Big Lost River (BLR) set. The BLR set is located south of the Big Lost River and was installed to monitor the northern perched water levels and to examine hydraulic connections between northern perched water and the Big Lost River.
- Sewage Treatment Lagoon (STL) set. The STL set is located west of the sewage treatment lagoons and was installed to define the perched water thickness and provide data on the hydraulic connection between the northern perched water and the sewage treatment lagoons.
- Percolation Pond (PP) set. The PP set is located north of the former percolation ponds. These wells were installed to monitor the upper and lower perched zones in the southern INTEC, to identify the hydraulic connection between the former percolation ponds and the southern perched water, and to provide monitoring points for the percolation pond tracer test.
- Tank Farm (TF) set. The TF set is located north of the tank farm and was installed to identify the effects of the Big Lost River on soil moisture and perched water at the alluvium/basalt interface, upper northern perched water, lower northern perched water, and the SRPA.
- Central Set (CS). The CS wells are located between the northern and southern upper perched water. These wells were installed to monitor conditions between the former percolation ponds and the tank farm.

Each of the well sets contained four to five well completions and were designed to collect specific data. The corehole (CH) completions were installed to collect soil and basalt core and monitor perched water. The alluvial (AL) completions were installed to monitor perched water at the alluvium/basalt interface. The shallow perched (SP) completions are monitored in the shallow perched water associated with the 110-ft to 140-ft interbeds. The deep perched (DP) completions targeted the deep perched zones at approximately 380-ft bls. Tensiometers and lysimeters were installed a various depths to monitor unsaturated conditions.

In addition to the OU 3-13, Group 4, wells, the ICDF construction project increased the monitoring network. In 2002, the ICDF installed six new perched water wells with multiple completions at varying depths (total of 15 completion intervals). Well locations for both groups are shown in Figure A-3-1. All of the perched water well locations and hydrographs are illustrated in Figures A-3-2 through A-3-8. In general, they are ordered by depth and increasing north to south direction. Data types, dates, and depths for all the wells are given in Table A-3-6.

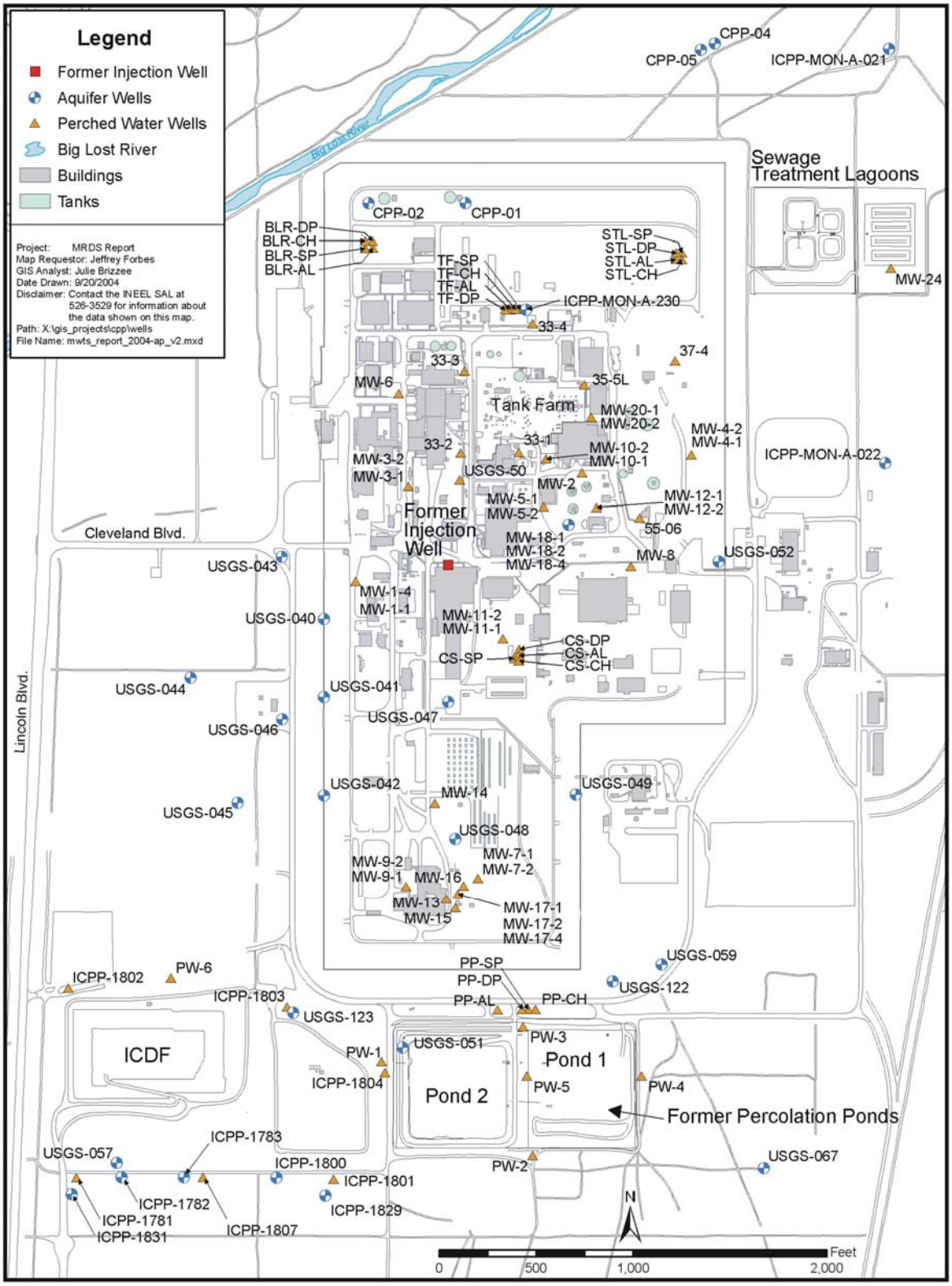

Figure A-3-1. Aquifer and perched water well locations.

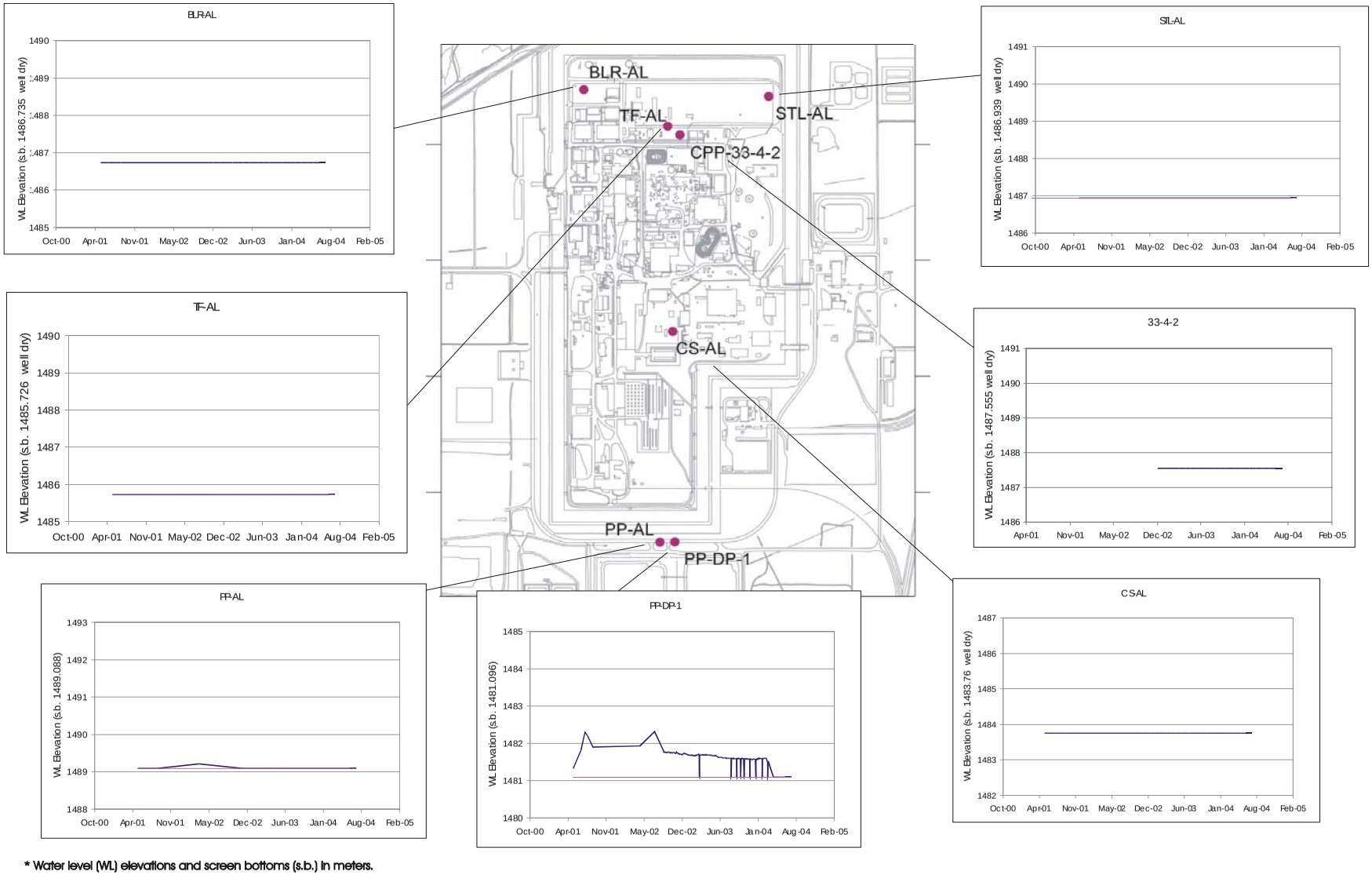

Figure A-3-2. Alluvium perched water well locations and hydrographs.

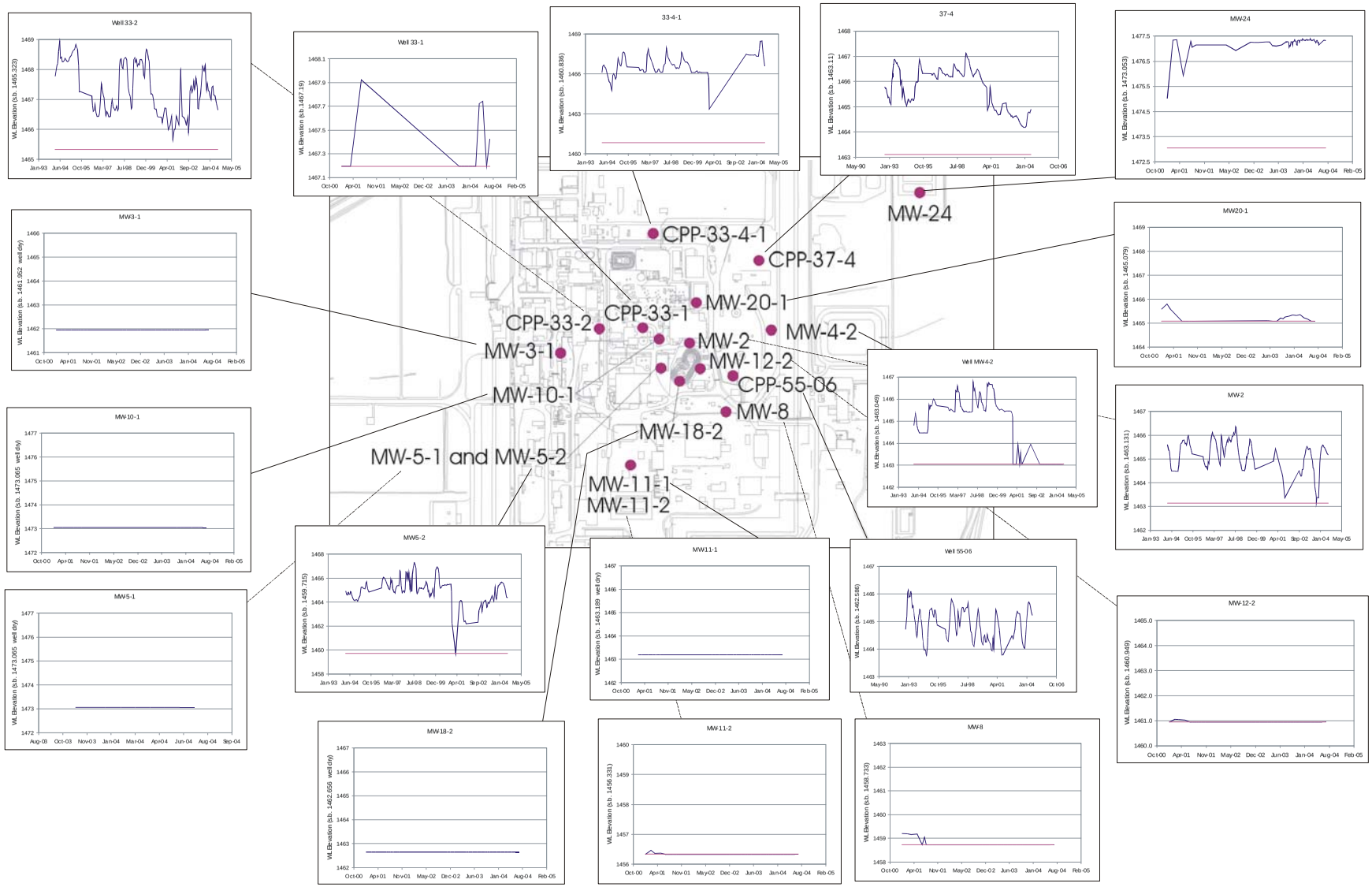

* Water level (WL) elevations and screen bottoms (s.b.) in meters.

Figure A-3-3. Northern upper shallow perched water well locations and hydrographs.

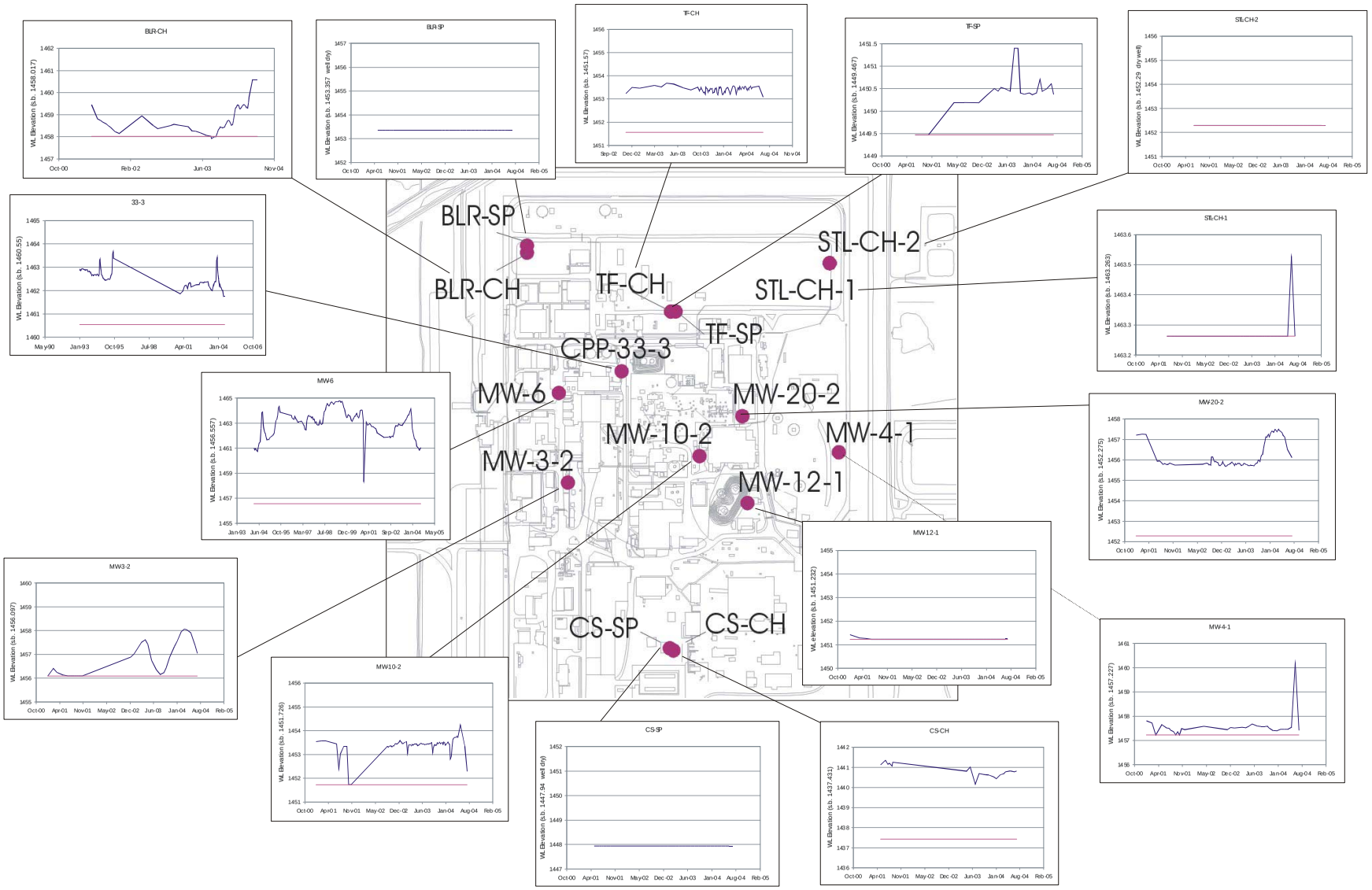

Figure A-3-4. Northern lower shallow perched water well locations and hydrographs.

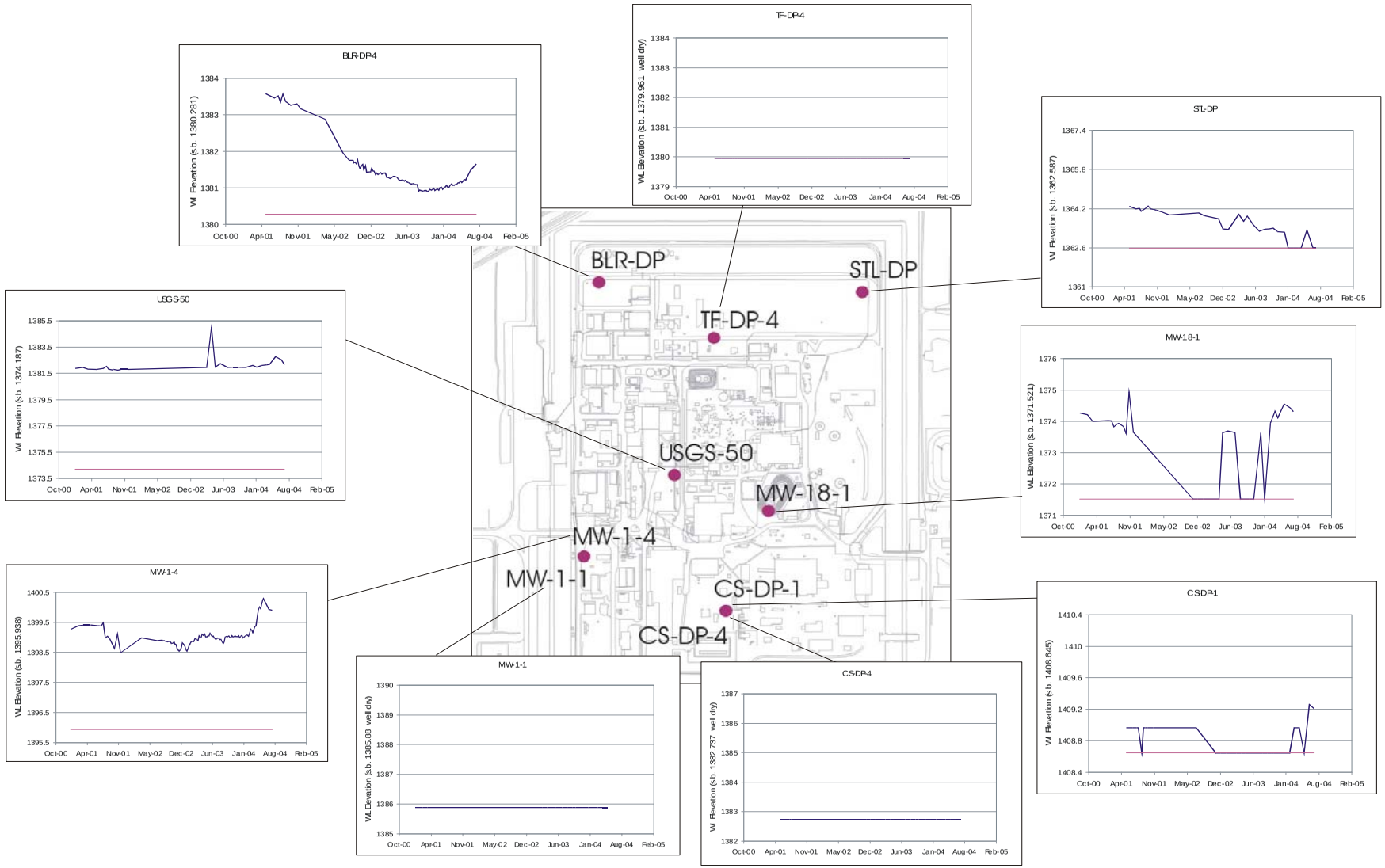

* Water level (WL) elevations and screen bottoms (s.b.) in meters.

Figure A-3-5. Northern deep perched water well locations and hydrographs.

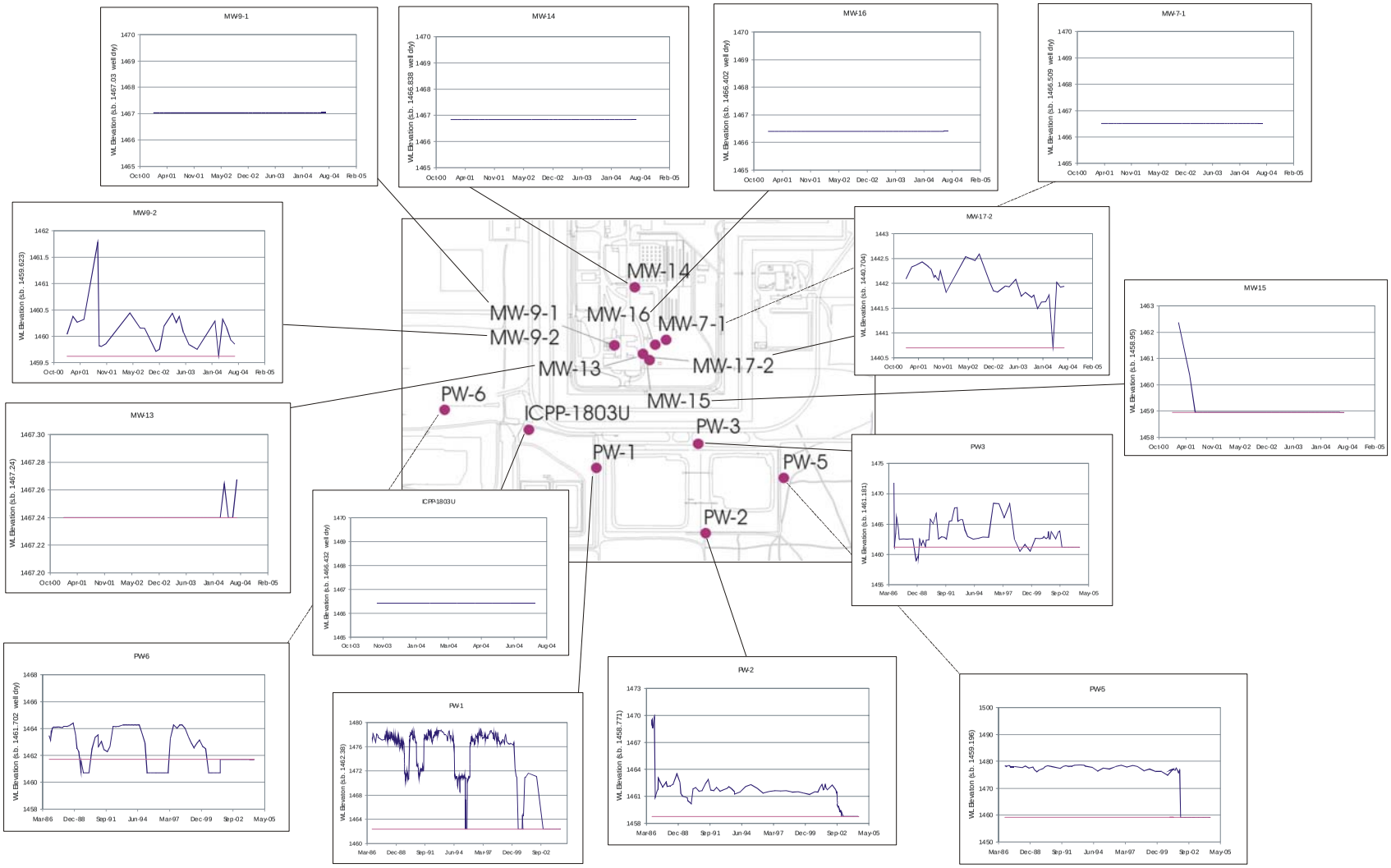

* Water level (WL) elevations and screen bottoms (s.b.) in meters.

Figure A-3-6. Southern upper shallow perched water well locations and hydrographs.

* Water level (WL) elevations and screen bottoms (s.b.) in meters.

Figure A-3-7. Southern lower shallow perched water well locations and hydrographs.

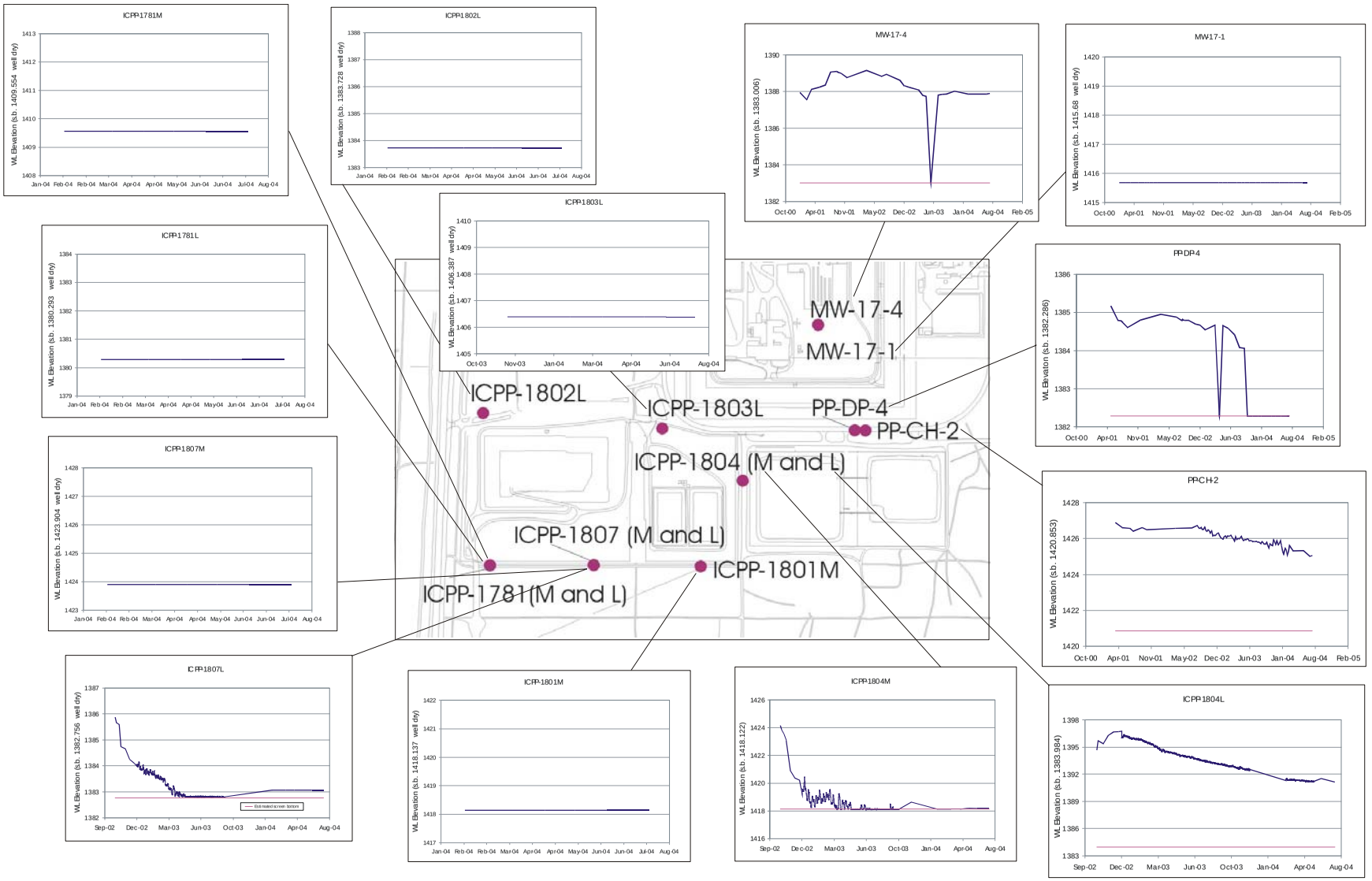

* Water level (WL) elevations and screen bottoms (s.b.) in meters.

Figure A-3-8. Southern deep perched water well locations and hydrographs.

Table A-3-6. Well summary.

Well ID	Well Name	Well Alias	Land Surface Elevation (ft)	Instrument (Depth from Land Surface) (ft)	Available Data
1428	ICPP-SCI-P-216	BLR-AL	4913.64	Lysimeter (32.3) Tensiometer (32.87) Piezometer (35.4-35.9)	 August 2001-Present Automated Data Dry
1429	ICPP-SCI-P-217	BLR-SP	4913.73	Lysimeter (166.38) Tensiometer (132.5, 166.75) Piezometer (140-145.5)	 August 2001-Present Automated Data Dry
1430	ICPP-SCI-P-218	BLR-DP	4913.48	Lysimeter (351.5) Tensiometer (352, 395) Screen (375-385) Screen (375-385)	 August 2001-Present Automated Data September 2002-Present Automated Data April 2001-Present Manual Measurement
1444	ICPP-SCI-P-248	BLR-CH	4913.52	Screen (120-130)	April, 2001-Present Manual Measurement
1431	ICPP-SCI-P-219	STL-AL	4909.31	Lysimeter (26) Tensiometer (26.5) Piezometer (30.4-30.9)	 August 2001-Present Automated Data Dry
1432	ICPP-SCI-P-220	STL-SP	4909.44	Lysimeter (103.25) Tensiometer (103.5, 146)	 August 2001-Present Automated Data
1433	ICPP-SCI-P-221	STL-DP	4909.43	Lysimeter (418) Tensiometer (384.5, 416) Screen (429-439)	 August 2001-Present Automated Data April 2001-Present Manual Measurement
1447	ICPP-SCI-P-251	STL-CH	4909.73	Piezometer (99-109) Screen (140-145)	June 2001-Present Manual Measurement Dry
1434	ICPP-SCI-P-222	PP-AL	4916.76	Lysimeter (26.6) Tensiometer (27.4) Piezometer (30.8-31.3)	 August 2001-Present Automated Data January 2001-Present Manual Measurement
1435	ICPP-SCI-P-223	PP-SP	4917.04	Lysimeter (108.3, 168.5) Tensiometer (108.8, 131.5, 169) Piezometer (180-182)	 August 2001-Present Automated Data Dry
1436	ICPP-SCI-P-224	PP-DP	4917.06	Lysimeter (382.5) Tensiometer (263.5, 383) Piezometer (50-55) Piezometer (50-55) Screen (372-382)	 August 2001-Present Automated Data August 2001-Present Automated Data April 2001-Present Manual Measurement April 2001-Present Manual Measurement
1446	ICPP-SCI-P-250	PP-CH	4916.59	Piezometer (187-192) Screen (235-255)	August 2002-Present Automated Data April 2001-Present Manual Measurement

Well ID	Well Name	Well Alias	Land Surface Elevation (ft)	Instrument (Depth from Land Surface) (ft)	Available Data
1443	ICPP-SCI-P-247	CS-AL	4914.48	Lysimeter (41) Tensiometer (41.5) Piezometer (45.5-46)	August 2001-Present Automated Data Dry
1437	ICPP-SCI-P-225	CS-SP	4914.46	Lysimeter (121.5, 154.5) Tensiometer (122, 155) Piezometer (159-164)	August 2001-Present Automated Data Dry
1438	ICPP-SCI-P-226	CS-DP	4914.54	Lysimeter (279.5) Tensiometer (280, 287, 383) Piezometer (288.5-293) Piezometer (288.5-293) Screen (368-378)	August 2001-Present Automated Data July 2001-Present Automated Data April 2001-June 2002 Manual Measurement Dry
1445	ICPP-SCI-P-249	CS-CH	4914.48	Screen (188.5-198.5)	April 2001-Present Manual Measurement
1439	ICPP-SCI-P-227	TF-AL	4912.43	Lysimeter (34.5) Tensiometer (35) Piezometer (37.5-38)	August 2001-Present Automated Data Dry
1440	ICPP-SCI-P-228	TF-SP	4912.22	Lysimeter (117.5, 156.4) Tensiometer (118, 157, 173) Piezometer (145-150)	August 2001-Present Automated Data March 2002-Present Manual Measurement
1441	ICPP-SCI-P-229	TF-DP	4912.43	Lysimeter (385) Tensiometer (350.5, 388.5) Screen (375-385)	August 2001-Present Automated Data Dry
1442	ICPP-SCI-P-230	TF-Aquifer	4912.41	Screen (443-483)	September 2001-Present Manual Measurement
1448	ICPP-SCI-P-252	TF-CH	4912.36	Screen (145-150)	March 2002-Present Manual Measurement
1781	ICPP-1781	ICPP-1781	4925.99	Screen (155-175, 279-299, 375-395)	February 2004-Present Manual Measurement
1801	ICPP-1801	ICPP-1801	4921.92	Screen (138-158, 247-267)	February 2004-Present Manual Measurement
1802	ICPP-1802	ICPP-1802	4925.12	Screen (186-206, 291-311, 363-383)	November 2003-Present Manual Measurement
1803	ICPP-1803	ICPP-1803	4921.99	Screen (88-108) Screen (135-155) Screen (285-305)	November 2003-Present Manual Measurement November 2004-Present Manual Measurement November 2003-Present Manual Measurement

Well ID	Well Name	Well Alias	Land Surface Elevation (ft)	Instrument (Depth from Land Surface) (ft)	Available Data
1804	ICPP-1804	ICPP-1804	4920.96	Screen (246-266) Screen (358-378)	October 2002-Present Manual Measurement December 2002-October 2003 Automated Data October 2002-Present Manual Measurement December 2002-Present Automated Data
1807	ICPP-1807	ICPP-1807	4924.13	Screen (144-164) Screen (230-250) Screen (364-384)	February 2004-Present Manual Measurement February 2004-Present Manual Measurement October 2002-Present Manual Measurement January 2003-October 2003 Automated Data
735	CPP-33-1	33-1	4914.33	Screen (89.0-90.0)	Dry
736	CPP-33-2	33-2	4913.29	Screen (85.8-105.8) Screen (85.8-105.8)	February 1994-May, 2003 Automated Data January 2001-Present Manual Measurement
737	CPP-33-3	33-3	4913.83	Screen (111.8-122.0) Screen (111.8-122.0)	January 1993-October, 1995 Automated Data January 2001-Present Manual Measurement
764	CPP-33-4	33-4	4911.02	Screen (98.2-118.3)	February 1994-April, 2001 Manual Measurement
806	CPP-37-4	37-4	4910.13	Screen (99.6-110) Screen (99.6-110)	February 1992-Present Automated Data January 2001-Present Manual Measurement
131	CPP-55-06	55-06	4911.61	Screen (93.1-113.1) Screen (93.1-113.1)	October 1992-Present Automated Data January 2001-Present Manual Measurement
1057	INTEC-MON-P-001	MW-1-4	4915.85	Screen (326-336) Screen (326-336)	August 2002-Present Automated Data January 2001-Present Manual Measurement
1057	INTEC-MON-P-001	MW-1-1	4915.85	Piezometer (359-369)	Dry
1058	INTEC-MON-P-002	MW-2	4912.3	Screen (102-112) Screen (102-112)	March 1992-Present Automated Data January 2001-Present Manual Measurement
1059	INTEC-MON-P-003	MW-3-2	4915.22	Screen (128-138)	January 2001-Present Manual Measurement
1059	INTEC-MON-P-003	MW-3-1	4915.22	Piezometer (116.3-118)	May 2001-Present Manual Measurement
1060	INTEC-MON-P-004	MW-4-2	4910.63	Screen (100.6-110.6) Screen (100.6-110.6)	February 1994-January, 2001 Automated Data April 2001-March, 2002 Manual Measurement
1060	INTEC-MON-P-004	MW-4-1	4910.63	Piezometer (128.0-129.7)	January 2001-Present Manual Measurement

Well ID	Well Name	Well Alias	Land Surface Elevation (ft)	Instrument (Depth from Land Surface) (ft)	Available Data
1061	INTEC-MON-P-005	MW-5	4915.59	Screen (106.5-126.5) Screen (106.5-126.5)	March 1994-May, 2003 Automated Data May 2001-Present Manual Measurement
1062	INTEC-MON-P-006	MW-6	4915.73	Screen (117-137) Screen (117-137)	February 1994-Present Automated Data January 2001-Present Manual Measurement
1063	INTEC-MON-P-007	MW-7-2	4916.38	Screen (132-142) Screen (132-142)	August 2002-Present Automated Data January 2001-Present Manual Measurement
1063	INTEC-MON-P-007	MW-7-1	4916.38	Piezometer (102.3-104)	Dry
1064	INTEC-MON-P-008	MW-8	4911.72	Screen (115-125)	January 2001-June, 2001 Manual Measurement
1065	INTEC-MON-P-009	MW-9-2	4918.79	Screen (120-130)	January 2001-Present Manual Measurement
1065	INTEC-MON-P-009	MW-9-1	4918.79	Screen (104.2-105.7)	Dry
1066	INTEC-MON-P-010	MW-10-2	4913.88	Screen (141-151) Screen (141-151)	August 2002-Present Automated Data January 2001-Present Manual Measurement
1066	INTEC-MON-P-010	MW-10-1	4913.88	Piezometer (76.5-78)	Dry
1067	INTEC-MON-P-011	MW-11-2	4913.99	Screen (131-136)	January 2001-August, 2001 Manual Measurement
1067	INTEC-MON-P-011	MW-11-1	4913.99	Piezometer (112-113.5)	Dry
1068	INTEC-MON-P-013	MW-12-2	4912.14	Screen (109-119)	January 2001-April, 2001 Manual Measurement
1068	INTEC-MON-P-013	MW-12-1	4912.14	Piezometer (148.6-150.3)	February 2001-April, 2001 Manual Measurement
1069	INTEC-MON-P-014	MW-13	4918.78	Screen (100-105)	Dry
1070	INTEC-MON-P-015	MW-14	4917.23	Screen (94-104)	Dry
1071	INTEC-MON-P-016	MW-15	4917.88	Screen (111.3-131.3)	January 2001-Present Manual Measurement
1072	INTEC-MON-P-017	MW-16	4918.03	Screen (97-107)	Dry
1073	INTEC-MON-P-018	MW-17-2	4918.42	Screen (181.7-191.7)	January 2001-Present Manual Measurement

Well ID	Well Name	Well Alias	Land Surface Elevation (ft)	Instrument (Depth from Land Surface) (ft)	Available Data
1073	INTEC-MON-P-018	MW-17-1	4918.42	Piezometer (263.8-273.8)	Dry
1073	INTEC-MON-P-018	MW-17-4	4918.42	Screen (360-381)	January 2001-Present Manual Measurement
1187	INTEC-MON-P-019	MW-18-2	4913.74	Screen (113.5-123.5)	Dry
1187	INTEC-MON-P-019	MW-18-1	4913.74	Piezometer (394-414)	January 2001-Present Manual Measurement
1074	INTEC-MON-P-020	MW-20-2	4913.08	Screen (133.2-148.4)	January 2001-Present Manual Measurement
1074	INTEC-MON-P-020	MW-20-1	4913.08	Piezometer (96-106) Piezometer (96-106)	August 2002-Present Automated Data April 2003-Present Manual Measurement
1093	INTEC-MON-P-024	MW-24	4906.35	Screen (53.5-73.5)	January 2001-Present Manual Measurement
257	PW-1	PW-1	4917.82	Screen (100-120) Screen (100-120)	August 2002-February, 2003 Automated Data January 2001-March, 2002 Manual Measurement
258	PW-2	PW-2	4916.99	Screen (111-131) Screen (111-131)	August 2002-May, 2003 Automated Data January 2001-December, 2002 Manual Measurement
259	PW-3	PW-3	4916.9	Screen (103-123) Screen (103-123)	August 2002-Present Automated Data January 2001-June, 2002 Manual Measurement
260	PW-4	PW-4	4915.05	Screen (110-150) Screen (110-150)	August 2002-Present Automated Data January 2001-Present Manual Measurement
261	PW-5	PW-5	4916.39	Screen (109-129)	August 2002-May, 2003 Automated Data
262	PW-6	PW-6	4920.61	Screen (105-125)	Dry
499	USGS-50	USGS-50	4913.5	Screen (357-405)	January 2001-Present Manual Measurement

A-3.5 Vadose Zone Water Chemistry

Contaminants have been observed in the INTEC perched water since the 1950s (Robertson et al. 1974), as summarized in the OU 3-13 RI/BRA (DOE-ID 1997). During the spring and summer of 2001, OU 3-13 Group 4 updated the concentration inventory by sampling existing and newly constructed perched water wells for radionuclides and general organic/inorganic chemistry (DOE-ID 2003a). This latter effort also verified the historical chemical analysis from previous investigations. Both data sets were summarized in the Monitoring Well and Tracer Study Report (DOE-ID 2003a). In addition to the Group 4 report, the wells installed during the ICDF construction were sampled for VOCs, SVOCs, metals, and major cations and anions in 2002 (Cahn and Ansley 2004).

The Monitoring Well and Tracer Study Report's (DOE-ID 2003a) analysis of the water chemistry data concluded that the former percolation ponds may impact perched water only as far north as the CS-SP well (DOE-ID 2003a). This conclusion was based on environmental isotopic signatures of the perched water and chloride concentrations in perched water and in the Snake River Plain Aquifer. The Monitoring Well and Tracer Study Report also concluded that the northern perched water in the vicinity of the tank farm receives water from many sources, including leaking pipes, precipitation, the Big Lost River, and possibly the sewage treatment lagoons because of elevated nitrate levels. The nitrate could be from tank farm leaks and spills or the sewage treatment lagoons. However, high radionuclide concentrations in the tank farm vicinity perched water indicate that the tank farm leaks and spills have impacted perched water. The ICDF well data obtained in 2002 suggested that the perched water (shallow, middle, and deep) had the same chemistry as percolation pond water.

These data correspond to the following categories:

- Field parameters (pH, conductivity, dissolved oxygen, temperature, total dissolved solids)
- Hazardous constituents (arsenic, barium, cadmium, chromium, lead, mercury, selenium, silver, fluoride, nitrate, lindane, endrin, methoxychlor, toxaphene, 2,4-D)
- Groundwater quality indicators (calcium, copper, iron, magnesium, manganese, sodium, potassium, chloride, bicarbonate alkalinity, sulfate, phenols, zinc)
- Radionuclides (gross alpha, gross beta, Pu-238, Pu-239/240, Tc-99, Am-241, U-233/234, U-235, U-238, Cs-134, Cs-137, Np-237, I-129, Ra-226, Ra-227, Sr-90, tritium)
- Miscellaneous parameters (Al, Ni, Br, CO_3).

A-3.6 Vadose Zone Water Sources

The perched water bodies at INTEC are a result of low-permeability interbeds, low-permeability basalt flows, and high surface recharge rates. The high INTEC recharge rates are from discharges to the former percolation ponds, natural flows from the Big Lost River, discharges to the sewage treatment lagoons, losses from the facility water distribution system, and infiltration from lawn irrigation and precipitation. Estimates of these discharges were presented in Appendix F of the OU 3-13 RI/BRA (DOE-ID 1997) and are reproduced in Table A-3-7.

To better understand these recharge sources and to identify plant operations responsible for them, a water system engineering study for INTEC was performed in 2003 (DOE-ID 2003b). The engineering study concluded that the INTEC facility uses approximately 1.65 M gal/day (0.344 M kg/day), which was considerably higher than the 0.228 million kg/day recharge rate assumed in Appendix A of the OU 3-13 RI/ BRA (Appendix A, DOE-ID 1997). Due to inherent uncertainty and unreliable data used in the 2003 study, the INTEC process water flow monitoring systems were upgraded in 2004. A separate study of water discharges to the subsurface in the vicinity of the Waste Calcining Facility (WCF) was performed in 2003 (DOE-ID 2004b). The study identified and quantified several facility-related water discharges in the northern INTEC. All of the WCF discharges are included in Table A-3-8.

The Big Lost River is an intermittent stream that flows adjacent to the northwest corner of INTEC. Most of the streamflow infiltrates through the river channel, INL Site spreading areas, or the playas located at the river's terminus, which is located approximately 15 miles north of INTEC. The Big Lost River recharge near INTEC was estimated using stream infiltration losses occurring between the INL Site diversion dam and the Lincoln Boulevard bridge near INTEC. In this river reach, Bennett (1990) estimated the average annual infiltration rate to be 9,800 acre-feet for the period 1965-1987. The distance between the INL Site diversion dam and the Lincoln Boulevard bridge is 10.7 miles, which results in a long-term infiltration rate of approximately 1,900 kg/day per meter of river length.

More recent daily streamflow records obtained from the gauging stations located at the INL Site diversion dam and Lincoln Boulevard bridge (USGS 2004) were used to estimate a transient infiltration rate adjacent to the INTEC. Daily stream -flow data are available from 1984 through the present time. The flow difference between the INL Site diversion dam and Lincoln Boulevard bridge gauges was used to estimate streamflow losses due to infiltration to the river channel along the 10.7-mile river reach. A time series analysis of the data was performed to estimate a lag time between the diversion dam and Lincoln Boulevard gauging station, and the result was a monotonically decreasing correlation with increasing lag. This indicated the water travel time between stations is less than 1 day and simply differencing the daily mean flow at each station for each day provided an adequate estimate of possible infiltration. The average daily infiltration rate for the period 1984-2003 was approximately 1,066 kg/day per meter of river length (Figure A-3-9). As indicated in Figure A-3-9, the river did not flow beyond the INL Site diversion dam during the years 1988 through 1992, 1994, and 2001 through 2003.

Using the changing perched water and soil moisture conditions as model calibration data requires using pre- and post-remedial action discharge rates. The pre-remedial action water sources are summarized in Table A-3-7 and represent the values used in the OU 3-13 RI/BRA. The selected remedy for OU 3-13, Group 4, (perched water) included surface water reduction which resulted in elimination or significant reduction in discharge rates from INTEC facility operations. The former percolation ponds were moved to a new location approximately 2 miles west of INTEC, and several changes were made to INTEC plant operations to reduce recharge sources. The post-remedial action water balance is summarized in Table A-3-8. The post-remedial action water balance, excluding the Big Lost River or precipitation, is 0.242 million kg/day (which is close to the OU 3-13 study value) and reflects the newer data. The differences between water sources in Tables A-3-7 and A-3-8 are due to changes in water use over time at the INTEC and possibly due to more or less conservative estimation methods between the OU 3-13 work and the more recent Group-4 water balance studies.

Some of the water sources provided in Table A-3-7 have removed since the model was constructed and calibrated. However, they remain in the model because they were performed after model development.

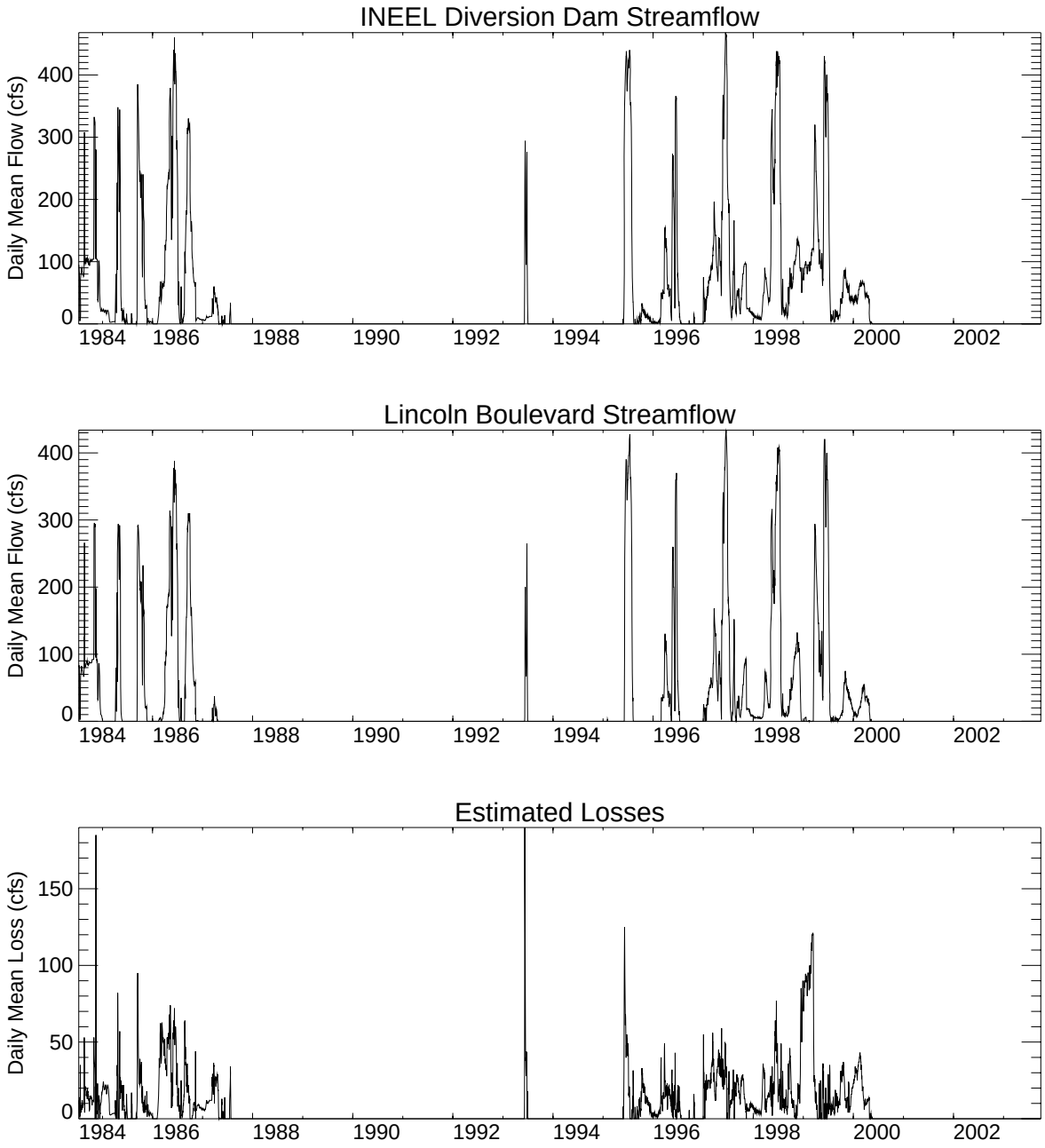

Figure A-3-9. Mean streamflow and Big Lost River losses between the INL Site diversion dam and Lincoln Boulevard bridge.

Table A-3-7. OU 3-13 RI/BRA model water balance (from Tables 1-8 and 1-9 of Appendix F in DOE-ID 1997).

Water Source	Mass Rate (m^3/day)	Notes
Precipitation Total	462.0	640,000 m^2@18 cm/year and 5,360,000 m^2@1 cm/year
Landscape irrigation total	13.50	—
Steam vent condensate total	17.31	—
Steam Vent Area 1	1.82	—
Steam Vent Area 2	2.29	—
Steam Vent Area 3	1.53	—
Steam Vent Area 4	1.00	—
Steam Vent S-3	3.36	—
Steam Vent S-19	2.09	—
Steam Vent S-76	0.45	—
Steam Vent S-78	0.23	—
Steam Vent S-180	0.78	—
Steam Vent 21	0.42	—
Steam Vent 24	1.62	—
Steam Vent 27	0.22	—
Steam Vent 30	0.67	—
Steam Vent UT-46	0.20	—
Steam Vent UT-47	0.23	—
Steam Vent UT-48	0.39	—
CPP-603 basins	0.51	Estimated from basin makeup water
Sewage treatment ponds	155.56	—
Fire water system leaks total	41.23	Calculated from average fire water system flow estimated prior to 1995
Former percolation ponds	5,838.87	—
Big Lost River	2,100.00	—

Table A-3-8. Current (post-remedial action) water balance from DOE-ID (2003b) and DOE-ID (2004b).

Water Source	Mass Rate (m^3/day)	Notes
Precipitation total	462.0	640,000 m^2@18 cm/year and 5,360,000 m^2@1 cm/year.
Landscape irrigation total	13.31	Daily average estimated from 2002 irrigation totals in DOE-ID (2003b). This is higher than the irrigation rates presented in DOE-ID (2004b). Plans to eliminate all irrigation during CY 2006.
Steam vent condensate total	0.30	All but two steam traps have been abandoned or are no longer in use. Rate estimated from RI/BRA for two traps. All have been eliminated.
CPP-603 basins	0	Basin water usage only replaces evaporative losses.
CPP-655 sanitary sewer	0.89	Building 655 septic tank discharge rate (DOE-ID 2004b).
Sewage Treatment Ponds	138.2	Daily average estimated from Nov-01 through Jul-03 totals. Effluent transferred to the vadose zone research park in 2004.
CPP-656 sanitary sewer	4.05	Building 656 septic tank discharge rate (DOE-ID 2004b).
CPP-1606 heating system	0.89	September-April heating steam condensate.
CPP-1608 heating system	0.89	September-April heating steam condensate.
CPP-697 heating system	0.89	September-April heating steam condensate.
Fire water system leaks total	81.77	Calculated from average fire water system flow estimated in 2003.
Steam drip at corner of CPP-649	0.15	—
Steam drip 125ft west of CPP-649	0.15	—
Former percolation ponds	0	Service waste water was transferred to the new location in August, 2002.
Fire hydrant testing	0.13	Fire hydrant testing water is directed towards drainage ditches or use diffusers to maximize evaporation.
Big Lost River	1.90 kg/day/m	Recharge per meter of river length from Bennett (1990).

A-3.7 Vadose Zone Solute Sorption Data

The sorption processes involve mass transfer from the solution to the solids. Sorption is a general term that can be further classified based on the type of process that binds the solute to the solid. These processes include (1) adsorption (solutes held at the mineral surface as a complex), (2) absorption (solutes incorporated into the mineral structure at its surface), and (3) ion exchange (ions sorbed to a surface through changing places with a similarly charged ion on the mineral surface) (Kehow 2001). Contaminant sorption to the subsurface media can significantly slow transport of many contaminants. Simulating sorption requires parameterizing the soil/rock bulk density and adsorption/desorption isotherms for each contaminant. The groundwater model assumes the sorption processes are reversible, and these models lump the processes into a single soil/water distribution coefficient (K_d) parameter. The simulation of the Site CPP-31 Sr-90 transport out of the alluvium did not use the constant K_d parameter approach. The simulation of Site CPP-31 Sr-90 transport used a geochemical model, which considered the important processes that would alter/control the strontium transport from the very high ionic strength of the acidic raffinate. The geochemical conceptual and numerical models are presented in Appendix J.

Reasonably conservative contaminant partition coefficients were identified for each of the COPCs identified in the OU 3-14 RI/FS Work Plan (DOE-ID 2004a) for the three (alluvium, basalt, and interbed)

material types used in the groundwater fate and transport model. Appendix D presents the COPC partition coefficients from site-specific or off-Site transport studies in similar geologic materials. Plutonium is thought to include an immobile and mobile fraction. The total mobile plutonium was estimated to be from 1 to 2.5% (Appendix D) and has a zero K_d. The OU 3-14 COPC and partition coefficients are presented in Table A-3-9. An in-depth discussion of the K_d uncertainty and variability can be found in Appendix D. The minimum Tc-99 K_d value reported in the literature was -0.1 mL/g. The negative value is the result of a column experiment derived K_d value in which the assumed conservative tracer moved slower than the Tc-99. The negative value can not be used to parameterize a contaminant transport model.

Table A-3-9. Preliminary COPCs and partition coefficients.

COPC	Alluvium K_d and (Range) (mL/g)	Interbed K_d and (Range) (mL/g)	Basalt K_d and (Range) (mL/g)
Am-241	400 (100-10,000)	400 (100-10,000)	0.85 (0-140)
C-14	1.6 (0.5-2.8)	1.6 (0.5-2.8)	0 (0-2.8)
Cs-137	50 (10-160)	50 (10-160)	25 (0-44)
Eu-154	400 (15-19,600)	400 (15-19,600)	0.85 (0-140)
H-3	0	0	0
I-129	1.5 (0.04-8.7)	0.7 (0.04-3)	0
Np-237	2 (0.1-60)	2 (0.1-60)	0 (0-8)
Pu-238,239,240[a]	1,000 (96-12,712)	1,000 (96-12,712)	70 (0-130)
Sr-90	12 (8-20)	50 (25-84)	0.5 (0-15)
Tc-99	0 (-0.1-1.4)	0 (-0.1-0.1)	0
U-234,235,238	1.6 (0.12-12)	1.6 (0.12-12)	0 (0-1.4)
Arsenic	40 (0.7-190)	45 (0.5-230)	2 (0-10)
Chromium	2.4 (0.08-12)	90 (9-673)	1.5 (0-50)
Mercury	118 (118-1,912)	156 (72-673)	0 (0-88)
Nitrate	0.1 (0-0.5)	0.1 (0-0.5)	0
Nitrite	0.1 (0-0.5)	0.1 (0-0.5)	0

a. Pu K_d is for the relatively immobile fraction only.

A-4 AQUIFER DATA SUMMARY

The Snake River Plain Aquifer is one of the largest and most productive aquifers in the United States, with approximately 9% of the aquifer lying beneath the INL Site. As with the vadose zone, historical investigations by DOE and USGS have provided an extensive set of data describing the aquifer and its hydrogeologic properties. Similar to the vadose zone, the Snake River Plain Aquifer comprises primarily alternating basalt flows and discontinuous interbeds (INEEL 2003b); however, unlike the vadose zone, only one primary sediment unit exists near the INTEC area. Properties specific to the saturated aquifer near INTEC are discussed in the following subsections.

A-4.1 Aquifer Geology/Lithology

For the purposes of contaminant transport predictions, it is necessary to define the top of the water table, the thickness of the aquifer, and the lithology. The depth to the top of the aquifer ranges between 200 ft in the northern and 900 ft in the southern portions of the INL Site, respectively. Under INTEC, the top of the aquifer is located at approximately 450 ft below land surface. Defining the thickness of the SRPA is more difficult, primarily because the thickness of interest for contaminant transport is much less than the total aquifer thickness. The thickness of the aquifer through which water actively flows is uncertain and is based on a limited number of fully penetrating wells (Figure A-4-1). Estimates near the INL Site vary from near zero to over 1,200 ft. To better define this thickness, deep well temperature logs were used by Smith in 2002. The temperature logs reflect an isothermal gradient in the upper portions of the aquifer, with normal temperature gradients occurring deeper. The isothermal region is attributed to cold recharge water moving fast enough to overcome the geothermal gradient. This isothermal area is thought to identify the portion of the aquifer actively conducting water and contaminants.

The lithology was primarily defined by the work by Anderson (1991) who estimated the areal extent of basalt flow groups and sedimentary interbeds in the upper 700 ft of subsurface. In the INTEC and Reactor Technology Complex (RTC), 23 basalt flow groups were identified and designated with informal letters B through I with the I flow being the oldest and deepest. The flow groups included 15 to 20 sedimentary interbeds which were designated by the two alphabetical characters of the basalt flow above and beneath the interbed. Flow group I tends to be many times thicker than other flows near the INL Site, and is overlain by the HI interbed. The HI interbed is widespread, occurs in most wells that penetrate to the flow group I (Anderson 1991), and is the primary sedimentary structure in the INTEC/RTC vicinity.

Data taken from 51 INL Site and USGS well logs were used to define the HI interbed thickness and surface elevation. Data pertaining to older INL Site and USGS wells can be found in Anderson (1989) and Anderson, (1991), and more recent data can be found in DOE-ID (2002). The data available to define the HI interbed thickness and elevation are contained in Table A-4-1. Analysis of this data shows that the HI interbed tends to dip in the southeast direction when viewed from a large scale (OU 3-13 RI/BRA aquifer model domain) and that the interbed tends to become thicker and more continuous in the southeast direction. Isopach maps of the HI interbed can be found in Appendix C. Well logs from Wells SPERT-IV and Site-09 (southeast of INTEC) indicate that the interbed can be approximately 90 ft thick in some areas.

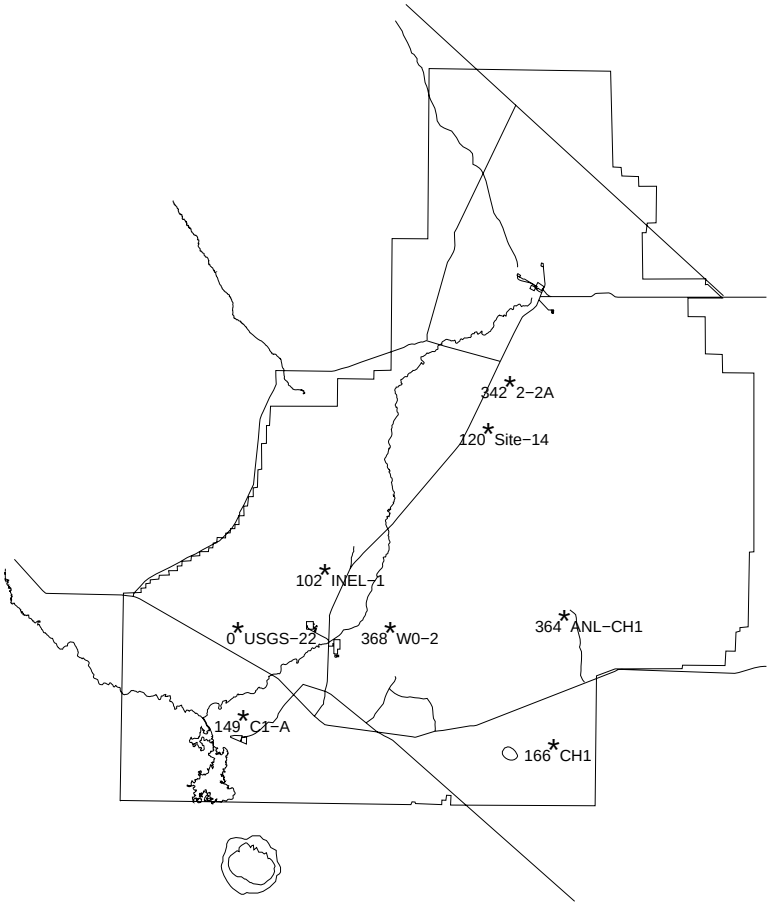

Figure A-4-1. Deep INL Site wells used to define the aquifer thickness (m).

Table A-4-1 HI interbed elevation and thickness data.

Well	Surface Elevation (ft)	Depth to HI Interbed Top (ft)	HI Interbed Thickness (ft)	Well	Surface Elevation (ft)	Depth to HI Interbed Top (ft)	HI Interbed Thickness (ft)
cfa-1	4928.31	623	48	usgs-047	4916.309	532	5
cpp-3	4916.047	519	7	usgs-048	4917.11	549	3
cpp-4	4909.282	523	0	usgs-049	4912.9	540	2
lf2-09	4932.227	625	14[a]	usgs-051	4918.74	561	4
lf2-10	4932.477	620	49	usgs-052	4909.557	526	5
mtr-test	4917.149	351	0	usgs-057	4922.487	567	5
npr-test	4933.146	556	42	usgs-058	4918.373	342	7

Well	Surface Elevation (ft)	Depth to HI Interbed Top (ft)	HI Interbed Thickness (ft)	Well	Surface Elevation (ft)	Depth to HI Interbed Top (ft)	HI Interbed Thickness (ft)
ow-1	5042.	758	5	usgs-066	4921	365	7
ow-2	5044.	781	6	usgs-067	4914	572	18
rwmc-m04d	5022.53	728	3	usgs-076	4930	528	4
site-09	4926.9	724	84	usgs-079	4931	487	4
site-19	4926.329	462	5	usgs-082	4908	557	9
spert-IV	4924	837	87	usgs-083	4943	716	36[a]
tra-06a	4926	489	6	usgs-085	4939	631	6[a]
tra-07	4931	495	6[a]	usgs-104	4989	688	12[a]
usgs-020	4916	611	65[a]	usgs-106	5015	652	0
usgs-034	4929	593	4	usgs-121	4910	517	5
usgs-038	4929	596	5	usgs-123	4920	559	4
usgs-039	4931	568	4	C-1A	5029.	698	5
usgs-040	4916	527	2	EOCR	4943	966	34
usgs-041	4917	530	4	NPR_WO-2	4930	571	27
usgs-042	4918	547	0	S5G-Test	4850	698	26
usgs-043	4916	516	4	WS-INEL-1	4878	670	29
usgs-044	4918	521	0	ICPP-1795	4340	587	7
usgs-045	4920	541	9	ICPP-1796	4331	605	27
usgs-046	4916	542	6	ICPP-1797	4328	601	16
usgs-059	4915	554	4	ICPP-1798	4315	621	57
usgs-065	4925	490	8[a]				

a. Well did not fully penetrate interbed.

CFA=Central Facilities Area.

CPP=Chemical Processing Plant (now INTEC).

MTR=Materials Test Reactor.

RWMC=Radioactive Waste Management Complex.

SPERT=Special Power Excursion Reactor Test.

TRA=Test Reactor Area (now RTC).

USGS=United States Geological Survey.

A-4.2 Aquifer Hydrological Data

A-4.2.1 Aquifer Hydraulic Conductivity

The results of aquifer well testing can be found in several studies. Ackerman (1991) analyzed 183 aquifer well tests and estimated the transmissivity to range from 1.1 to 760,000 ft^2/day. Wood (1989) summarized well pumping tests near the Test Area North and estimated the average transmissivity to be

13,000 ft^2/day. Magnuson and Sondrup (1998) reports the aquifer transimissivities in the vicinity of the SDA to be in the range of 1.1 to 1,000,000 ft^2/day. ICP (2004) estimated the hydraulic conductivity of Well ICPP-MON-A-230 at the INTEC to be in the range of 2,000 to 4,000 ft/day. Most of the hydraulic data were obtained from single and partially penetrating well tests conducted in the uppermost portion of the aquifer. These transmissivity data were converted to hydraulic conductivity using the well screen thickness, are presented in Table A-4-2, and are thought to be representative of basalt properties.

There are less data available for the HI interbed. Pumping tests have been performed by the State of Idaho (Frederick and Johnson 1996) using packers to isolate the interbed from the surrounding basalt. Geotechnical analysis of interbed samples collected for DOE-ID (2004c) from boreholes ICPP-1795, ICPP-1797, and ICPP-1798 has also provided permeability estimates south of the INTEC. The results of the pumping tests and geotechnical analysis are provided in Table A-4-3.

Table A-4-2 Snake River Plain Aquifer hydraulic conductivity values.

Well Name	Hydraulic Conductivity (ft/day)	Well Name	Hydraulic Conductivity (ft/day)	Well Name	Hydraulic Conductivity (ft/day)
tf-aquifer	2560.	site-19	155.8	usgs-012	104.8
anp-05	1923.1	spert-1	7.1	usgs-014	611.1
anp-06	6666.7	spert-2	299.6	usgs-015	4.5
ara-02	1018.5	tan-01	192.1	usgs-024	200.
arbor-test	5600.	tan-02	160.	usgs-030	5657.9
area-II	754.7	tan-03	182	usgs-031	118.9
cfa-2	1.1	tan-04	49	usgs-037	246.2
cpp-1	973.3	tan-05	335	usgs-040	390.9
cpp-2	2162.2	tan-06	14	usgs-043	355.6
cpp-3	7378.6	tan-07	48	usgs-051	15.8
cpp-4	0.9	tan-08	10	usgs-057	109.8
ebr-I	2.7	tan-09	28	usgs-058	740.
ebr-II-1	5200.	tan-10	502	usgs-076	754.0
ebr-II-2	110.	tan-10a	31	usgs-082	608.7
eocr	967.7	tan-11	16	usgs-083	3.8
fet-disp	156.2	tan-12	3.7	usgs-086	6.5
firesta-2	2000.	tan-13a	14	usgs-087	9.8
hwy-3	3.3	tan-14	0.2	usgs-088	0.2
iet-disp	1.6	tan-15	64	usgs-089	0.9
loft-1	310.	tan-16	122	usgs-090	15.8
loft-2	46.0	tan-18	233.3	usgs-097	582.0
lptf-disp	34.0	tan-19	291.7	usgs-098	826.5
mtr-test	1418.4	tan-19	98.9	usgs-099	1746.0

Well Name	Hydraulic Conductivity (ft/day)	Well Name	Hydraulic Conductivity (ft/day)	Well Name	Hydraulic Conductivity (ft/day)
npr-test	245.7	tan-20	0.9	usgs-100	177.2
nrf-1	3953.5	tan-21	9.6	usgs-101	12.6
nrf-2	4473.7	tan-22a	214.7	usgs-103	8843.0
nrf-3	500.	tan-23	477.2	usgs-104	0.1
omre	1.1	tan-23a	100	usgs-105	634.3
p&w-1	5000.	tan-24	43.5	usgs-106	565.0
p&w-2	2058.8	tan-24a	418.2	usgs-107	327.1
p&w-3	177.2	tan-25	37.5	usgs-108	961.5
pstf	57.3	tan-27	135	usgs-109	604.4
rwmc-m01s	0.7	tan-28	36.7	usgs-110	51.4
rwmc-m03s	33.7	tan-29	55.2	usgs-111	0.2
rwmc-m04d	0.1	tan-30a	35.1	usgs-112	666.7
rwmc-m06s	1.2	tan-ch1	14.1	usgs-113	1958.8
rwmc-m07s	33.3	tra-01	7300	usgs-114	0.1
rwmc-m10s	0.1	tra-03	990.1	usgs-115	0.3
rwmc-prod	226.7	tra-04	1048.2	usgs-116	1.2
rwmc-tw	5512.	tra-disp	151.2	usgs-117	0.2
s5g-test	5797.1	tsf05	0.3	usgs-119	0.01
site-06	18.9	usgs-009	2107.1	usgs-120	2340.4
site-14	368.1	usgs-011	2333.3	wsi-1	1.6

Table A-4-3 Summary of HI interbed permeability values.

Well	Hydraulic Conductivity (ft/day)	Reference
USGS-44	2.28E-01	Fredrick and Johnson (1996)
USGS-45	1.80E-01	Fredrick and Johnson (1996)
USGS-46	1.80E-01	Fredrick and Johnson (1996)

Well	Hydraulic Conductivity (ft/day)	Reference
USGS-59	8.39E-02	Fredrick and Johnson (1996)
ICPP-1795	2.30E-04	DOE-ID (2004c)
ICPP-1795	5.42E-04	DOE-ID (2004c)
ICPP-1797	2.83E+01	DOE-ID (2004c)
ICPP-1797	1.96E+00	DOE-ID (2004c)
ICPP-1798	1.53E-01	DOE-ID (2004c)
ICPP-1798	3.30E+00	DOE-ID (2004c)

A-4.3 Aquifer Water Chemistry

As with the INTEC perched water, contaminants have been observed in the aquifer since the early 1950s. The early aquifer contaminants originated from direct disposal of service waste via the CPP-3 injection well. The radioactive service wastes discharged to the injection well included fission and activation by-products from spent nuclear fuel reprocessing at the INTEC with additional minor contributions from laboratory sink drains.

The PEW evaporator system collected dilute radioactive wastes from a variety of sources and concentrated the dilute waste before sending the concentrate (bottoms) to the tank farm. The PEW vapors were condensed, sampled, and then sent to the service waste. The PEW did not effectively remove the more volatile radionuclides. These volatile radionuclides entering the service waste stream have resulted in large aquifer contamination plumes. To quantify the extent of contamination, DOE and USGS have drilled 68 wells downgradient of the INTEC. Groundwater monitoring data are available from the early 1950s to present in some wells and are presented as part of the aquifer calibration information in Section A-8.

A-5 VADOSE ZONE AND AQUIFER CONCEPTUAL MODELS

This study conceptualizes flow and transport through the vadose zone and aquifer as transient processes in three dimensions. The 3-D model domains are necessary to capture the spatial distribution of the vadose zone and aquifer lithology, water recharge sources, and COC sources. Developing a 1-D model of vadose zone flow and transport would lump most of the vadose zone processes into a simple response function and would require calibrating the 1-D model to large-scale tracer data. Large-scale tracer test data are not available for the INTEC, but there are large amounts of data available that represent different portions of the vadose zone. These data often suggest that water and solute movement is subhorizontal and highly spatially variable. The spatial variability invalidates use of 1-D or 2-D models. On the other hand, a 3-D model may be calibrated to a variety of data and data types, each of which may be available for different areas within the vadose zone. These data include perched water elevations, perched water chemistry, 3-D lithological data, and limited small-scale tracers (i.e., radionuclide and contaminants that only partially penetrate vadose zone).

The vadose zone and aquifer models are time-dependent and use three linked simulation domains. The simulation domains consist of (1) a submodel of the tank farm area alluvium including the fractured basalt down to the 110-ft interbed; (2) the large-scale INTEC vadose zone from north of the Big Lost River to south of the former percolation ponds, including the alluvium, fractured basalt, and interbeds down to the water table; and (3) the aquifer, which extends from approximately the INTEC to the southern INL Site boundary. Flow and transport through the three domains are simulated independently and are linked together with the transient water and contaminant flux from each model feeding the next model domain immediately below. Conceptualization and initial parameterization of the vadose zone models are presented in Section A-5.1. Conceptualization and initial parameterization of the aquifer model are presented in Section A-5.2. The simulation code is discussed in Section A-5.3.

A-5.1 Vadose Zone Model and Parameterization

As described above, the vadose zone model is based on a three-dimensional conceptualization through which transient infiltration and transport occurs. In this model, the following assumptions were made:

- Flow in the fractured basalt is controlled by the fracture network and can be represented by a high-permeability, low-porosity equivalent porous medium.
- Surface water sources are not transient with the exception of the fluxes from the former percolation ponds and recharge from the Big Lost River. Variation in discharge and pumping rates in the other service and potable water wells will be neglected.
- The bottom boundary of the vadose zone model is represented by 101.3 Kpa in the water phase. This corresponds to free drainage at just saturated conditions.
- Lateral boundary conditions are no-flow. This might force water to flow through the vadose zone model near the Big Lost River, and might overly constrain infiltration to remain within the model boundaries, but these boundaries are far from the contaminant sources and should not have an undue negative impact.
- The magnitude of the flux entering through the upper boundary is constrained by field data. Perched water levels and contaminant arrival histories will be used to constrain the in situ distribution of transport velocity through adjustment of permeability and porosity.

Under these assumptions, flow through the vadose zone and within the aquifer can be simulated separately. Transient water and contaminant flux leaving through the lower vadose zone model boundary are first computed using the vadose zone models. The vadose zone model parameters were extracted from the data presented in Section A-3. Details of incorporating the physical data into the numerical framework (model parameterization) are discussed below. Parameterization in order of presentation include hydrogeology/ lithology (Section A-5.1.1), spatial extent and discretization (Section A-5.1.2), infiltration (Section A-5.1.3),

and contaminant sources (Section A-5.1.4). The vadose zone model was calibrated to perched water and water quality trends of Tc-99, Sr-90, H-3, and nitrate. The vadose zone model calibration is presented separately in Section A-6.

A-5.1.1 Representation of Lithology

The continuous nature of a numerical model requires interpolation of the sparse observations of hydraulic properties onto a relatively dense simulation grid. As presented in Section A-3, the primary lithology is characterized by fractured basalt that is overlain by alluvium and interspersed with sediment units. Also, as discussed in Section A-3, the moisture content and unsaturated hydraulic characteristics are very much different for basalt than for sediments. These differences - and their magnitudes - present a unique interpolation problem and essentially require that the subsurface lithology be treated as a binary system, with hydraulic properties assigned to the model grid according to the distribution of lithologic type.

As presented in Section A-3.1, the vadose zone lithology is comprised of primary features (alluvium, 110-ft interbed, 140-ft interbed, massive basalt, and 380-ft interbeds); secondary features (miscellaneous sediments); and basalts. The 121 wells in the INTEC facility were used to define the lithology and textural materials in this model. There were six basic phases of this step as listed below:

1). Digital elevation models of the surface elevation at INTEC were assigned to the top layer of the model grid.

2). Wells within and near the model boundaries were selected. Based on the in-depth lithologic, geologic, and hydrologic characterization summarized in Section A-3.1, textural class and lithologies were assigned over the depth of each well in 1-ft increments. At the end of this step, each foot of elevation in each well had been assigned a textural indicator and a lithology flag. The textural indicator was used in Steps 4 and 5, and the lithology flag determined whether the depth increment belonged to the alluvium, basalt, the 110-ft, 140-ft, Interbed below the massive basalt, or 380-ft interbed, or to the secondary discontinuous sediments.

3). The thickness of the alluvium in each well was selected as the first continuous variable to be interpolated. Interbed tops and thicknesses for the 110-ft, 140-ft, Interbed below the massive basalt (BM interbed), and 380-ft interbed constituted the remaining eight continuous variables. Alluvium thickness was available for all but one well. However, not all of the primary sedimentary structures were observed in each well, nor did all wells penetrate each interbed. In wells deep enough to penetrate a given unit, the thickness was assigned a zero if the interbed was not present. Those wells were not used to define the interbed top elevation. After the top and thickness of each unit were defined at all well locations, the data for each unit individually were subjected to a geostatistical analysis to determine spatial correlation structure. The analysis included anisotropic variography, trend surface analysis, and cluster analysis. Results of these analyses for the nine variables are contained in Appendix C and are summarized in Table A-5-1.

Table A-5-1 Geostatistical parameters for the nine continuous variables describing lithology.

Variable	Model	Nugget ($unit^2$)	Partial Sill ($unit^2$)	Horizontal Range (m)	Vertical Range (m)
Alluvium Thickness (m)	Spherical	0	10	600	Not Applicable
110-ft Interbed Thickness (m)	Spherical	1	5.5	350	Not Applicable
140-ft Interbed Thickness (m)	Gaussian	0	7	200	Not Applicable
Below Massive Basalt (BM) Interbed Thickness (m)	Spherical	0	11	250	Not Applicable
380-ft Interbed Thickness (m)	Spherical	0	3.7	550	Not Applicable
110-ft Interbed Top Elevation (m amsl)	Spherical	1	5	550	Not Applicable

Variable	Model	Nugget ($unit^2$)	Partial Sill ($unit^2$)	Horizontal Range (m)	Vertical Range (m)
140-ft Interbed Top Elevation (m amsl)	Spherical	0	10	400	Not Applicable
Below Massive Basalt (BM) Interbed Top Elevation (m msl)	Spherical	0	40	400	Not Applicable
380-ft Interbed Top Elevation (m msl)	Spherical	0	25	600	Not Applicable

4). Data used in Step 3 were removed from the full set, leaving the lithology and textural information for basalt and discontinuous sediments. Based on textural class, the basalt segments were either assigned either a high or low basalt permeability flag. Also, based on textural category, sediment units were assigned either a high or low sediment permeability flag. The geostatistical correlations for these four categorical variables were then determined using indicator variography for the four permeability categories. The following criteria were used for selecting the lithologic flag:

- High-permeability sediment was assigned to material primarily described as sand or gravel.
- Low-permeability sediment was assigned to any material primarily described as silt, clay, silt-stone, or sandstone.
- High-permeability basalt was assigned to material described as cinders, rubble, void, fractured, scoriaceous, porous, broken, ash, void, top, bottom, or vesicular.
- Low-permeability basalt was assigned to any material described as dense, massive, central, middle, hard, or solid.
- High-permeability sediment or basalt was conservatively assigned to any material if the well log only provided a general basalt or sediment description.
- If no material description was available for a depth interval, it was assumed to be the same as the previous depth interval.

5). The textural information for the each of the primary sedimentary units was also assigned either a high or low permeability class based on the previous criterion, resulting in an additional five categorical variables. These were also subjected to rigorous indicator variography. Results of the indicator variography are presented in Table A-5-2.

Table A-5-2 Geostatistical parameters for the nine categorical variables based on textural class.

Variable	Model	Nugget ($unit^2$)	Partial Sill ($unit^2$)	Horizontal Range (m)	Vertical Range (m)
Alluvium Permeability Category NE-SW (E-W)	Spherical	0 (0.01)	0.05 (0.03)	300	Not Applicable
110-ft Interbed Permeability Category	Spherical	0	0.2	100	Not Applicable
140-ft Interbed Permeability Category	Spherical	0	0.2	100	Not Applicable
Below Massive Basalt (BM) Interbed Permeability Category	Spherical	0	0.25	400	Not Applicable
380-ft Interbed Permeability Category	Spherical	0	0.2	300	Not Applicable

Variable	Model	Nugget (unit^2)	Partial Sill (unit^2)	Horizontal Range (m)	Vertical Range (m)
High-Permeability Interbed Sediment not Included in the Four Main Interbeds	Exponential	0.008	0.01	100	30
Low-Permeability Interbed Sediment not Included in the Four Main Interbeds	Exponential	0	0.028	100	30
High-Permeability Basalt	Exponential	0	0.09	80	30
Low-Permeability Basalt	Exponential	0	0.055	80	30

6). Ordinary kriging was used to interpolate the nine continuous variables describing the alluvium and primary sediment interbed tops and thicknesses. Indicator kriging was used to interpolate the nine categorical variables used to determine the permeability within the basalts, primary sedimentary interbeds and secondary sedimentary segments.

The geostatistical approaches used and results of each analysis were based on the rigorous analysis presented in Appendix C. That appendix also presents a discussion of data clustering, trend analysis, and predictive uncertainty. It is worthwhile to mention that the resultant horizontal correlation lengths range from 80 to 600 m which are on the order of the grid block lengths. As a result, the statistical distributions are not exactly reproduced in the model. The resultant distribution of alluvium and subsurface interbed structure is presented in Figure A-5-1 as viewed from the south. The fractured basalt is represented between the colored areas.

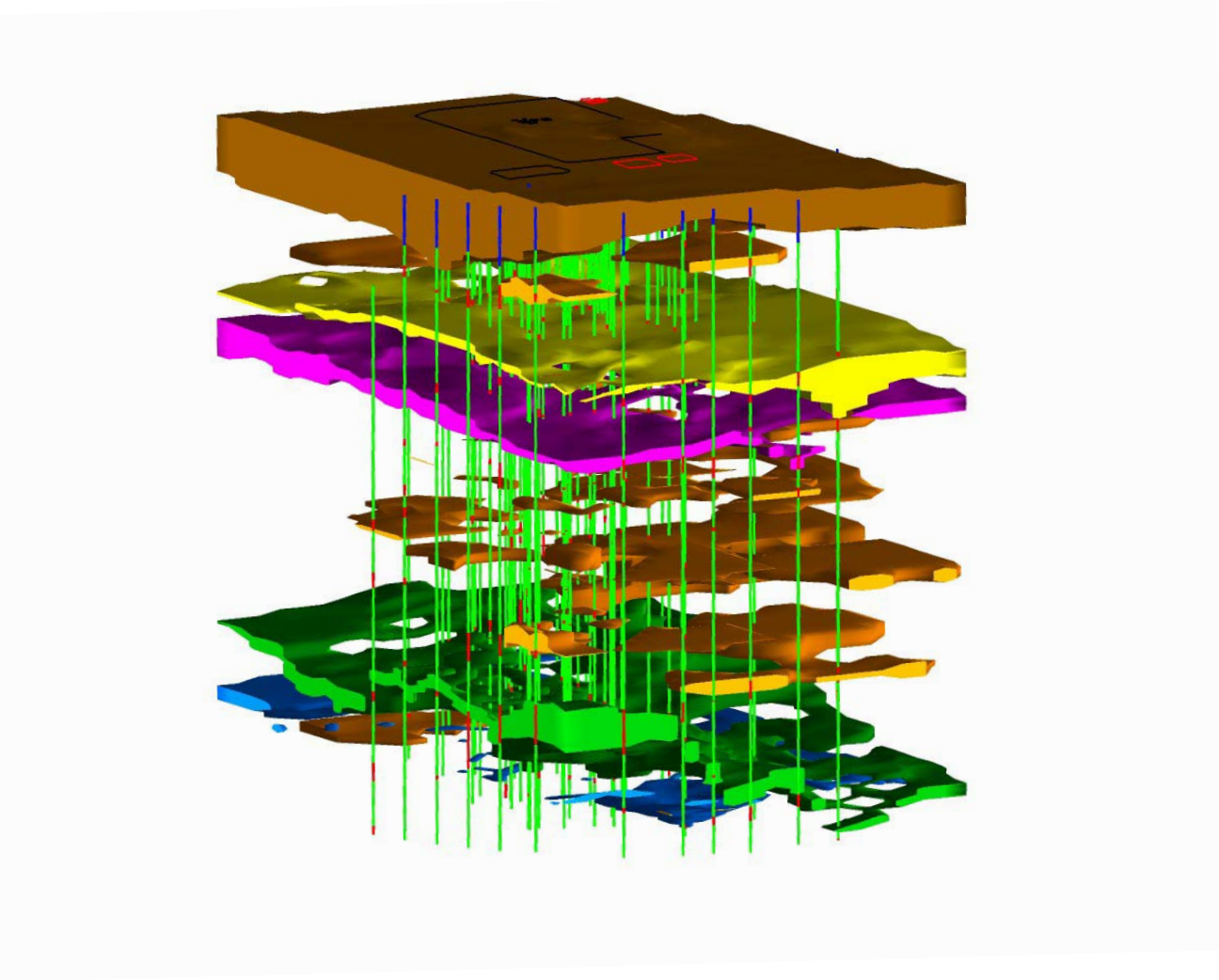

Figure A-5-1. Vadose zone structure. (Surficial alluvium is brown, 110-ft interbed yellow, 140-ft interbed pink, Below Massive Basalt (BM) interbed green, 380-ft interbed blue, and other interbed soils orange. The wells are represented with blue surficial alluvium, green basalt, and red interbed. The INTEC fence, former percolation ponds, and ICDF are outlined on the surface.)

A-5.1.2 Vadose Zone Simulation Domain and Discretization

The vadose modeling used two separate models to predict contaminant fate and transport from land surface to the Snake River Plain Aquifer. The first small-scale model was constructed to represent detailed releases from the tank farm alluvium. It is referred to throughout this document as the "submodel". The second model is larger in scale and includes the entire INTEC facility from land surface to the Snake River Plain Aquifer. It is referred to as the "large scale, or base-grid model" in the remainder of this document. The contaminant flux leaving the tank farm submodel was placed into the large-scale model immediately below the alluvium/fractured basalt interface. Although the TETRAD simulator has local grid refinement capabilities, it was not used in the vadose zone model to create the tank farm area. A submodel approach was used to improve computational efficiency of the vadose zone models. A linked domain is only necessary if there is feedback between the domains. Drainage out of the alluvium into the fractured basalt below is essentially one-way because the matric potential in the fractured basalt is much less than that in the alluvium.

Selection of the submodel grid was guided by the need to encompass all the OU 3-14 soil sites and maintain grid blocks small enough to accurately simulate the water velocity resulting from the historical liquid releases. This area extended from approximately 100 m northwest of Site CPP-31 to 150 m southeast of Site CPP-31 and used a 20 by 20 grid with 10 m x 10 m grid block sizes. The upper boundary was land surface and the lower boundary was the surface of the 110-ft interbed. The lower boundary was chosen to provide a saturated (perched water) boundary condition, although the contaminant flux from the tank farm submodel was taken at the alluvium/fractured basalt interface. Figure A-5-2 illustrates the submodel's horizontal discretization.

Selection of the large-scale vadose zone model grid was guided by the need to include spatially variable lithology and water recharge sources that may impact contaminant migration from the tank farm near surface to the aquifer. This area includes the Big Lost River to the north and the former location of the percolation ponds to the south. The vadose zone model domain extends in the north-south direction from approximately 300 m north of the northern INTEC fence line to 800 m south of the location of the former percolation ponds. The east-west model domain extends from approximately 200 m west of Lincoln Boulevard to 400 m east of the INTEC steam generating plant. The model's horizontal grid used a 20 by 30 grid with 100 m x 100 m grid block sizes. The model grid was chosen to be large enough to capture major historical and current INTEC recharge sources (i.e., the Big Lost River and former percolation ponds) while being computationally tractable. Large aspect ratios will result in relatively large numerical dispersion which will reduce the required "physical" dispersivity to capture contaminant and water arrival histories.

The vadose zone model's vertical domain extended from land surface to the Snake River Plain Aquifer and used a 1-m vertical discretization in the alluvium and 2-m vertical discretization in the basalt and interbeds. The alluvium discretization was chosen to better define contaminant source depth. Figure A-5-3 illustrates the vadose zone model's horizontal discretization, and Figure A-5-4 illustrates the vadose zone's model vertical discretization. Figure A-5-4 also illustrates the location of the simulated sediment (alluvium and interbed) within the basalt. The white grid blocks are simulated sediment and the red grid blocks are fractured basalt.

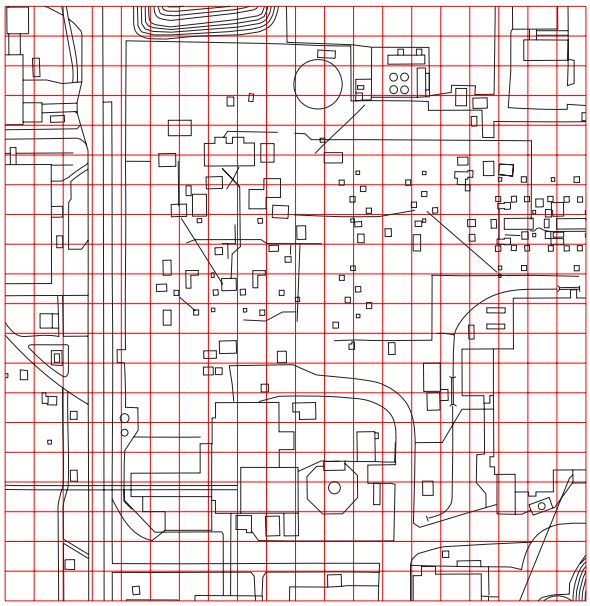

Figure A-5-2. Tank farm submodel vadose horizontal discretization.

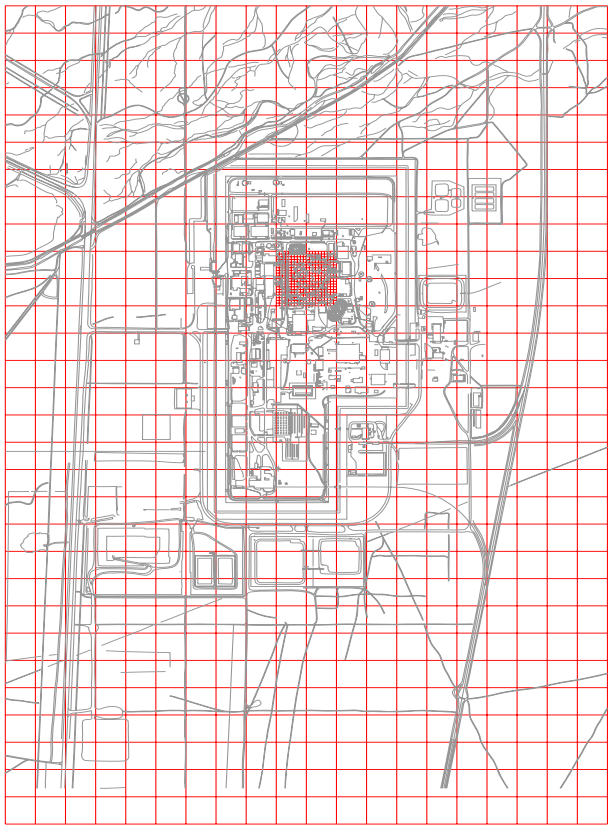

Figure A-5-3. Large-scale vadose zone model horizontal discretization.

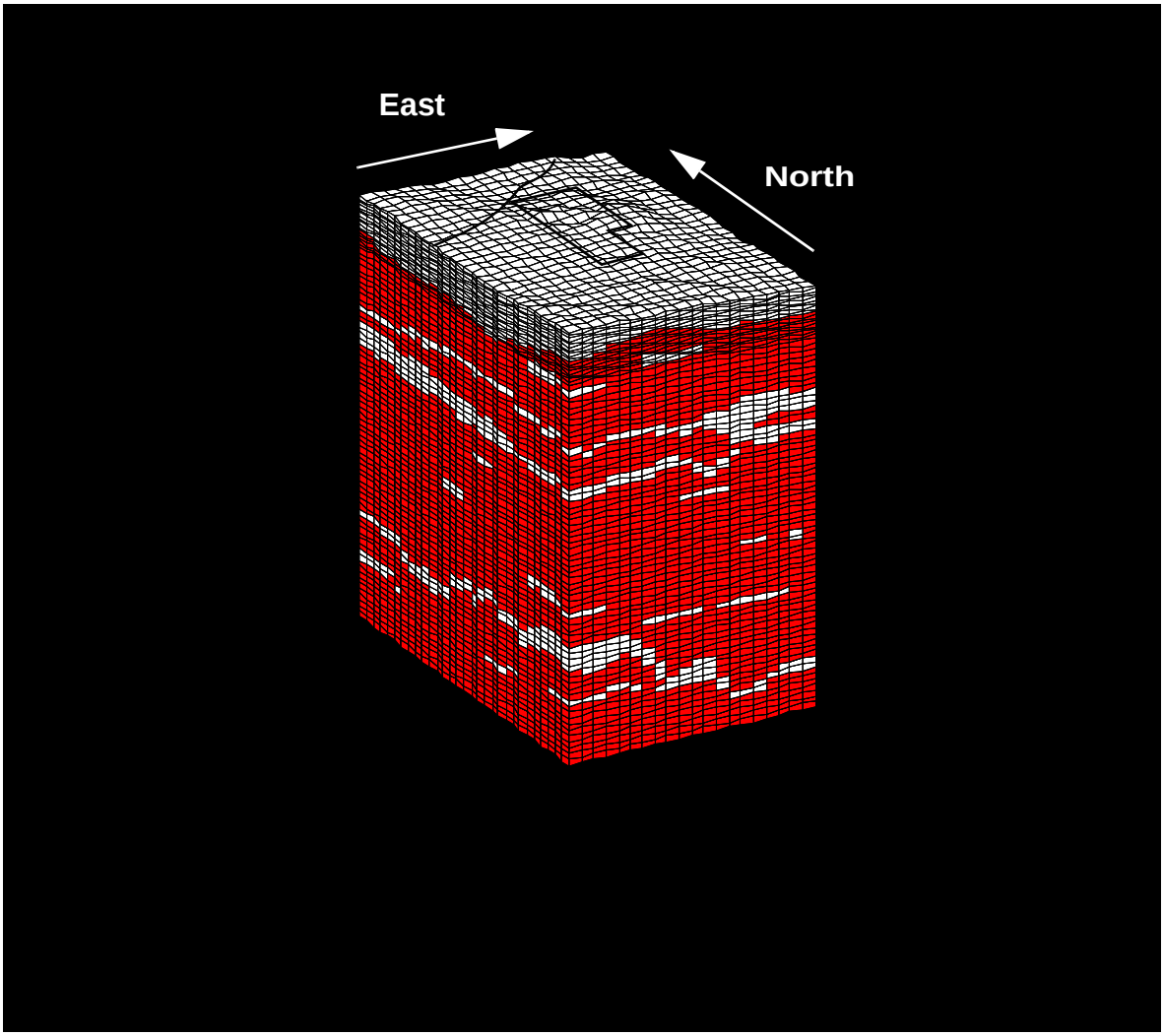

Figure A-5-4. Vadose zone model vertical discretization with 35x vertical exaggeration.

A-5.1.3 Incorporating Infiltration

Infiltration discussed in this section includes recharge from natural and anthropogenic sources. These water sources were presented in Section A-3. For the purposes of simulation, infiltration rate was assumed to be spatially and temporally varying across the INTEC to account for water system leaks, landscape irrigation, sewage effluent, Big Lost River fluxes, etc. In addition, the magnitude of the infiltration rates were time-dependent to account for the reduction in infiltration due to OU 3-13 remedial actions. The pre- and post-remedial action rates identified in Section A-3.6, with some adjustment due to reevaluation of OU 3-13 water sources (Big Lost River and precipitation infiltration), were applied as specified flux to the model surface grid blocks. The pre-remedial action rates represent conditions prior to the percolation pond relocation and implementation of facility-related water recharge controls. The post-remedial action rates represent current conditions. The pre-remedial action infiltration rates were switched to the post-remedial action rates on August 26, 2002. This was the date the percolation ponds were relocated to the vadose zone research park.

The reevaluation of the OU 3-13 water sources included increasing the amount of water from precipitation in the pre-remedial action water balance from 10 cm/year to 18 cm/year to be consistent with the tank farm infiltration study and using a transient Big Lost River infiltration rate from recent USGS streamflow recordings at the INL Site diversion dam and the Lincoln Boulevard bridge (see Section A-3.6). The daily

USGS streamflows (and estimated losses to infiltration) were averaged over 1-year periods when implemented into the model as summarized in Table A-5-3. Figure A-5-5 and Table A-5-4 illustrate the areal distribution and amount of water in the pre-remedial action time periods. Figure A-5-6 and Table A-5-5 illustrate the areal distribution and amount of water in the post-remedial action time period. The area subject to water line leaks was assumed to include the entire developed area at the INTEC, including the steam generation plant located east of the east security fence.

Table A-5-3 Simulated annual average Big Lost River infiltration rate.

Year	Infiltration per Meter of River Length (m^3/day)
1954-1984	1.9
1985	1.7
1986	3.2
1987	0.8
1988-1992	0.
1993	0.5
1994	0.
1995	1.3
1996	0.9
1997	2.9
1998	2.8
1999	4.2
2000	1.1
2001-2004	0.

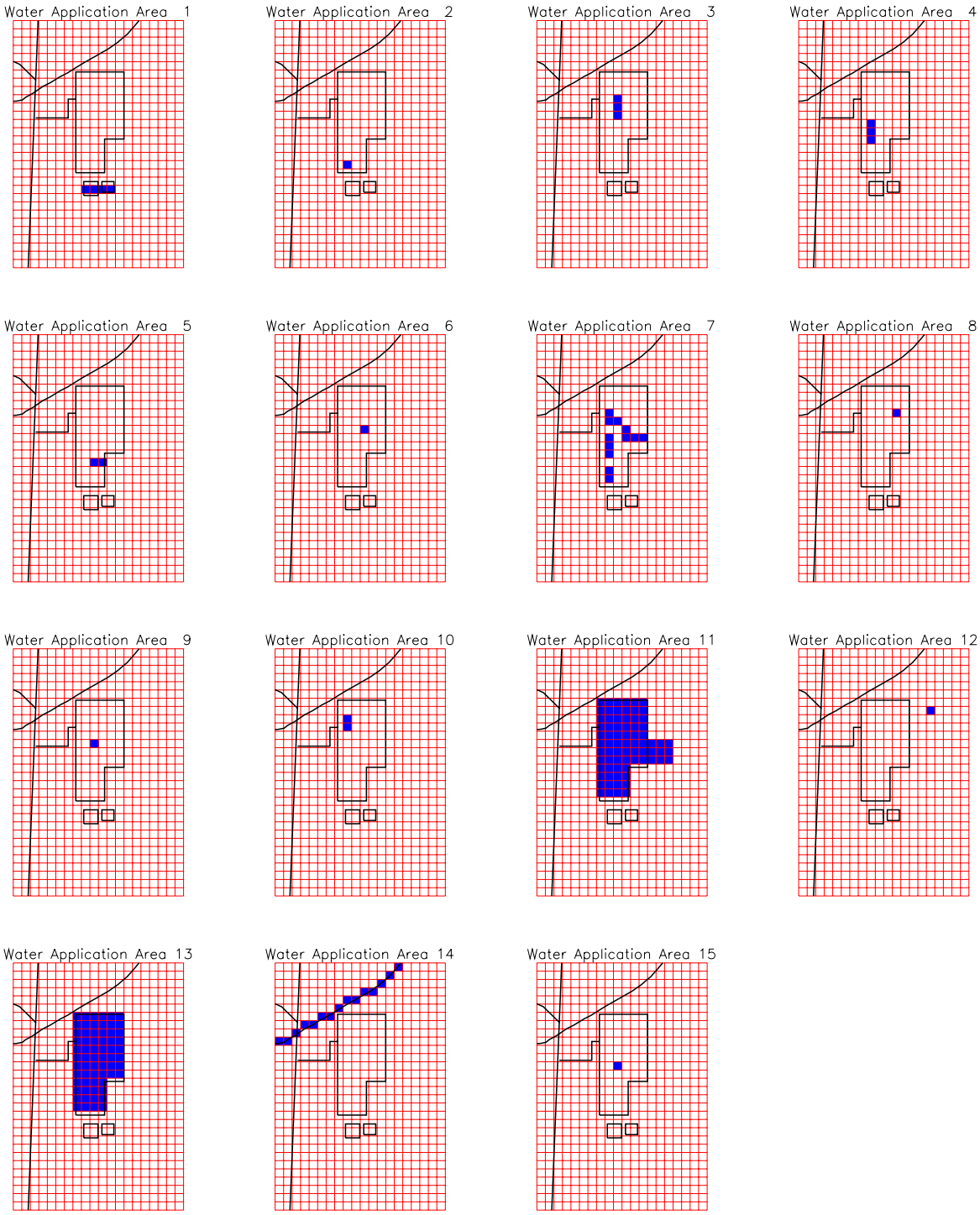

Figure A-5-5. Areal distribution of the pre-remedial action rates.

Table A-5-4 Water application rates for the pre-remedial action corresponding to areas illustrated in Figure A-5-5.

Area Number in Figure A-5-5.	Source Area	Application Rate (kg/day)
1	Percolation ponds	5,838,000
2	Building 603 basins	511
3	Steam vent area	1,821
4	Steam vent area	2,888
5	Steam vent area	1,528
6	Steam vent area	1,002
7	Individual steam vents	10,672. (kg total)
8	Lawn irrigation area	2,245
9	Lawn irrigation area	2,250
10	Lawn irrigation area	8,981
11	Fire water line leaks	41,230
12	Sewage treatment infiltration trench	155,565
13	Developed area precipitation infiltration	315,400
14	Big Lost River	Variable (see Table A-5-3)
15	CPP-3 injection well during failure	Variable (1.321e+10 kg total)

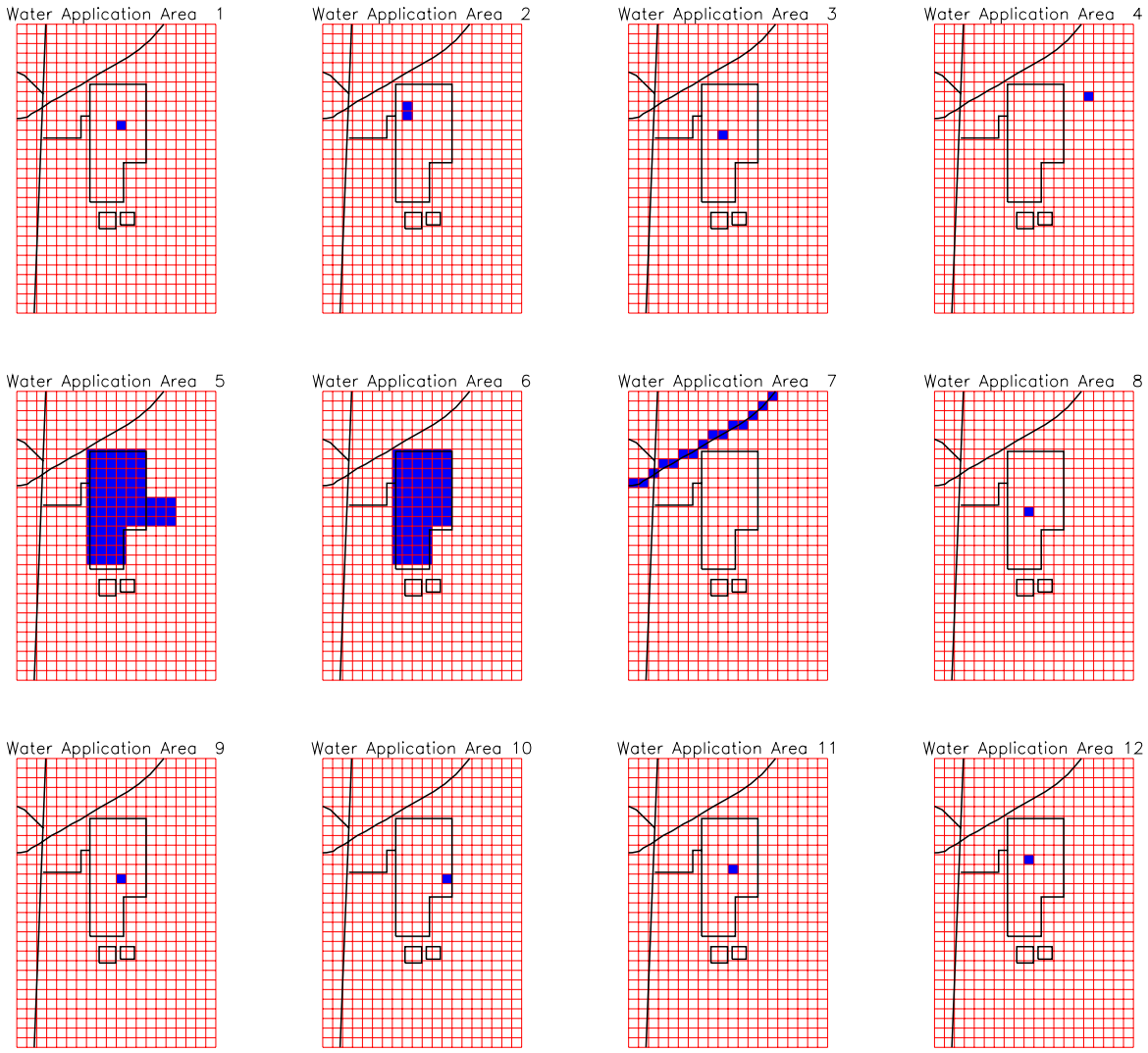

Figure A-5-6. Areal distribution of the post-remedial action water balance.

Table A-5-5 Water application rates for the post-remedial action period corresponding to areas illustrated in Figure A-5-6.

Area Number in Figure A-5-6.	Source Area	Application Rate (kg/day)
1	Steam vent area	303
2	Lawn irrigation	10,646
3	Lawn irrigation	2,661
4	Sewage Treatment Lagoon*	138,181
5	Fire water line leaks with fire hydrant testing	81,901
6	Developed area precipitation infiltration	315,400
7	Big Lost River	Variable (see Table A-5-3)
8	CPP-655 sanitary sewer	890
9	CPP-656 sanitary sewer	4,050
10	CPP-1606 and CPP-697 heating system	1,776
11	CPP-1608 heating system	888
12	CPP-649 steam drip	300
*The sewage treatment effluent was transferred to the vadose zone research park in 2004. However, the model was constructed prior to the transfer and the sewage treatment effluent is included in the simulations.		

A-5.1.4 Contaminant Source Terms for Model Calibration

Parameterizing source terms involved assigning inventories, locations, and times to the known releases. The volume of water and contaminant concentration from each source was quantified and input into the model as a flux rate. The model contaminant source terms were constructed from the data presented in the OU 3-14 RI/BRA, Section A-5, and the OU 3-13 RI/BRA (DOE-ID 1997). The source used in model calibration were the same as those used in the baseline risk assessment and are presented in Section A-8.2.

A-5.1.4.1 Contaminant Source Parameterization

Each of the tank farm and non-tank farm sources are represented in the model as liquid releases placed in specific grid blocks. A complete description of the model source terms is provided in Section A-8.2. The model assumes equilibrium partitioning of sorbing contaminants onto the soil or rock (except Sr-90, see Appendix J). The highly sorbing contaminants will partition into the solid phase after one time step and will behave as a leaching source until sufficient water passes through the source grid block to wash the contaminants deeper into the vadose zone. The source location within the 3-D model domain was the grid block center nearest to the location of the actual leak/spill provided in the OU 3-14 Work Plan (DOE-ID 2004a). Table A-5-6 summarizes each OU 3-14 source location source within the tank farm submodel using a numbering scheme that assigns a unique number to each horizontal model grid block location. Table A-5-7 summarizes each OU 3-13 source location within the large-scale vadose zone model using a a similar numbering scheme. The model's horizontal discretization and surface grid block number scheme for source identification is illustrated in Figures A-5-7 and A-5-8 for the tank farm submodel and large-scale vadose zone model, respectively. Grid blocks in the tank farm submodel are 10 x 10 x 1 m. Grid blocks in the upper 18 model layers of the large-scale vadose zone model are 100 x 100 x 1 m, grid blocks in the lower layers are 2 m in the vertical direction.

A-5.1.5 Vadose Zone Initial Conditions

The simulation initial conditions were achieved using the natural recharge sources of 1 cm/year infiltration from precipitation and the long term average Big Lost River infiltration rate (1.9 m/year per meter). The model was run for 1,000 years prior to the transport simulation start time. The 1,000 year initial condition time period was determined by monitoring the maximum grid block pressure change between simulation time steps and extending the initial condition time period until the pressure change is approximately zero.

Table A-5-6 OU 3-14 contaminant source locations and liquid release rate used in tank farm submodel.

Source Identification	Horizontal Grid Block Number	Vertical Layer
CPP-31	250,251,231,232	4
CPP-28	191	3
CPP-79 deep 1967	171	13
CPP-79 deep 1973	171	13
CPP-79 shallow	171	4
CPP-27/33 1964 scrub solution	111,112,131	4
CPP-27/33 1966-1967 scrub solution	111,112,131	4
CPP-27/33 1964-1974 decon solution	111,112,131	4
CPP-15	50	2
CPP-16	228	2
CPP-20	129	2
CPP-24	206,207	2
CPP-25	128	2
CPP-26	258,259,260, 278,279,280, 298,299,300	2
CPP-30	277	2
CPP-32E	257	2
CPP-32W	276	2
CPP-58E 1975 (now CPP-87/89) CPP-58E 1976 (now CPP-87/89) CPP-58W	24,25,26,27,28,29 44,45,46,47,48,49	2

Table A-5-7 Contaminant source locations and liquid release rate used in the large-scale model (OU 3-13 sources).

Source Identification	Horizontal Grid Block Number	Vertical Layer
CPP-89	390	3
CPP-35	371	3
CPP-36/91	391	3
CPP-01/04/05	250	3
CPP-08/09	249	3
CPP-10	250	3
CPP-11	250	3
CPP-03	250,251	3
CPP-17A	271	3
CPP-37A	433	3
CPP-37B	433	3
CPP-14	411	3
CPP-34	474	3
CPP-13	392	3
CPP-06	229	3
CPP-19	289	3
CPP-22	228,229,208	3
CPP-90	370	3
Other Sources		
Service waste injection well (CPP-23)	350 in vadose zone during well collapse	51-61 in vadose zone during well collapse
Early service waste ponds	189,190,191, 192	9
CPP-80	389	3

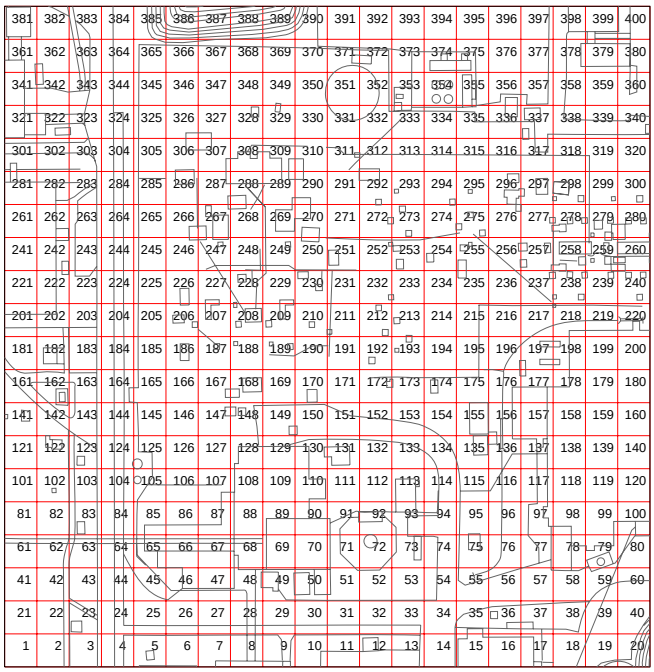

Figure A-5-7. Tank farm submodel horizontal discretization with OU 3-14 source location numbering scheme.

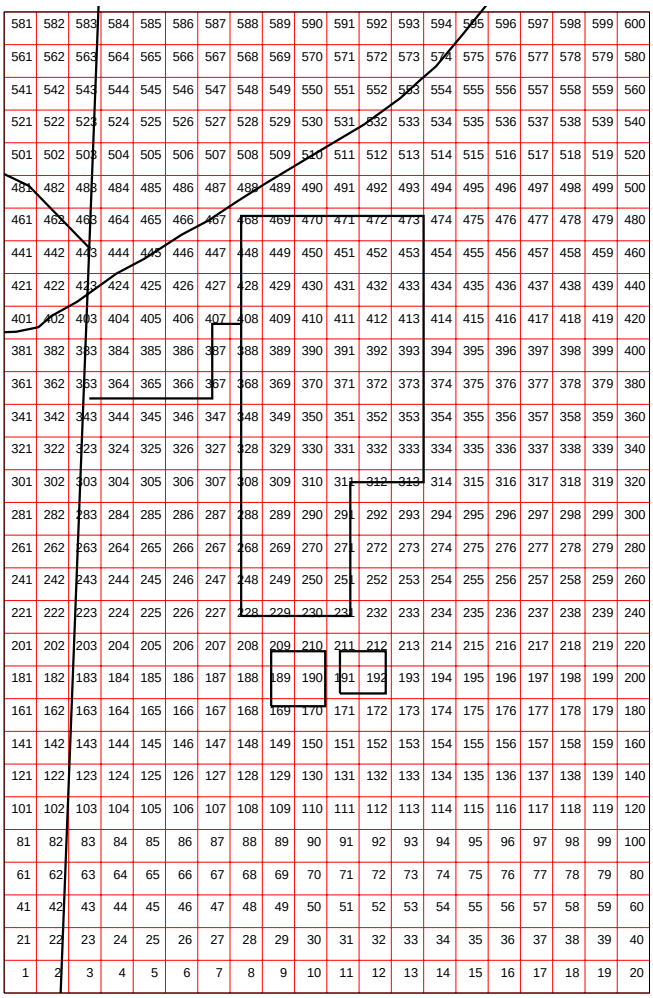

Figure A-5-8. Large-scale vadose zone model horizontal discretization with OU 3-14 source location numbering scheme.

A-5.2 Aquifer Model and Parameterization

The aquifer is parameterized as a three-dimensional flow field with vertical infiltration from the top, a no-flow boundary at the bottom, and lateral Dirichlet boundaries (prescribed head) allowing inflow from the sides. In this model, the following assumptions were made:

- Flow in the fractured basalt is controlled by the fracture network and can be represented by a high-permeability, low-porosity equivalent porous medium.
- The aquifer model domain is assumed to be fully saturated, and the response to pumping and recharge is assumed to behave as if confined. However, a transient water and contaminant flux is placed as an upper boundary condition.

- The top boundary is a vertical flux provided by the vadose zone model near INTEC, the lateral boundary conditions are Dirichlet (prescribed head) allowing inflow from the sides, and the bottom boundary is no flow.
- Isothermal temperature adequately denotes the thickness of the actively flowing portion of the aquifer.
- Water levels measured in the summer of 2004 are representative of the long-term natural gradient.

Details of incorporating the physical data into the aquifer model's numerical framework (model parameterization) are discussed below. Parameterization in order of presentation include hydrogeology/ lithology (Section A-5.2.1), spatial extent and discretization (Section A-5.2.2), and boundary conditions and water sources (Section A-5.2.3).

A-5.2.1 Representation of Lithology and Hydrology

The lithology of the aquifer is more uniform than that of the vadose zone. Basalt units tend to be thicker and the sedimentary interbeds are fewer in number. The region extending from north of INTEC to the south of RWMC is primarily comprised of the E through H basalt flows, the HI interbed, and the I basalt flow (Section A-4, and Anderson 1991). In general, the I basalt flow is significantly thicker (Anderson 1991) and may be less permeable than the E through H basalt flows. In the I basalt flow, the high-permeability interflow rubble zones represent a smaller fraction of the total flow thickness. The HI sedimentary interbed separates the overlying higher-permeability basalts from the underlying lower permeability I basalt and may act as a weak confining layer. This separation is captured in the aquifer model through the use of three distinct lithologic types. These include the H basalt, the HI interbed, and the I basalt.

In the model, the H basalt extends downward from the water table and is bounded below by the HI interbed. The I basalt extends from the bottom of the HI interbed to the lower model boundary. The water table elevation was determined by a planar fit to water level data as described above. The top elevation and thickness of the HI interbed was determined in a manner analogous to that used for the primary sedimentary structures in the vadose zone model (i.e., variography and kriging). Elevation of the lower model boundary was based on the thickness of the actively flowing portion of the aquifer (Section A-4.1). These features are illustrated in Figures A-5-11 and Figure A-5-9.

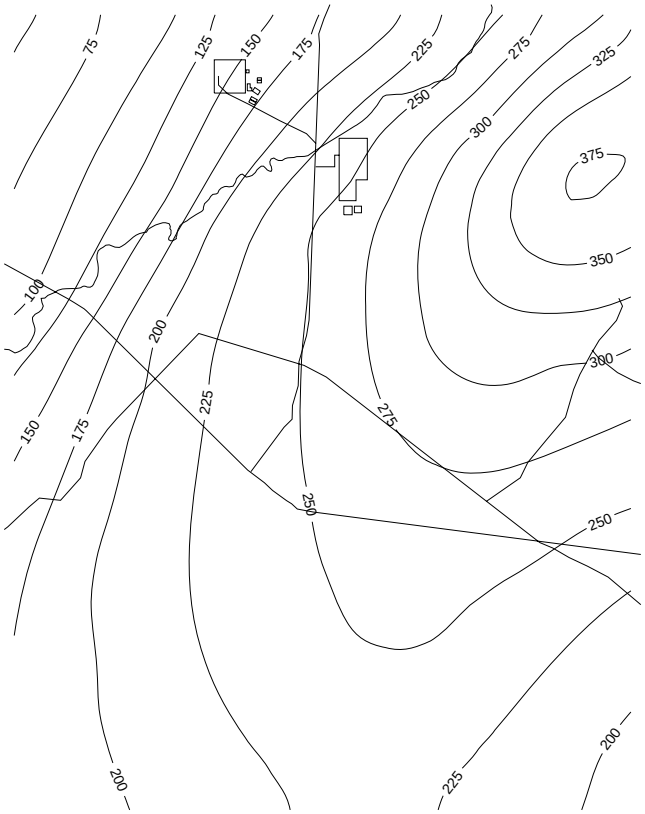

Figure A-5-9. Aquifer model thickness (m).

Nested variograms were used to describe the HI interbed thickness and top elevation (Table A-5-9). Both parameters exhibited smooth variation at short correlation and larger variance at longer lag distances. Kriging the HI interbed resulted in a thick region through the east-central areas of the model grid, with the thick regions extending further south than north. Most of the HI interbed in the west was very thin, and, in the north-central regions, the HI interbed had zero thickness. The krigged top elevation was low in the east, had a ridge running from the center of the southern border to the northeast corner, and was mostly level with a bump in the center North boundary. The low elevation areas in the south correspond to the thick interbed areas. The interpolated thickness and elevation both conformed quite well to observed values where data were available. However, in the northwest and southeast corners, large areas were without data. Uncertainty in the krigged results is high in those areas as reflected by high kriging variance (Appendix C).

Variography was used to determine the geostatistical parameters describing aquifer pump test-derived permeability within the H and upper I basalt units. The variogram for aquifer permeability was modeled with a one-structure variogram, although two structures may have been present. Both variograms were used to predict natural log of permeability onto the grid with almost identical results. Parameters for the simpler one-structure model were used for this work, and the parameters are given in Table A-5-8. Natural log permeability was then interpolated onto the model grid using ordinary kriging. Actual permeability was obtained through back-transformation. A complete description of the variogram structures and ranges used in predicting the aquifer's H basalt permeability field can be found in Appendix C.

Initial permeability values for the current model's HI interbed were estimated from perched water slug tests and core analysis of the HI interbed. Initial permeability values for the current model's I basalt were taken from the OU 3-13 RI/BRA. Figure A-5-10 illustrates the initial H basalt hydraulic conductivity.

Table A-5-8 Geostatistical parameters for the HI interbed thickness and elevation.

Variable	Model	Nugget ($Unit^2$)	Partial Sill ($Unit^2$)	Horizontal Range (m)	Vertical Range (m)
HI interbed thickness (range less than 2,300 m)	Gaussian	0.	10	2,300	Not Applicable
HI interbed thickness (range greater than 2,300 m)	Spherical	0.	55 (45 plus the sill of 10 from the first structure)	4,500	Not Applicable
HI interbed elevation (range less than 2,300 m)	Gaussian	0.	340	2,000	Not Applicable
HI interbed elevation (range less than 2,000 m)	Spherical	0.	800 (460 plus the sill of 340 from the first structure)	3,500	Not Applicable
HI interbed elevation (range greater than 2,000 m)	Spherical	0.	1700 (900 plus the sill of 800 from the second structure)	6,000	Not Applicable
H and I basalt permeability (natural log K)	Spherical	2	9	4,000	Not Applicable

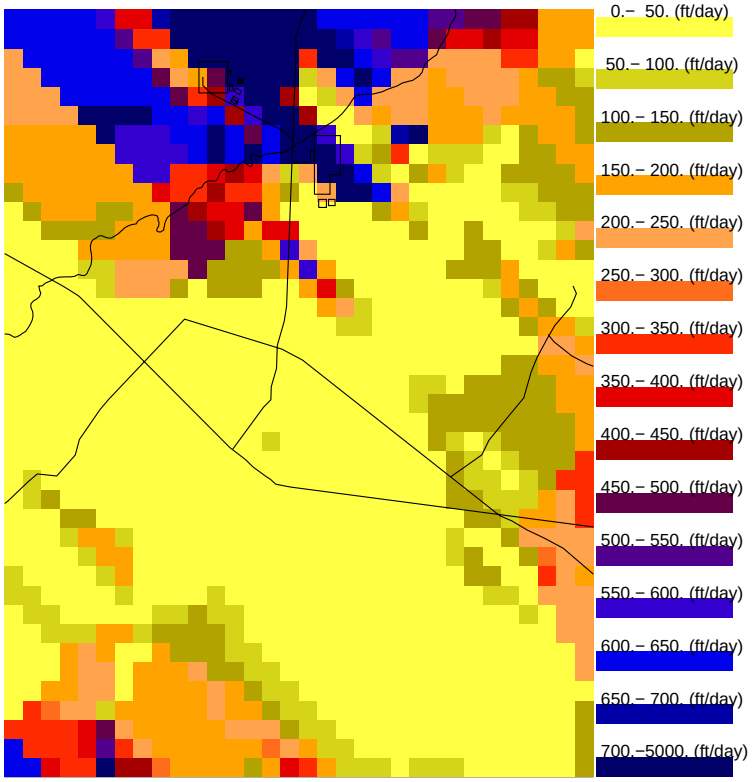

Figure A-5-10. Initial H basalt hydraulic conductivity field.

A-5.2.2 Aquifer Simulation Domain and Discretization

Selection of the aquifer model grid was guided by the need to predict aquifer water quality resulting from historical injection of INTEC contaminants, influx of water and contaminants from the vadose zone, and the three-dimensional aquifer thickness. The aquifer model domain extends from approximately 2.5 km north of the INTEC to the southern INL boundary in the north to south direction, and approximately 5.5 km east of the INTEC to slightly east of the RWMC in the east to west direction. The model was discretized using 400 x 400 m grid blocks in the horizontal, as illustrated in Figure A-5-1. Local horizontal refinement corresponding to the discretization level applied in the vadose zone model is within the footprint of the INTEC (100 x 100 m grid block size) with a 200 x 200 m transition grid surrounding the vadose zone foot print. This local refinement was only performed in the top five layers of the aquifer model. Variable vertical discretization following the HI interbed was applied.

The model's top surface corresponded to a planar fit through the observed water table elevation, and the model's bottom surface was created from the thickness estimates discussed in Section A-4.1. Correspondingly, the total aquifer model thickness varied between 32 m and 379 m. The vertical discretization included five uniform 2 m layers directly beneath the water table, which were increased in thickness to the midpoint between the water table and the HI interbed surface. At this point the vertical discretization gradually decreased until 2 m thickness was reached within the HI interbed. The thickness gradually increased again until the aquifer bottom was reached. The decreasing layer thickness near the water table and around the HI interbed places more computation nodes where they are needed (i.e., high-gradient areas). In total, 27 model layers were

used and the minimum grid block thickness was 2 m. The aquifer model vertical discretization is illustrated in Figure A-5-12. The simulated HI interbed is depicted in red and basalt is depicted in white.

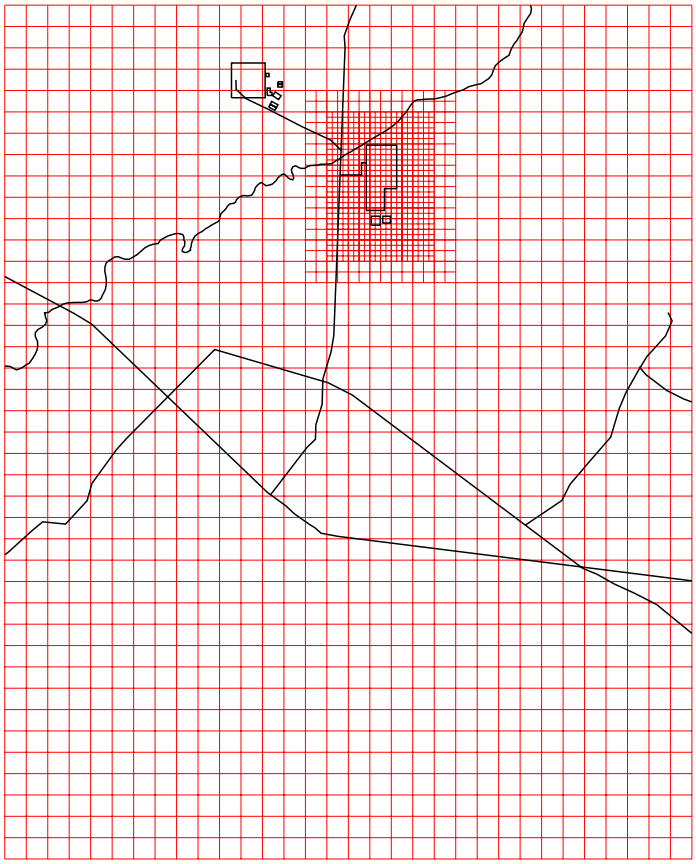

Figure A-5-11. Aquifer model domain and horizontal discretization.

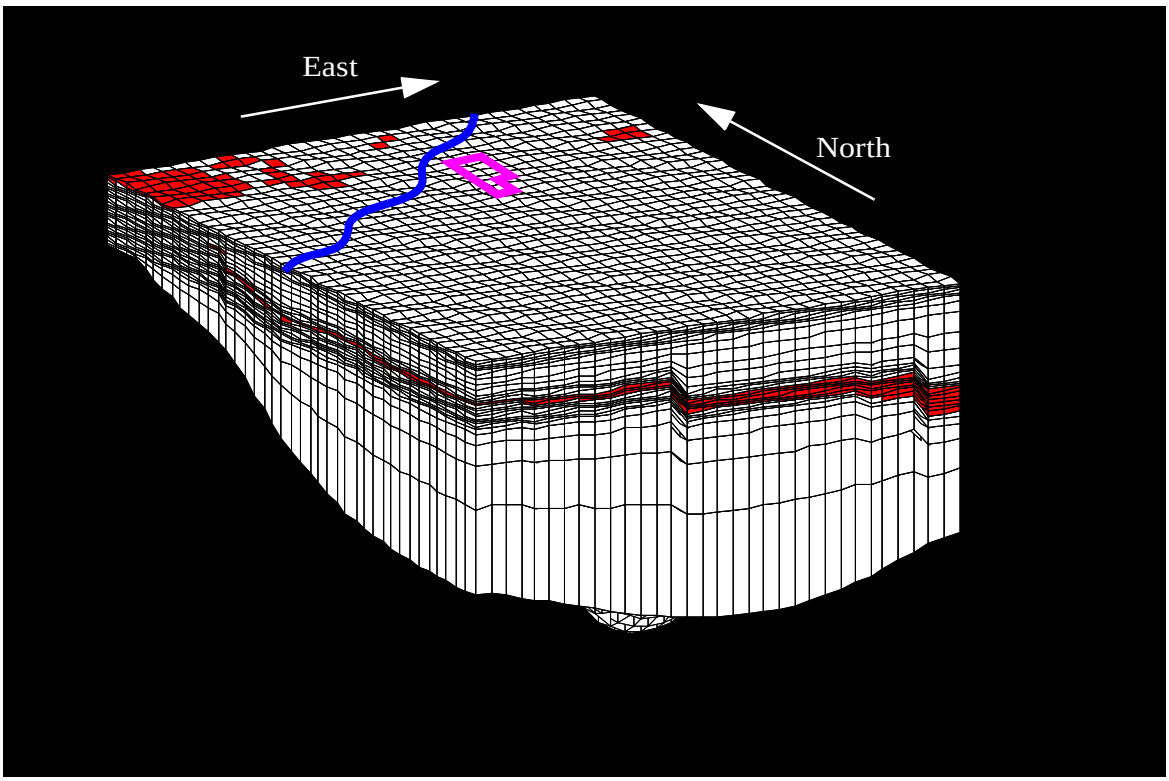

Figure A-5-12. Aquifer model vertical discretization with 30x vertical exaggeration.

A-5.2.3 Aquifer Boundary Conditions and Water Sources

The Snake River Plain Aquifer underlies INTEC and is located approximately 460 ft bgs. Water generally flows through the Snake River Plain Aquifer under unconfined conditions, but may be confined in local areas. It is mainly recharged from underflow originating from regional basins adjacent to the INL Site and from regional groundwater flow. Additional recharge can be attributed to intermittent streams that terminate on the INL Site and to precipitation. In this model, the following assumptions were made:

- The underflow contributions are not transient and the aquifer behaves as though confined.
- Variation in discharge and pumping rates in the service and potable water wells will be neglected. With the exception of CPP-03, the pumping rates will be simulated as steady state. The variability in injection rate for CPP-03 will be accounted for.
- Water levels from summer 2004 are representative of the natural gradient and will form the basis of model calibration to observed heads.
- Underflow contributions are accounted for by using steady-state Dirichlet boundary conditions. This allows matching water levels (2004 heads) throughout the simulation domain but does not constrain the magnitude of the flux entering through those boundaries. The flux will be constrained through the transport velocity. Transport velocity will be constrained by adjusting the permeability and porosity distribution to obtain matches to key contaminant arrival histories downgradient of their sources.

Under these assumptions, flow through the vadose zone and flow within the aquifer can be simulated separately. Transient water and contaminant flux leaving through the lower vadose zone model boundary are first computed using the vadose zone model. These fluxes then are used as recharge sources applied to the

upper boundary condition of the aquifer model. Precipitation, and recharge from the former percolation ponds and Big Lost River occurring within the vadose zone footprint are not directly simulated in the aquifer model but are accounted for in the flux from the vadose zone model used as the upper aquifer model boundary condition.

Water sources and sinks directly accounted for in the aquifer model include (1) infiltration from the vadose zone, (2) recharge from the Big Lost River reaches extending outside of the vadose zone footprint, (3) infiltration from precipitation, (4) reinjection of CPP-3 disposal well water, (5) pumping from CPP-1 and CPP-2 service water production wells, (6) pumping from the CPP-4 and CPP-5 potable water sources, (7) pumping from the RTC production well, (8) injection into the RTC disposal well and ponds, and (9) production in the CFA-1 and CFA-2 water supply wells. Infiltration from the vadose zone water and infiltration from the Big Lost River were applied to the upper layer of aquifer grid blocks as specified flux. The CPP-3, CPP-5, CPP-4, CPP-2, CPP-1, RTC production, and RTC disposal wells were simulated as injection/ production wells in the TETRAD software with well screen intervals defined in the corresponding model grid blocks. The amount of water injected in the RTC disposal well included the injection well water and RTC disposal pond water. This was done to simplify model parameterization, while including the TRA water sources. As discussed in Sections A-5.3.1, Big Lost River fluxes were transient values (See Section A-5.3.1 and Table A-5-1). The aquifer model water sources are summarized in Table A-5-9.

A-5.2.4 Aquifer Initial Conditions

The simulation initial conditions were achieved using the natural recharge sources of 1 cm/year infiltration from precipitation, the long term average Big Lost River infiltration rate (1.9 m/year per meter), and the steady-state Dirichlet lateral boundary conditions. The model was run for 1,000 years prior to the transport simulation start time. As with the vadose zone model, the 1,000 year initital condition time period was determined by monitoring the maximum grid block pressure change between simulation time steps and extending the initial condition time period until the pressure change is approximately zero. The aquifer model achieved steady-state conditions long before 1,000 years, but running a longer initialization period did not increase the computational burden because time steps are allowed to increase after a near steady-state is achieved.

Table A-5-9 Aquifer model water sources and amounts.

Water Source	Application Amount	Notes
Recharge from vadose zone	Spatially and temporally variable (0.01 m/year to approximately 70 m/year)	Transient drainage from the vadose zone model is the aquifer model upper boundary condition.
Big Lost River infiltration	Temporally variable (0. to 3.2 m^3/day per m of river length)	Infiltration is only applied outside the vadose zone footprint.
CPP-3 injection	Temporally variable (0 to 7,000 m^3/day)	Injection rate was determined from service waste disposal records.
CPP-1 pumping	2,785 (m^3/day)	Service water production estimated from INTEC water balance (DOE-ID 2003b).
CPP-2 pumping	2,785 (m^3/day)	Service water production estimated from INTEC water balance (DOE-ID 2003b).
CPP-4 pumping	68 (m^3/day)	Potable water production estimated from INTEC water balance (DOE-ID 2003b).
CPP-5 pumping	68 (m^3/day)	Potable water production estimated from INTEC water balance (DOE-ID 2003b).

Water Source	Application Amount	Notes
TRA-4 pumping	5,968.95 (m^3/day)	Potable water production estimated from Five-Year Review Report for the Test Reactor Area (DOE-ID 2005a).
TRA-DISPOSAL cold waste pond injection	2,017 (m^3/day)	Potable water production estimated from Five-Year Review Report for the Test Reactor Area (DOE-ID 2005a).
CFA-1 pumping	358 (m^3/day)	Obtained from CFA operation records.
CFA-2 pumping	770 (m^3/day)	Obtained from CFA operation records.

A-5.3 Simulation Code

The TETRAD multipurpose simulator (Vinsome and Shook 1993), Version 12.7, was chosen to simulate water and contaminant migration through the vadose zone and aquifer. This code was chosen because it is robust, multiphase, multicomponent, and three-dimensional and can simulate dual porosity systems. TETRAD was originally developed as an enhanced oil recovery simulator for the petroleum industry. It has been successfully applied to simulate groundwater flow and transport at the INL Site for Waste Area Groups 1, 3, and 7. TETRAD has undergone limited verification and validation (Shook 1995) to demonstrate proficiency of the TETRAD simulator for use in modeling environmental fate and transport processes.

To solve the governing equations for variably saturated flow, TETRAD requires parameterization of saturation versus capillary pressure and saturation versus permeability for each lithologic material. The van Genuchten (1980) equations were used to describe the constitutive relationships for the alluvium and interbed (sediment). TETRAD uses two-phase van Genuchten constitutive equations, as adapted by Parker et al. (1987) with slight modifications to the normalized saturation terms. The van Genuchten constitutive relations are

$$\bar{S}_w = \frac{S_w - S_{wr}}{1 - S_{wr}} \; ; \quad \bar{S}_a = \frac{S_a}{1 - S_{wr}}; \quad \bar{S}_o = \frac{S_o}{1 - S_{wr}} \tag{1}$$

$$\bar{S}_L = \bar{S}_o + \bar{S}_w \tag{2}$$

$$P_{c\,ow} = \frac{\sigma_{ow}\,\rho_{fw}\,g}{\sigma_{aw}\,\alpha}\,[(\bar{S}_w)^{-1/\gamma} - 1]^{1/\beta} \Leftrightarrow \bar{S}_w = \left[1 + \left(\frac{\alpha\,P_{c\,ow}\,\sigma_{aw}}{\rho_{fw}\,g\,\sigma_{ow}}\right)^{\beta}\right]^{-\gamma} \tag{3}$$

$$P_{c\,ao} = \frac{\sigma_{ao}\rho_{fw}\,g}{\sigma_{aw}\,\alpha}\,[(1 - \bar{S}_a)^{-1/\gamma} - 1]^{1/\beta} \Leftrightarrow \bar{S}_a = 1 - \left[1 + \left(\frac{\alpha\,P_{c\,ao}\,\sigma_{aw}}{\rho_{fw}\,g\,\sigma_{ao}}\right)^{\beta}\right]^{-\gamma} \tag{4}$$

$$P_{c\,aw} = \frac{\rho_{fw}\,g}{\alpha}\,[(1 - \bar{S}_a)^{-1/\gamma} - 1]^{1/\beta} \Leftrightarrow \bar{S}_a = 1 - \left[1 + \left(\frac{\alpha\,P_{c\,aw}}{\rho_{fw}\,g}\right)^{\beta}\right]^{-\gamma} \tag{5}$$

$$k_{rw} = (\bar{S}_w)^{1/2}\,[1 - [1 - (\bar{S}_w)^{1/\gamma}]^{\gamma}]^2 \tag{6}$$

$$k_{ro} = (\bar{S}_o - \bar{S}_{or})^{1/2}\,[[1 - (\bar{S}_w)^{1/\gamma}]^{\gamma} - [1 - (\bar{S}_L)^{1/\gamma}]^{\gamma}]^2 \tag{7}$$

$$k_{ra} = (\bar{S}_a)^{1/2} [1 - (\bar{S}_L)^{1/\gamma}]^{2\gamma} \quad (8)$$

where

S_w = water saturation

S_o = oil saturation

S_a = air saturation

S_{wr} = residual water saturation

S_{or} = residual oil saturation

α = curve fitting parameter, related to inverse air entry potential (m^{-1},van Genuchten Alpha)

β = curve fitting parameter, affects nonlinearity of characteristic curve (van Genuchten n)

$\gamma = 1 - 1/\beta$

σ_{aw} = air-water interfacial tension (N/m)

σ_{ow} = oil-water interfacial tension (N/m)

σ_{ao} = air-oil interfacial tension (N/m)

ρ_{fw} = fresh water density (kg/m^3)

g = gravitational acceleration (m/s^2).

Determining constitutive relationships for fractured media continues to be an active research area. A Brooks-Corey (1966) analytical formulation was used to describe the constitutive relationships for the fractured basalt, which was treated as an equivalent porous media. The general Brooks-Corey formulas implemented in TETRAD are

$$P_{c\,aw} = A_{aw}(1 - S_w)^{B_{aw}} \quad (9)$$

$$k_{ri} = A_i((S_i - S_{ir})/(1 - S_{ir}))^{B_i} \quad (10)$$

where

$P_{c\,aw}$ = capillary pressure between air and water (kPa)

k_{ri} = relative permeability of any phase *i*

S_i and S_{ir} = saturation and residual saturation of any phase *i*

A_{aw} (kPa), B_{aw}, A_i, and B_i = fitting parameters for the Brooks-Corey functions.

A-6 SIMULATION CODE

The TETRAD multipurpose simulator (Vinsome and Shook, 1993), Version 12.7 ms was chosen to simulate water and contaminant migration through the vadose zone and aquifer. This code was chosen because it is robust, multiphase, multicomponent, and three-dimensional and can simulate dual porosity systems. TETRAD was originally developed as an enhanced oil recovery simulator for the petroleum industry. It has been successfully applied to simulate groundwater flow and transport at the INL Site for Waste Area Groups 1, 3, and 7. TETRAD has undergone limited verification and validation (Shook 1995) to demonstrate proficiency of the TETRAD simulator for use in modeling environmental fate and transport processes.

The general conservation equation solved by the TETRAD simulator for accumulation, flux, decay or degradation, and sources for any component i can be written as

$$\frac{\partial W_i}{\partial t} + \vec{\nabla} \cdot \vec{N}_i - R_i + q_i = 0 \qquad \text{(A-6-1)}$$

where

$\frac{\partial W_i}{\partial t}$ = is the accumulation term that consists of net changes in the concentration of the component *i* in any phase, including the adsorbed phase

$\nabla \bullet \vec{N}_i$ = is the flux of component *i*

R_i = the change in concentration arising from decay of component *i*

q_i represents sources or sinks of component *i*.

The accumulation term can be written as

$$W_i = \varphi(S_w \rho_w w_i + S_g \rho_g y_i + S_o \rho_o x_i) + ((1-\varphi)\rho_s V_i)/M_i \qquad \text{(A-6-2)}$$

where

φ = the porosity

S_j = the phase saturations (*w* aqueous, *g* gaseous, *o* oleic)

ρ_j = the phase molar densities

w_i, y_i, and x_i = the mole fractions of *i* in the aqueous, gaseous, and oleic phases, respectively

ρ_s = the solid phase density

V_i = the mole fraction of *i* adsorbed on the solid phase

M_i = the molecular weight of *i*.

A generalized adsorption relationship is available in TETRAD that allows for adsorption onto the solid phase from any of the other three phases.

The flux term in Equation (A-6-3) is comprised of an advection and dispersion term for each phase given by

$$\vec{N}_j = [\rho_w \vec{u}_w w_i - \vec{\vec{D}}_{iw} \cdot \vec{\nabla}(\rho_w w_i)] + [\rho_g \vec{u}_g y_g - \vec{\vec{D}}_{ig} \cdot \vec{\nabla}(\rho_g y_i)] + [\rho_o \vec{u}_o x_i - \vec{\vec{D}}_{io} \cdot \vec{\nabla}(\rho_o x_i)] \quad \text{(A-6-3)}$$

In Equation (A-6-3) the $\vec{u}_j$ are the phase advective fluxes, given by the multiphase version of Darcy's law:

$$\vec{u}_j = \frac{k k_{rj}}{\mu_j}(\vec{\nabla} P_j - \rho_j \vec{g}) \quad \text{(A-6-4)}$$

where

k = the intrinsic permeability

k_{rj} = the relative phase permeability

μ_j = the phase viscosity

P_j = the phase pressure

$\vec{g}$ = gravitational constant in vector form.

$\vec{\vec{D}}_{ij}$ = the phase-dependant dispersion tensor comprised of molecular diffusion modified by porosity, phase saturation, tortuosity, and mechanical dispersion consisting of phase dispersivities modified by directional components of advective phase fluxes (Bear 1972).

The reaction term in Equation (A-6-1) accounts for decay or degradation of component i and is written as:

$$R_i = -A_{i\varsigma}[m_j + V_i(1-\varphi)\rho_r] + A_{\omega i}[m_\omega + V_\omega(1-\varphi)\rho_r]; \varsigma \neq \omega \quad \text{(A-6-5)}$$

where m_i is the total aqueous mass of i. The first term on the right hand side of Equation (A-6-5) accounts for i decaying with a rate constant $A_{i\varsigma}$ into component ς, whereas the second term on the right-hand side is the formation of i from destruction of component ω with a rate constant $A_{\omega i}$. The final term on the right-hand side in Equation (A-6-1) is the source/sink term, q_i. This term accounts for the addition or extraction of component i through wells or boundary conditions.

To solve the governing equations for variably saturated flow, TETRAD requires parameterization of saturation versus capillary pressure and saturation versus permeability for each lithologic material. The van Genuchten (1980) equations were used to describe the constitutive relationships for the alluvium and interbed (sediment). TETRAD uses two-phase van Genuchten constitutive equations, as adapted by Parker et al. (1987) with slight modifications to the normalized saturation terms. The van Genuchten constitutive relations are

$$\bar{S}_w = \frac{S_w - S_{wr}}{1 - S_{wr}} \; ; \quad \bar{S}_a = \frac{S_a}{1 - S_{wr}}; \quad \bar{S}_o = \frac{S_o}{1 - S_{wr}} \quad \text{(A-6-6)}$$

$$\bar{S}_L = \bar{S}_o + \bar{S}_w \quad \text{(A-6-7)}$$

$$P_{c\,ow} = \frac{\sigma_{ow}\,\rho_{fw}\,g}{\sigma_{aw}\,\alpha}\,[\,(\bar{S}_w)^{-1/\gamma} - 1\,]^{1/\beta} \Leftrightarrow \quad \bar{S}_w = \left[1 + \left(\frac{\alpha\,P_{c\,ow}\,\sigma_{aw}}{\rho_{fw}\,g\,\sigma_{ow}}\right)^{\beta}\right]^{-\gamma} \tag{A-6-8}$$

$$P_{c\,ao} = \frac{\sigma_{ao}\rho_{fw}\,g}{\sigma_{aw}\,\alpha}\,[\,(1-\bar{S}_a)^{-1/\gamma} - 1\,]^{1/\beta} \Leftrightarrow \quad \bar{S}_a = 1 - \left[1 + \left(\frac{\alpha\,P_{c\,ao}\,\sigma_{aw}}{\rho_{fw}\,g\,\sigma_{ao}}\right)^{\beta}\right]^{-\gamma} \tag{A-6-9}$$

$$P_{c\,aw} = \frac{\rho_{fw}\,g}{\alpha}\,[\,(1-\bar{S}_a)^{-1/\gamma} - 1\,]^{1/\beta} \Leftrightarrow \quad \bar{S}_a = 1 - \left[1 + \left(\frac{\alpha\,P_{c\,aw}}{\rho_{fw}\,g}\right)^{\beta}\right]^{-\gamma} \tag{A-6-10}$$

$$k_{rw} = (\bar{S}_w)^{1/2}\,[1 - [1 - (\bar{S}_w)^{1/\gamma}\,]^{\gamma}]^2 \tag{A-6-11}$$

$$k_{ro} = (\bar{S}_o - \bar{S}_{or})^{1/2}\,[[1 - (\bar{S}_w)^{1/\gamma}\,]^{\gamma} - [1 - (\bar{S}_L)^{1/\gamma}\,]^{\gamma}]^2 \tag{A-6-12}$$

$$k_{ra} = (\bar{S}_a)^{1/2}\,[1 - (\bar{S}_L)^{1/\gamma}\,]^{2\gamma} \tag{A-6-13}$$

where

S_w = water saturation

S_o = oil saturation

S_a = air saturation

S_{wr} = residual water saturation

S_{or} = residual oil saturation

α = curve fitting parameter, related to inverse air entry potential (m^{-1},van Genuchten Alpha)

β = curve fitting parameter, affects nonlinearity of characteristic curve (van Genuchten n)

$\gamma = 1 - 1/\beta$

σ_{aw} = air-water interfacial tension (N/m)

σ_{ow} = oil-water interfacial tension (N/m)

σ_{ao} = air-oil interfacial tension (N/m)

ρ_{fw} = fresh water density (kg/m^3)

g = gravitational acceleration (m/s^2).

Determining constitutive relationships for fractured media continues to be an active research area. A Brooks-Corey (1966) analytical formulation was used to describe the constitutive relationships for the fractured basalt, which was treated as an equivalent porous media. The general Brooks-Corey formulas implemented in TETRAD are

$$P_{c\,aw} = A_{aw}(1 - S_w)^{B_{aw}} \quad \text{(A-6-14)}$$

$$k_{ri} = A_i((S_i - S_{ir})/(1 - S_{ir}))^{B_i} \quad \text{(A-6-15)}$$

where

$P_{c\,aw}$ = capillary pressure between air and water (kPa)

k_{ri} = relative permeability of any phase *i*

S_i and S_{ir} = saturation and residual saturation of any phase *i*

A_{aw} (kPa), B_{aw}, A_i, and B_i = fitting parameters for the Brooks-Corey functions.

The residual saturation was 0.01. Numeric values for the A_{aw} (kPa), B_{aw}, A_i, and B_i curve-fitting parameters were 32kPa, 1.5, 1, and 2, respectively.

A-6.1 Modifications to Version 12.7 Resulting in Version 12.7ms

Modifications to improve the computation efficiency for environmental modeling applications with the TETRAD, Version 12.7, simulator were described in Shook et al. (2003). The modified code resulting from this effort is called TETRAD, Version 12.7ms. Modifications were performed as part of an in-house laboratory-directed research and development project and consisted of allowing component-specific convergence criteria to be specified. This allowed tighter convergence criteria on those components representing contaminants and looser criteria for those components representing pure water, air, and a required nonaqueous phase liquid. Given the much larger mass of water and air present in the simulations, allowing appropriate convergence criteria for each component was a logical change.

Two additional changes were implemented in the TETRAD simulator during the transition from Version 12.7 to Version 12.7ms: (1) an implementation of a Millington formulation for calculating tortuosity during the simulation, based on total porosity and gaseous phase saturation; and (2) modifications to limit repetitive time-step output for problems with frequent surface or internal boundary condition changes (e.g., emulating barometric pressure fluctuations or positive pressures imposed downhole during drilling of wells). These two changes only affected input and output from the TETRAD simulator and did not affect the solution method used internally in the simulator.

A-6.2 Quality Assurance

The TETRAD 12.7ms simulator is a proprietary code and its use constitutes an off-the-shelf application by modeling staff from the INL Site. Quality assurance and quality control for these types of simulations consist of ensuring that results are reproducible. This requires archiving a version of the simulator, the model inputs, the model outputs, and the processing codes used to create the inputs and outputs. An extensive searchable electronic archive is maintained by the OU 3-14 project for this purpose.

A-7 VADOSE ZONE MODEL CALIBRATION

In this section, the adjustment of model parameters necessary to match simulated water levels and contaminant arrival histories to observed vadose zone data is presented. This calibration step is required because many of the model parameters tend to be scale-dependent. For example, the permeability measured in an interbed core sample may not adequately represent the interbed permeability represented by the numerical grid block volume. Further, it is not feasible for a large-scale numerical model, based on averaged hydrologic and transport properties and discrete grid sizes, to exactly represent each field observation of moisture content, perched water level, or solute concentration. Instead, the best overall match between simulated and observed water and solute movement becomes the target goal. Results presented here represent the best match between simulated and measured values achieved during the parameter adjustment or calibration process. The degree of agreement between the model and calibration data was quantitatively assessed through the use of a comparative statistical indicator (i.e., the root mean square error) and qualitatively assessed by graphically comparing simulated and observed data. The model calibration was performed manually, as opposed to being achieved through an automated or more rigorous parameter estimation process. As a result, it is neither unique, nor mathematically optimal.

The primary objective of the vadose zone flow calibration was to match the distribution of perched water. Specific aspects of the perched water distribution were the focus of calibration, including the (1) absence of perched water in some wells, (2) long-term water levels available in other wells, and (3) transient behavior of perched water resulting from recent perturbations in recharge rates. Recent perturbations include the current hydrologic drought, which began in 1997, and the relocation of the percolation ponds in 2002. Both of these changes have altered the recharge rate enough to result in the decline of perched water levels in some locations.

The primary objective of the vadose zone transport calibration was to match the timing and concentration of contaminant arrival in the perched water bodies and aquifer resulting from releases in the tank farm. Four contaminants were identified as having reasonably accurate source terms. These were Tc-99, Sr-90, H-3, and I-129. Although discussed in this section, nitrate was not used in calibration because arrivals in perched water did not coincide with the known nitrate sources. The highest emphasis was on matching the Tc-99 and Sr-90 concentration histories because their sources in the tank farm were large relative to the service waste releases. The Sr-90 calibration is presented separately in Appendix J, along with the geochemical model development. Less emphasis was placed on matching the H-3 and I-129 because of the difficulty in differentiating the arrival of H-3 and I-129 in the deep perched water from tank farm sources as opposed to the distribution originating during the injection well failure.

Concentration of the calibration targets and of all COCs are very small (dilute) and, because they are dissolved constituents in water, they do not affect transport velocity. However, the hydraulic and transport parameters cannot be obtained independently because, in unsaturated flow, the permeability and porosity influence both water pressure and transport velocity. As a result, the vadose zone model is calibrated in two iterative stages. In the first stage, the constitutive hydraulic model parameters are adjusted to match the observed water levels in the perched zones. In the second stage, transport parameters (porosity and dispersivity) are adjusted to obtain a match between simulated and observed contaminant arrival at monitoring locations. Changes in perched water levels resulting from the second step are reevaluated in an iterative fashion.

The model calibration process was performed in the following steps, beginning with the spatial distribution of lithology interpolated onto the grid in Section A-5, and the associated high/low-permeability flags for each grid block:

1). Assign constitutive parameters to the high/low-permeability groups. At the end of this step, the complete description of the six material types (2-alluvium, 2-basalt, and 2-interbed) was available.

2). Assign and adjust constitutive parameters (alpha and n), porosity and dispersivity to each material type. Initial parameterization of the model used the measured data discussed in Section A-3.2 and

the range of values permitted in the calibration process was constrained by the range of observed values.

3). Run the model to obtain the distribution of perched water and the arrival history for calibration targets.

4). Compare predicted perched water levels and contaminant arrival histories to observed data.

5). Adjust the lithologic database used to define permeability groups and use kriging to assign the permeability groups to model grid.

6). Go back to Step 1, reassigning the constitutive parameters to the changed lithology blocks.

At the end of several iterations, the parameters that provided the best visual agreement and minimized the difference between simulated and measured data were obtained. This calibration process is fairly standard with the exception of adjusting the lithology in Step 5. Adjusting the lithological description was an added step made necessary by the available material description in many well logs. In many wells, the material description was vague and did not differentiate between high- and low-permeability sediment or between high- and low-permeability basalt. In the initial assignment of material types, the material types were always assumed to be high permeability if the general description was “basalt” or “sediment” in the well logs. This default results in overestimating the areal extent of high permeability and prevents the formation of perched water in some locations. The high permeability identified in well logs at locations of known perched water was switched to low permeability and the geostatistics of the overall lithology were reestimated and the field reinterpreted using kriging (i.e., as described in Appendix C). Likewise, a few locations identified as low permeability in the well logs were changed to high permeability, if perched water was not observed in the field data but was predicted by the simulation.

Only a subset of the data presented in Section A-3 was used in the model calibration because the complete data set was too voluminous or would not provide useful information for model calibration. The specific observational data used in this calibration process are presented in Section A-7.1 along with a description of any data manipulation needed prior to model calibration. Final vadose zone model calibration results are presented in Sections A-7.2 and A-7.3 even though the calibration of flow and transport was achieved simultaneously. In these latter two sections, the match between simulated and observed values was evaluated qualitatively and quantitatively. Qualitative assessment of perched water simulations included time series plots of predicted and observed values versus time and vertical plots of simulated saturation versus depth. Qualitative assessment of contaminant arrival is similar, with predicted and observed values presented as a function of time. The root mean square (RMS) statistic was chosen to quantitatively evaluate the match between the field data and simulation results. The RMS statistic illustrates the average relative error between two data sets. The RMS is defined as

$$RMS = \sqrt{\frac{\sum_{i=1}^{k} (s_i - f_i)^2}{k}} \qquad \text{(A-7-1)}$$

where

f_i = field data point

s_i = simulation data point

k = number of comparison points.

The RMS was not calculated if the observed or simulated well screen locations did not have perched water present, and the average RMS presented in Section A-7.2 does not include these cases. The RMS was calculated separately for each well over the monitoring period.

The log of the simulated and observed perched water concentrations was taken before calculating the RMS error for the transport model calibration. This was done to reduce the bias of the error statistic towards wells with the highest concentrations. Perched water contaminant concentrations vary over many orders of magnitude in the vadose zone and using the log of the concentration provides a better estimation of the model's agreement with all the data. The RMS error was not calculated if either the simulated or observed concentration was zero, and the average RMS error presented in Section A-7.3 does not include these data.

A-7.1 Specific Data Used In Vadose Zone Model Calibration

Calibration data were taken from the OU 3-13 RI/BRA (DOE-ID 1997), the OU 3-13 Group 4 MWTS report (DOE-ID 2003a), and ongoing remedial investigations at INTEC and ICDF. The specific vadose zone calibration data included (1) observed transient responses in perched water levels following the relocation of the percolation ponds and resulting from changes in Big Lost River fluxes and (2) perched water concentrations. The perched water level data used in the model calibration are discussed in Section 7.1.1, and the concentration data and the perched water chemistry data are presented in Section A-7.1.2.

A-7.1.1 Water Level Data

Perched water levels in the 1992 through 2004 time period were used for calibration. Sources for these data include measurements taken manually and measurements obtained through automated field instrumentation. The raw water level data contained various irregularities and were reviewed and corrected as needed. Some of the automated water level data contained nearly 50,000 data points per well which was reduced before they could be efficiently used in model calibration. Often, both manual and automated water level measurements were available for the same well location and the data sets were combined before reducing the data. The techniques used to reduce the water level data are discussed below.

- Manual Water Level Data

The manual water level data were reviewed to locate any "suspect" data points (i.e., anomalously high or low elevations relative to the surrounding data). At locations where measurements were "suspect," the original field logbooks/field notes were reviewed and corrections were made. This included (1) correcting for transcription errors from the logbook to the project spreadsheet, (2) correcting surface casing stick-up values used to calculate depth to water, and (3) removing data points that were unrealistically different from measurements made the month prior/following. Since all measurements were made using the depth to water below measuring point, the stick-up value of the surface casing where the measuring point is located was subtracted from the field-measured value. These stick-up values came from WAG 3, Group 4, field measurements and from the ICDF well completion diagrams. Finally, the depth to water from land surface was subtracted from the brass cap elevation at each location to determine a water level elevation which was then converted to meters for the model. These data were flagged within their respective files to indicate that the source for the measurement was manual.

Dates for manual water level measurements reflect the general day on which water level measurements were taken and may not have been the exact date of data collection. The discrepancy in exact date arises because the recorded date corresponded to the start of a sampling campaign, which may have taken several days.

- Automated Water Level Data

Several of the wells contain one of four different automated pressure transducers: Solinst Leveloggers, Insitu Minitrolls, In-situ Hermit dataloggers, and Sentinel dataloggers. In these wells, water levels were either recorded as head above the monitoring unit, depth to water from a known elevation, or an actual water level elevation, depending on the instrument. All data were converted to depth below a measurement location.

Files containing head measurements as depth to water were first checked to ensure that the data conversions were correctly applied. These measurements were compared to the manually recorded data taken during the same time period to confirm that the automated measurements were correct. Where discrepancies existed, logbooks describing the transducer installation and/or manual water level measurements were reviewed and the discrepancies were corrected. If data did not accurately represent water levels at that location over time, they were removed from the data set. Examples of these data points include automated measurements taken during water sampling events and erroneous automated measurements occasionally recorded by the instrument. The Hermit transducers were programmed to record water levels below a given elevation and did not require conversions. The Sentinel data contain the oldest automated data collected in this study. These recorders report water level elevation. Logbooks describing their installation have not been located and manual water level measurements have not been found for this time period. These data were flagged within their respective files to indicate that the source for the measurement was automated and the type of instrument that took the reading.

- Water Level Data Reduction

Prior to data reduction, the number of measured data points in most wells containing automated measuring instrumentation ranged from 234 (Well PW-3) to 42,611 (Well CPP-37-4). Using data collected every 30 minutes for model calibration is not efficient and adds little additional information to the slowly changing seasonal trends. To improve calibration efficiency, most of the automated water level data sets were reduced to a few hundred data points. The data were averaged over a number of observations while preserving seasonal variations and the influence of changing recharge rates. The data reduction algorithm averaged the data points over a selected time-window range. Water levels within a given time window were averaged and the averaged value was assigned to the center of the time increment. The mean and variance statistics of the raw and reduced data were calculated and compared to ensure that the data character had not significantly changed during the data reduction.

A-7.1.2 Water Chemistry Data

Perched water chemistry and COC concentrations were collected from the INL Environmental Data Warehouse (EDW), the INL's Hydrologic Data Repository (HDR), and the MWTS report (DOE-ID 2003a). For the purposes of calibration, focus was on tritium, Sr-90, I-129, and Tc-99. In general, chemistry data are sparse, many INTEC perched water wells have never been sampled for these data, and only a few recent measurements are available in most wells. In a few wells, some data are available beginning in the early 1960s and extending through 2004.

As with the water level data, concentration data contained various irregularities and required review and correction. Data quality indicators are associated with chemistry data indicating nondetected values, estimated values (rather than measured), and rejected samples (U and/or UJ, J, and R). For calibration and plotting purposes, U and UJ flagged data indicate nondetect and were recorded as zero. In these data, samples were flagged nondetect if the radionuclide analytical results were not statistically positive at the 95% confidence level. Although the choice of confidence level is somewhat arbitrary, in practice 90%, 95%, and 99% levels are often used in science and engineering to denote the data has acceptable error, with 95% being the most commonly used value. The J-flagged data indicated that the sample concentration was a recorded estimate in the EDW/HDR data base. These values were retained. R-flagged data indicated that the sample was rejected and the data points were removed from the calibration data set. Flags were included in the model input file to record relevant information associated with the sample result.

A-7.2 Vadose Zone Flow Calibration Results

Observations of perched water elevations indicate that northern INTEC wells respond to variations in Big Lost River flow, and that southern INTEC wells responded to the removal of the percolation ponds. In between those two regions, the discharge rates prior to taking remedial action were quite similar to the rates after remedial action was taken. The relatively small change was reflected in the lack of transient perched

water level response in the central INTEC region. In the final calibration results presented here, the predicted high saturation elevations are generally in agreement with this observed behavior. On the average, the simulated decline in perched water elevations resulting from the percolation pond relocation was less than observed. The model predicted that the positive pressure would become negative but that the saturations would remain high. The model did not predict that percolation pond water would spread horizontally to the contaminated perched water in northern INTEC. This will result in the model predicting higher interbed contaminant concentrations in northern INTEC perched water and aquifer than was predicted by the OU 3-13 model.

The vadose zone model predicted the existence of perched water bodies beneath the Big Lost River and the percolation ponds. The model predicted positive pressure to only occur beneath these areas. However, both the pre- and post-remedial action discharge rates were sufficient to result in nearly saturated conditions in the low permeability interbed material. The saturation in all low-permeability interbed areas within the INTEC fence line was very near saturation.

Hydraulic parameters used in the final calibrated model are presented in Table A-7-1. The constitutive relationships used for the fractured basalt were those used by Magnuson (1995) and are discussed in Section A-6. However, the residual saturation was increased to 0.01 and the B_i parameter in Equation 6-15 was increased to 2.0. These values did not significantly change water and solute transport results but greatly reduced simulation run times. The very small residual saturations in Table A-7-2 for the alluvium and low-permeability interbeds were adjusted up from the zero value reported in the MWTS report (DOE-ID 2003a) to prevent numerical problems. These values represent a best fit to the measured moisture versus matric potential data. The reported moisture characteristic data are not accurate at the dry extreme, but the simulated recharge does not allow soil to drain to these conditions. The calibrated high permeability interbed porosity was 0.60. This value is within the range of measured values of interbed porosity obtained from core samples documented in DOE-ID 2003a and is representative of the data measured from the highest permeability cores.

The predicted and observed saturations are spatially and temporally varying. To simplify presentation, we first illustrate the distribution of perched water following the relocation of the percolation ponds (2002) and during the peak flow year for the Big Lost River recorded at Lincoln Boulevard bridge gauge (1999) in Figure A-7-1. This figure shows that areas of positive pressure (saturation = 1, and represented by red) and areas that are near saturation (0.99, represented by blue) are aerially extensive. It also illustrates that high saturations occur in the low- and high-permeability interbeds near the Big Lost River and percolation ponds, in addition to occurring in the low-permeability interbeds between these two primary recharge areas. These high saturations result in ephemeral perched water forming at the well screens as observed in many of the INTEC perched water wells where only small amounts of water can be withdrawn from the well.

The distribution of water and association with specific media are further illustrated in the vertical well profiles given in Figures A-7-2 through A-7-5. In the low-permeability interbeds, the saturations are nearly one; in the high-permeability interbeds, the saturations approach 0.5; and, in the basalt regions, the saturations are much lower. The vertical moisture profiles presented in Figures A-7-2 through A-7-5 correspond to dates in the 2003-2004 time period where field data are available and include the locations of the well screen top and bottom (dashed blue horizontal lines) and the observed elevations of the perched water (red horizontal line). If the red horizontal line is at the plot bottom, the well was dry. The wells are ordered from the north to the south with wells north of CPP-3 presented in Figures A-7-2 and A-7-3 and wells south of CPP-3 presented in Figures A-7-4 and A-7-5. The calibration results for the northern upper shallow, northern lower shallow, northern deep, southern shallow, and southern deep perched water zones and discussions of observed and simulated perched water behavior are further discussed in Sections A-7.2.1 through A-7.2.5, respectively.

Table A-7-1 Final calibrated hydraulic parameters.

Material Type	Horizontal Permeability	Horizontal Hydraulic Conductivity	Porosity	Permeability Anisotropy	Residual	van Genuchten Parameters	
	(mD)	(cm/sec)		(Horizontal to Vertical)	Saturation	Alpha (1/m)	n
High-permeability alluvium	34,570	2.79E-2	0.32	1 to 1	0.0002	100	1.40
Low-permeability alluvium	1	8.04E-7	0.39	1 to 1	0.0002	0.2	1.34
High-permeability interbed	4,107	3.30E-3	0.60	1 to 1	0.11	10.5	1.29
Low-permeability interbed	3	2.41E-6	0.49	1 to 1	0.0002	0.01	1.38
High-permeabilitybasalt	42,310.	3.40E-2	0.03	10 to 1	0.01	a	a
Low-permeability basalt	5,230.	4.20E-3	0.03	10 to 1	0.01	a	a

a. The basalt did not use the van Genutchen constitutive relationship (see Section A-6.)

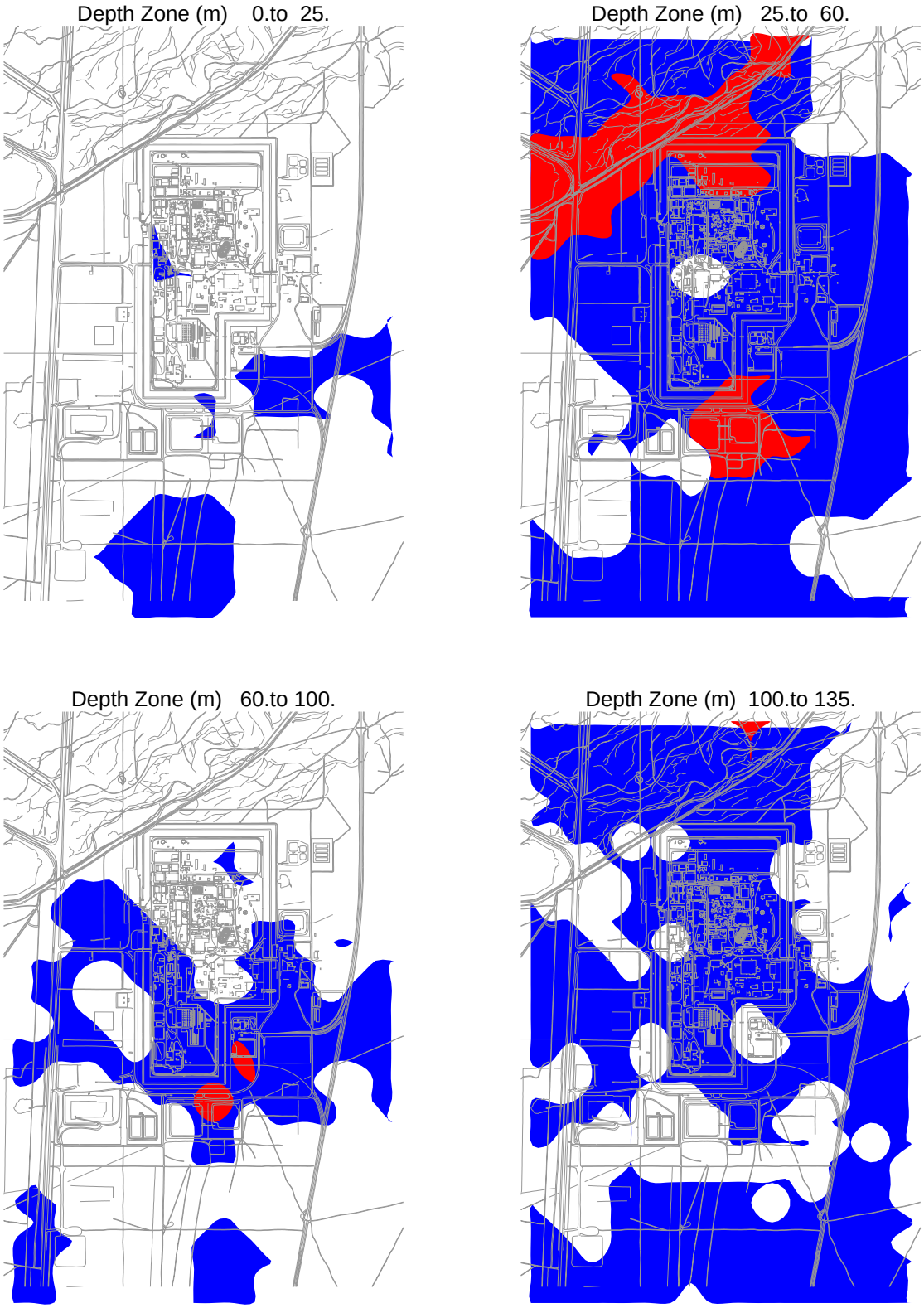

Figure A-7-1. Horizontal extent of simulated perched water at different depth intervals during the peak Big Lost River flow in 1999 (blue saturation = 0.99, red saturation = 1.0).

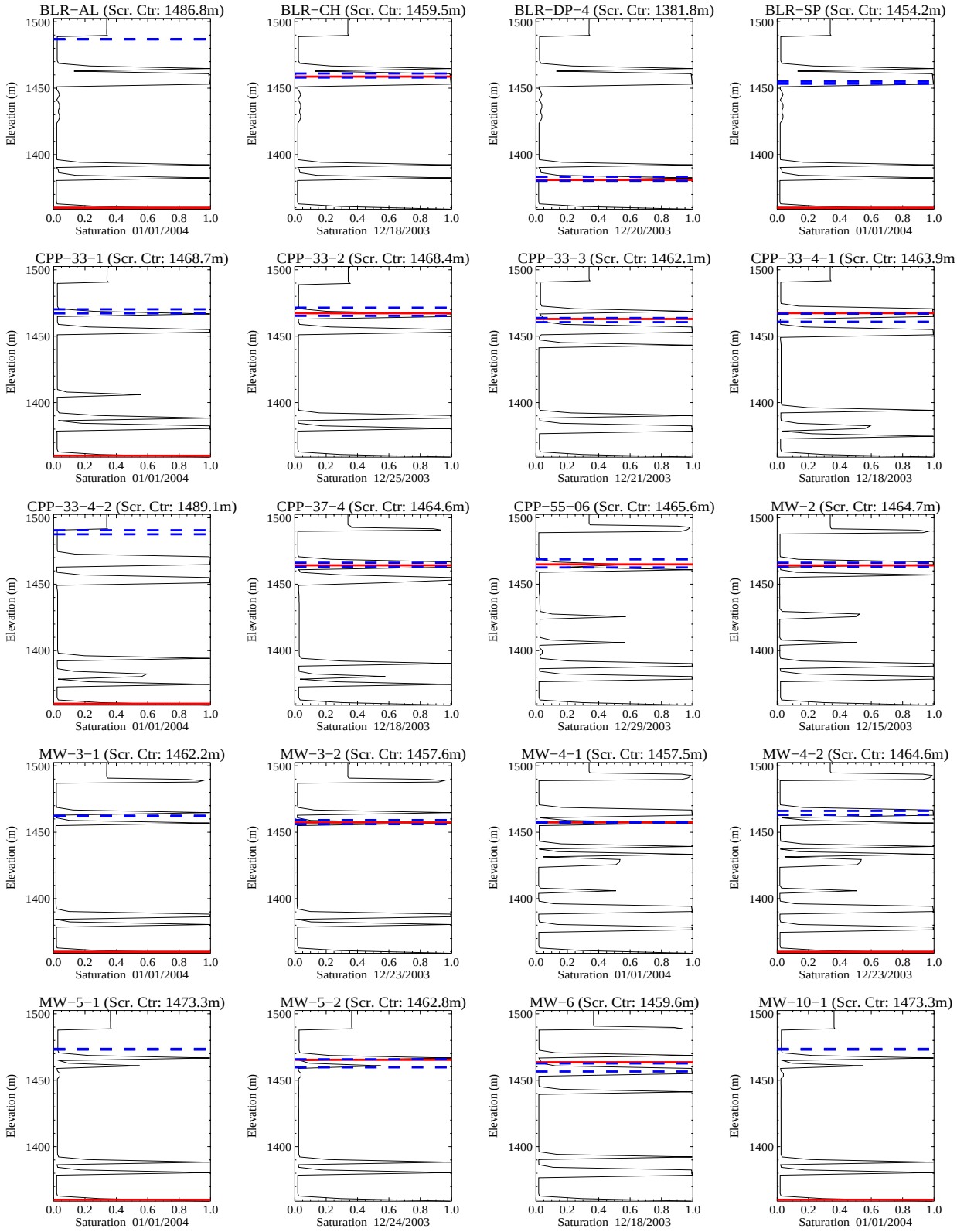

Figure A-7-2. Simulated saturation versus depth for northern perched water well locations after percolation pond relocation (dashed blue line = well screen top and bottom, red line = water elevation).

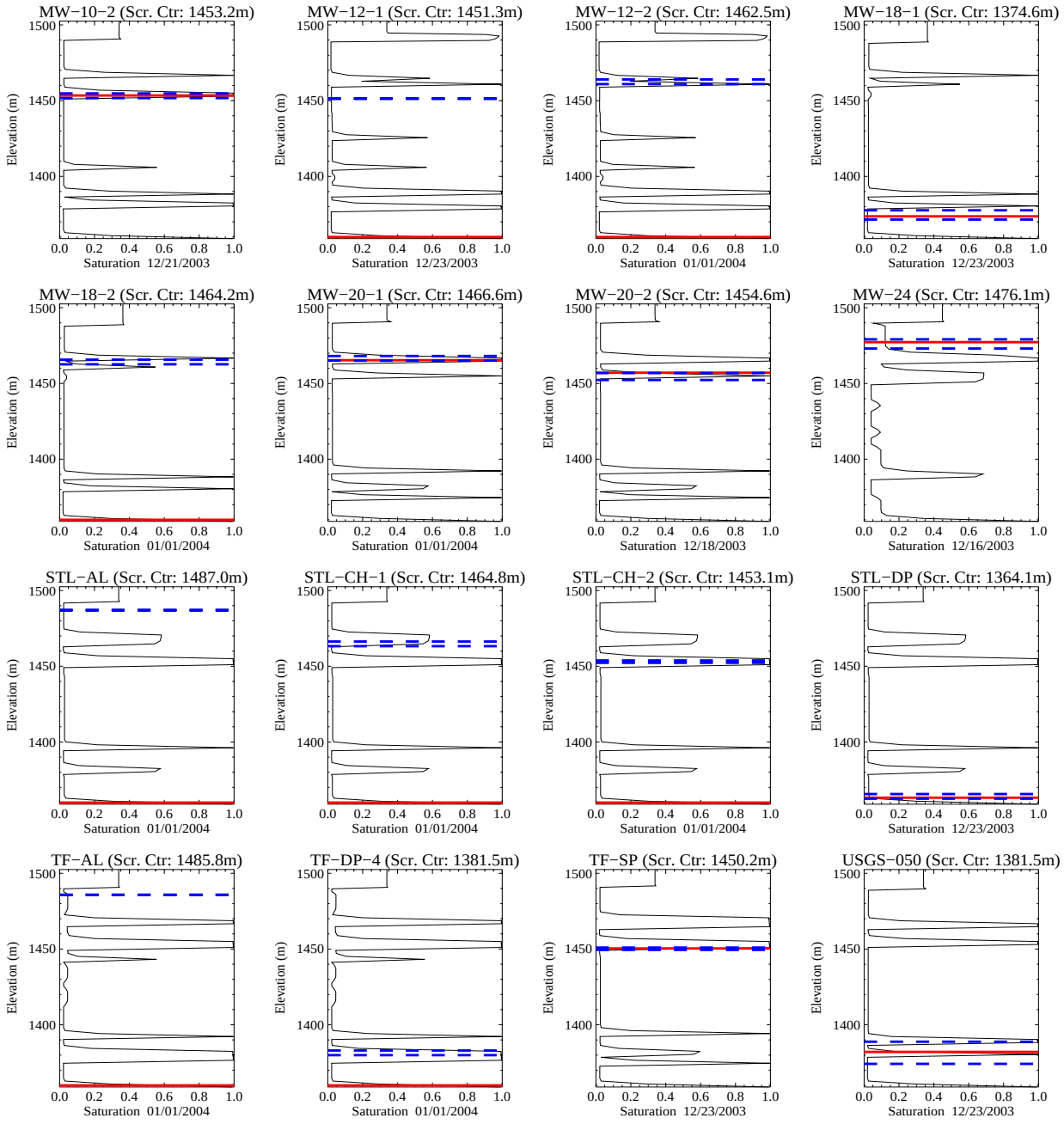

Figure A-7-3. Simulated saturation versus depth for northern perched water well locations after percolation pond relocation (continued) (dashed blue line = well screen top and bottom, red line = water). elevation).

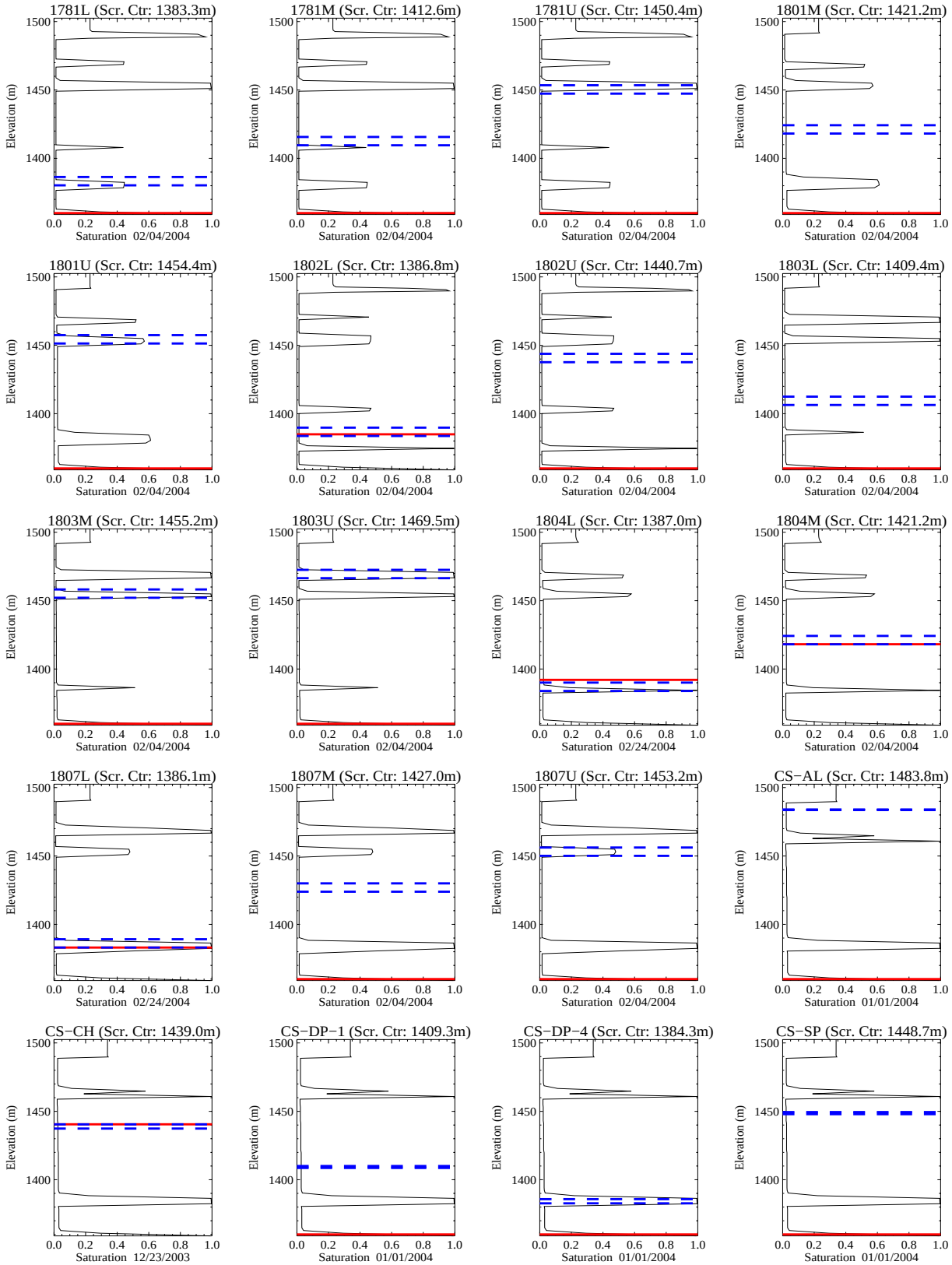

Figure A-7-4. Simulated saturation versus depth for southern perched water well locations after percolation pond relocation (dashed blue line = well screen top and bottom, red line = water elevation).

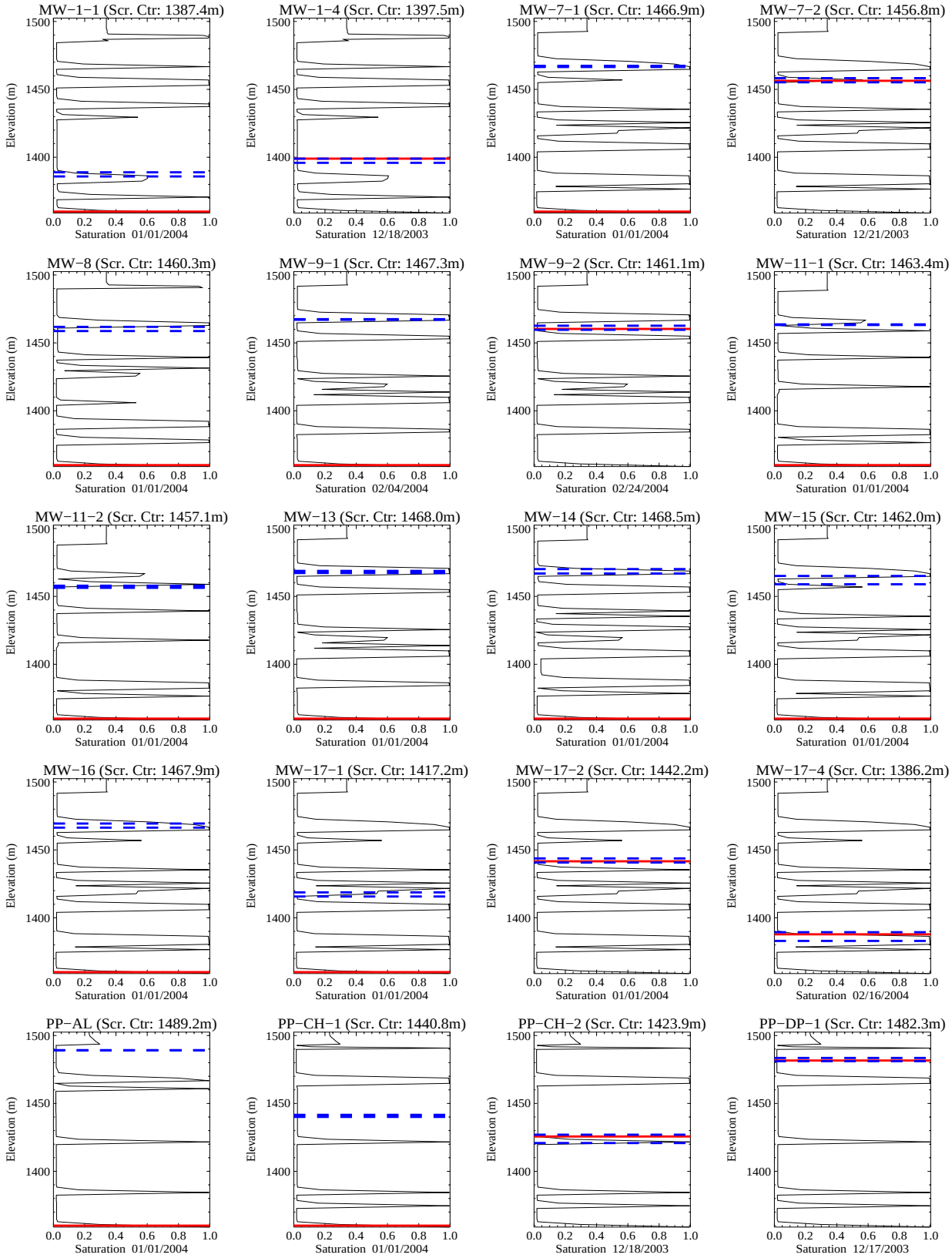

Figure A-7-5. Simulated saturation versus depth for southern perched water well locations after percolation pond relocation (dashed blue line = well screen top and bottom, red line = water elevation).

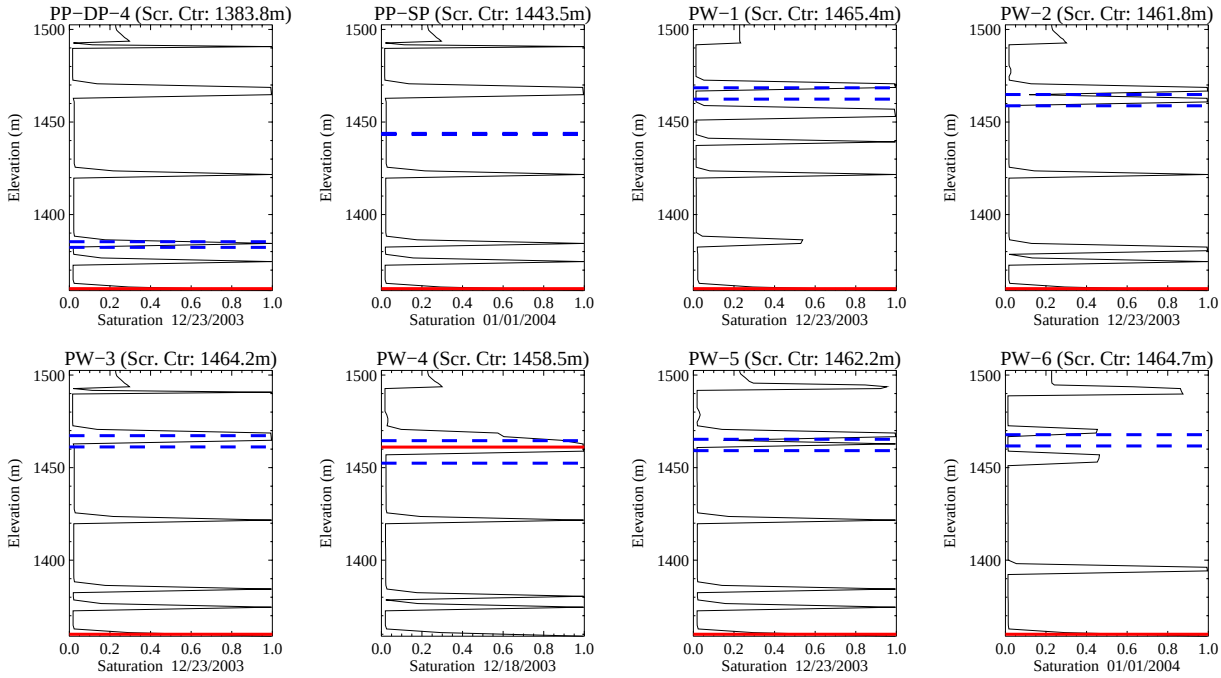

Figure A-7-6. Simulated saturation versus depth for southern perched water well locations after percolation pond relocation (dashed blue line = well screen top and bottom, red line = water elevation).

A-7.2.1 Northern Upper Shallow Perched Water

The northern upper shallow perched water is associated with the 110-ft interbed. The recharge sources may include the Big Lost River, the sewage treatment lagoons, precipitation, irrigation, and facility releases from leaking pipes and steam vents. A recent geochemical study of perched water indicates the sewage lagoons probably had little influence on the northern shallow perched water (EDF-5758). The northern upper shallow perched water region was defined to include all well screens located north of the CPP-3 injection well and located higher than 4,780-ft elevation.

Most of the observed data from the northern upper shallow perched water wells reflect seasonal fluctuations corresponding to increased spring recharge from snowmelt, precipitation, flow in the Big Lost River, and anthropogenic sources. Some of the wells in this region have responded to the recent hydrologic drought that began in 2000. Wells responding to the drought include MW-4-2 and CPP-37-4, which exhibit a clear decline in perched water elevation since 2000. This can be more clearly seen in Figure A-3-3 of Section A-3.4. In contrast, water levels have been increasing in BLR-CH since 2003. The increase in the BLR-CH well is thought to be due to facility discharge, but the source is unknown. A match to this increase by the model would not be expected.

In general, the simulated high saturation elevations were in good agreement with observed data. Notable exceptions are wells MW-24 and CPP-55-06, where the elevation of predicted 0.95 saturation was lower than observed, and well MW-3-2, where elevation of the 0.95 saturation was predicted to occur at a higher elevation than observed. These observations suggest that the elevation of the interpolated interbeds in these areas is slightly different than the actual elevation. Observed data from CPP-33-1, MW-3-2, MW-2, MW-4-1, MW-4-2, MW-12-2, and MW-20-1 show that these wells experienced intermittent dry periods, which were not captured in the simulations. The intermittent dry periods could be inferred as absences in the otherwise continuous time series data. Wells BLR-AL, CPP-33-4-2, MW-5-1, MW-10-1, TF-AL and STL-AL did not have perched water present in either the simulations or observations.

Observed data reflect a transient response to quarterly variations in Big Lost River recharge. These quarterly variations were reflected in the model period spanning 1985-2004 (see Sections A-5.1.3). However, these observed temporal changes were not captured in the simulated northern upper shallow high saturation elevations except the BLR-CH well, which showed a slight increase in elevation during peak river flow. This suggests a lack of hydraulic connectivity between the Big Lost River water and the 110-ft interbed. In contrast, a transient response was predicted in most of the northern lower locations (see Section A-7.2.2). This is because the dip of the simulated 110-ft interbed beneath the river is away from the tank farm, but the dip of the 140-ft interbed is towards the tank farm. In all of the simulated responses, short-time-scale seasonal trends in observed data were not captured. The lack of seasonal response is a direct consequence of assuming precipitation is a steady-state process.

Time series plots of observed and simulated high saturation elevation for the northern perched water body are illustrated in Figures A-7-7 and A-7-8. The elevation of the model grid block nearest to the well screen in which a saturation above 0.95 was predicted was used to reflect the plotted value. The red lines correspond to this approximate elevation and the black crosses correspond to the observed elevation. Wells in which perched water was neither predicted or observed correspond to plots without data. Plots with only a red line indicate the model predicted the presence of perched water, but the observations indicated that the well is dry. Plots with only black crosses indicate perched water was measured but that perched water was not predicted to exist.

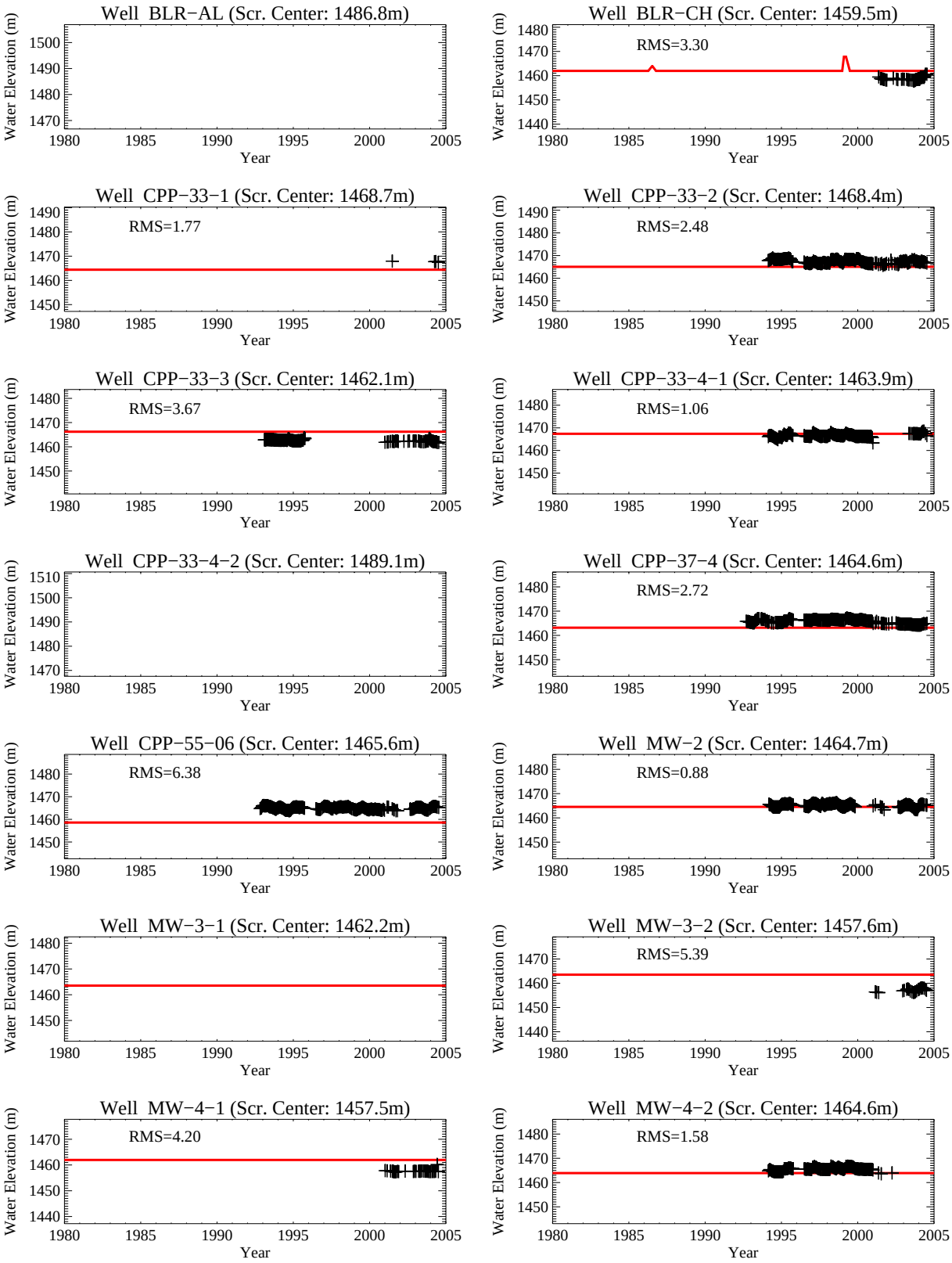

Figure A-7-7. Time series water elevation plots for the northern upper shallow perched water (red line = predicted elevation of 0.95 saturation, back crosses = measured data).

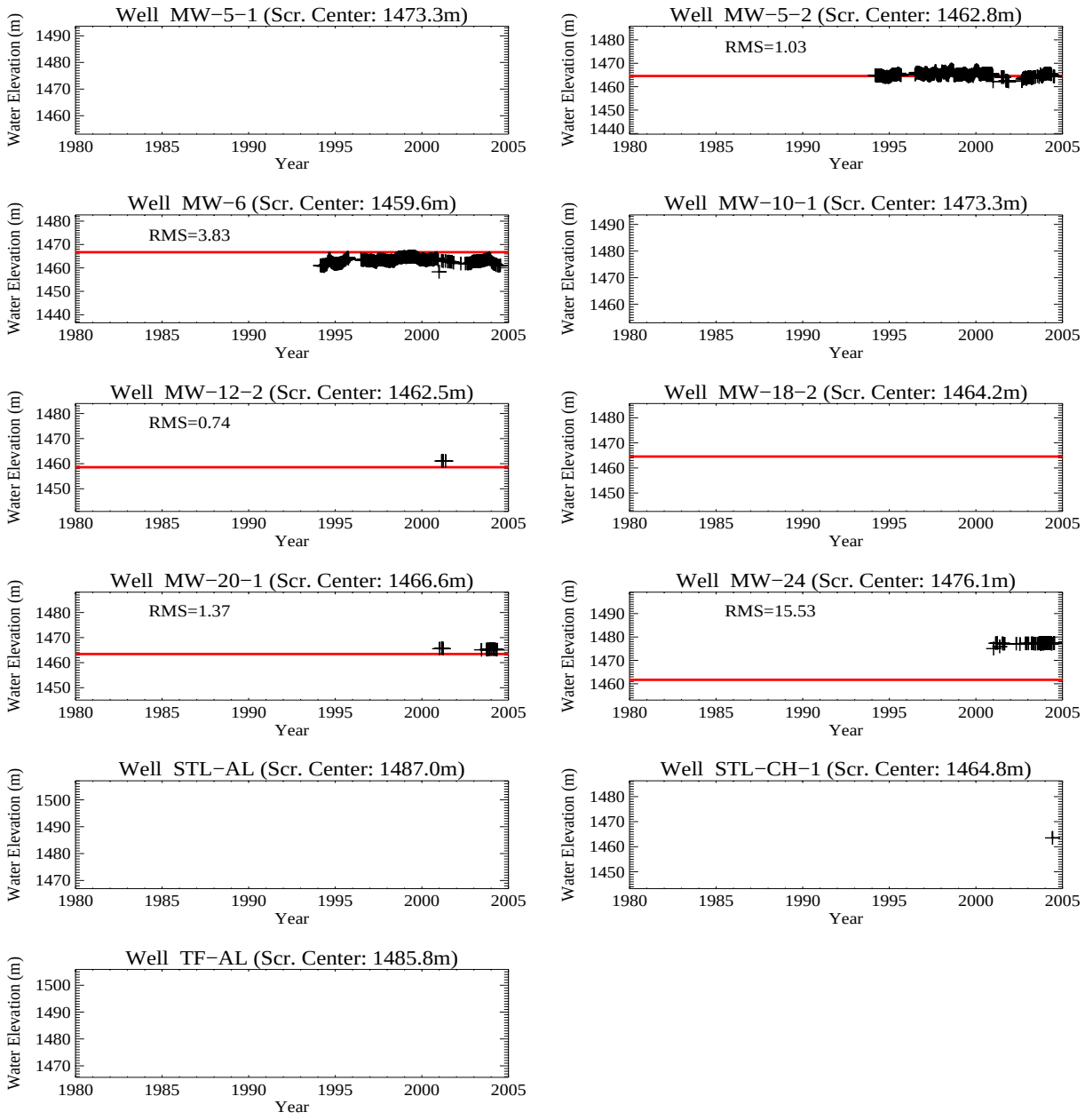

Figure A-7-8. Time series water elevation plots for the northern upper shallow perched water, continued. (red line = predicted elevation of 0.95 saturation, back crosses = measured data).

A-7.2.2 Northern Lower Shallow Perched Water

The northern lower shallow perched water is associated with the 140-ft interbed, and the primary water sources are most likely the same as those for the northern upper shallow perched water. This region was defined to include all well screens located north of the CPP-3 injection well and located lower than 4,789-ft, but higher than 4,741-ft, elevation. Observational data are only available from the last couple of years in these

wells and, as a result, do not reflect the temporal variation in water levels that were observed in the northern upper shallow perched water.

In general, the simulated high saturation elevations were in good agreement with observations. Exceptions include well MW-12-1, in which the predicted water elevations were higher than observed, and Wells BLR-SP and STL-CH-2, which were predicted to have perched water present but did not have perched water observed. Additional anomalies include wells MW-10-2, MW-12-1, and TF-SP, which have historically been dry intermittently but were predicted to have perched water present throughout the simulated time period.

A transient response to the simulated Big Lost River fluctuations was predicted in all the northern shallow perched wells except MW-12, which suggests that the northern lower shallow perched water wells are recharged by the Big Lost River. This was not seen in the observed data, although several of the northern lower shallow perched water wells were constructed after the start of the 2001 hydrologic drought. These predicted responses suggest that the 140-ft interbed may be responsible for moving river water laterally. Time series plots of observed and simulated high saturation elevations for the northern perched water body are illustrated in Figure A-7-9.

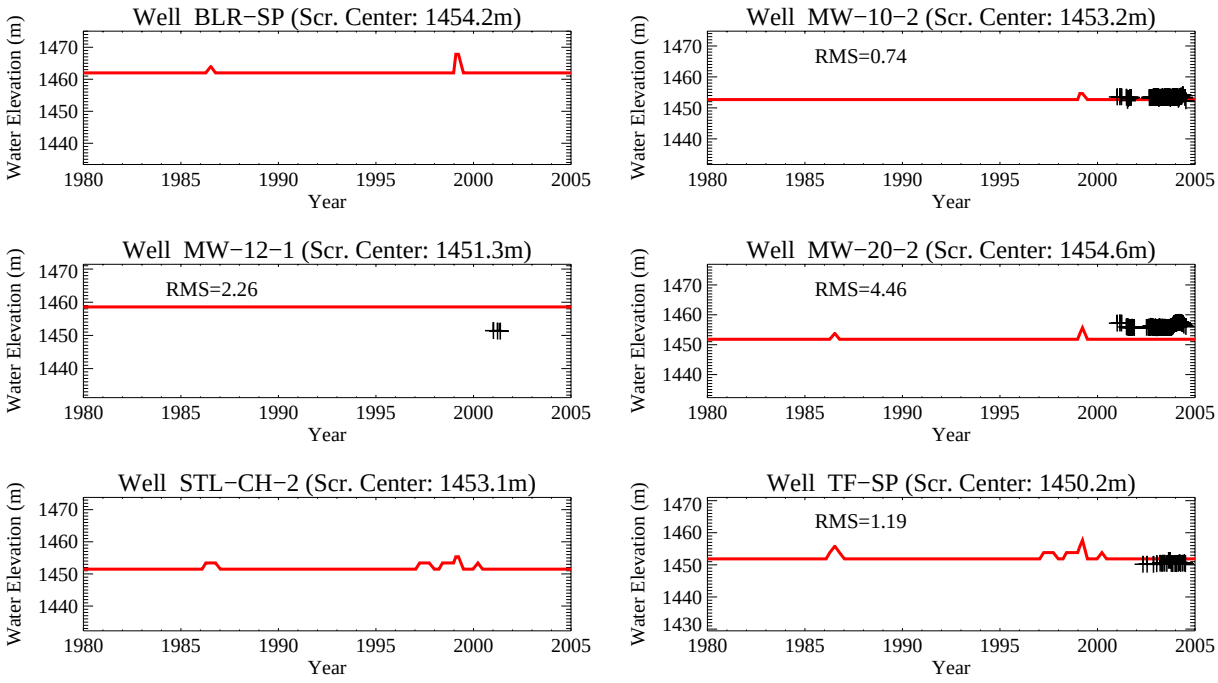

Figure A-7-9. Time series water elevation plots for the northern lower shallow perched water (red line = predicted elevation of 0.95 saturation, back crosses = measured data).

A-7.2.3 Northern Deep Perched Water

Predictions discussed in this section correspond to well screens located lower than 4,741 ft in elevation and located north of the CPP-3 injection well. Perched water in this region is thought to be associated with the 380-ft interbed, although it has been encountered deeper than the 380-ft interbed at wells STL-CH, MW-18, and USGS-50. Deep perched water southwest of the tank farm has also been encountered in well MW-1 at approximately 320 ft and may be associated with low-permeability basalt at this depth. As with the northern shallow perched water zone, the northern deep perched water recharge sources may include the Big Lost River, the sewage treatment lagoons, precipitation, irrigation, and facility releases from leaking pipes and steam vents. However, the CPP-3 injection well and the USGS-50 well may have also contributed to the deep perched

water. The CPP-3 injection well collapsed during the late 1960s and was not repaired until 1970. During the repair period, USGS-50 was used as a temporary injection well.

The simulated and observed high saturation elevations generally had good agreement with the exception of well STL-DP and well TF-DP-4. The observed perched water at well STL-DP could not be matched with the model because this location is within basalt (high permeability and low porosity equivalent porous media representative of flow in fractures). Although low-permeability basalt exists in the vadose zone model, the hydraulic parameters do not significantly differ from the high-permeability basalt values and are not conducive to forming perched water. Globally reducing the low permeability enough to produce perched water in the basalt resulted in grossly overestimating the perched water extent in the basalt, and these parameters were not selected for the calibrated model. Other observations include

- Perched water elevations in wells BLR-DP and STL-DP have been declining in response to the recent hydrologic drought. The decline was not captured by the simulations although the longer term average was.
- Wells MW-18-1and STL-DP have both been intermittently dry. This intermittent behavior was not captured in the simulations.
- The elevation of perched water predicted in well MW-18-1 was higher than the observed elevation.
- Well TF-DP-4 did not have observed perched water present, but the simulation predicted perched water was present.

Time series plots of observed and simulated high saturation elevations for the northern perched water body are illustrated in Figure A-7-10.

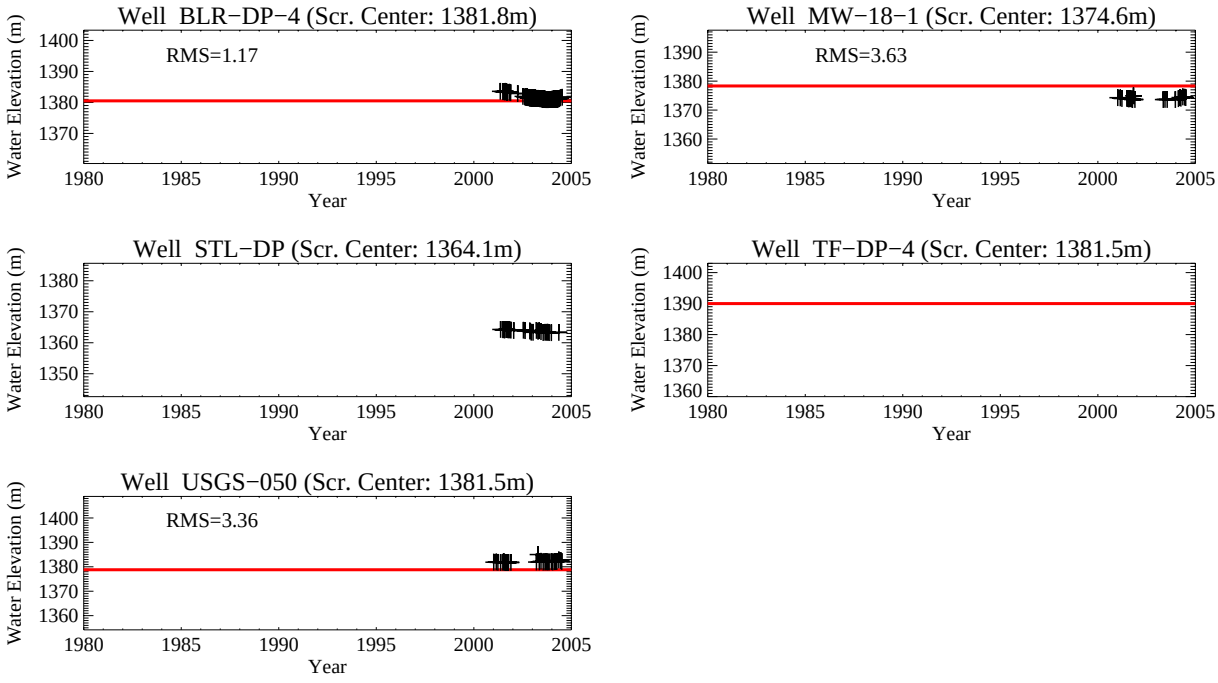

Figure A-7-10. Time series water elevation plots for the northern deep perched water (red line = predicted elevation of 0.95 saturation, back crosses = measured data).

A-7.2.4 Southern Shallow Perched Water

The southern shallow perched water region includes all well screens located south of the CPP-3 injection well and located higher than 4,741-ft elevation. As explained in Section A-3.4, there are two shallow perched water zones in this region. The first is near Building CPP-603 and is associated with the 140-ft interbed, and the second is a larger region located beneath the former percolation ponds and is associated with the 110- and 140-ft interbeds.

Time series plots of observed and simulated high saturation elevation for the northern perched water are illustrated in Figures A-7-11 and A-7-12. The transient decline in simulated perched water following the relocation of the percolation ponds was not as dramatic as the observed perched water decline. Wells PW-1, PW-2, PW-3, and PW-5, which are located near the former percolation ponds, went dry after percolation pond relocation on August 26, 2002. A decline in simulated water elevations was predicted in these wells, but they were predicted to remain nearly saturated through the end of the calibration period in 2005. However, the model did predict that positive pressures below the percolation ponds would quickly become negative after the percolation ponds were removed. The apparent discrepancy is, in part, due to the cutoff value chosen to represent saturation in the simulation results as opposed to using tensiometric data during the drainout period. The elevation of the model grid block nearest to the well screen in which a saturation above 0.95 was predicted was used to reflect the perched water elevation. If a higher threshold saturation was used, the wells would appear to drain faster. The 0.95 threshold value was chosen to be consistent with the results of the large-scale infiltration test and the resultant fractured basalt constitutive relationships used in this and other INL vadose zone models (Magnuson 1995).

Predicted high saturation elevations in wells PW-4 and PW-5 were lower than observed, while predicted elevations in wells MW-9-2, PP-DP-1, PW-2, and PW-3 were higher than observed. These results suggest that the simulated interbed elevation is slightly different than the actual interbed elevation in these areas. The predicted perched water decline in well PW-4 was very close to that observed. Wells MW-8, MW-9-2, MW-11-2, MW-13, MW-15, and PP-DP had intermittent dry periods which were not predicted. Wells 1781U, 1801U, 1807U, CS-AL, CS-SP, MW-7-1, MW-9-1, MW-11-1, MW-14, MW-16, and PW-6 did not have perched water present in the simulations or observations. The location of well PW-6 is approximately 1,000 ft west of the former percolation ponds. Intermittent perched water and contamination most likely originating from the former percolation ponds have been measured in this well. However, the vadose zone model did not predict water from the percolations ponds would travel this far west. This is because the simulated 110-ft interbed becomes discontinuous southeast of the INTEC facility.

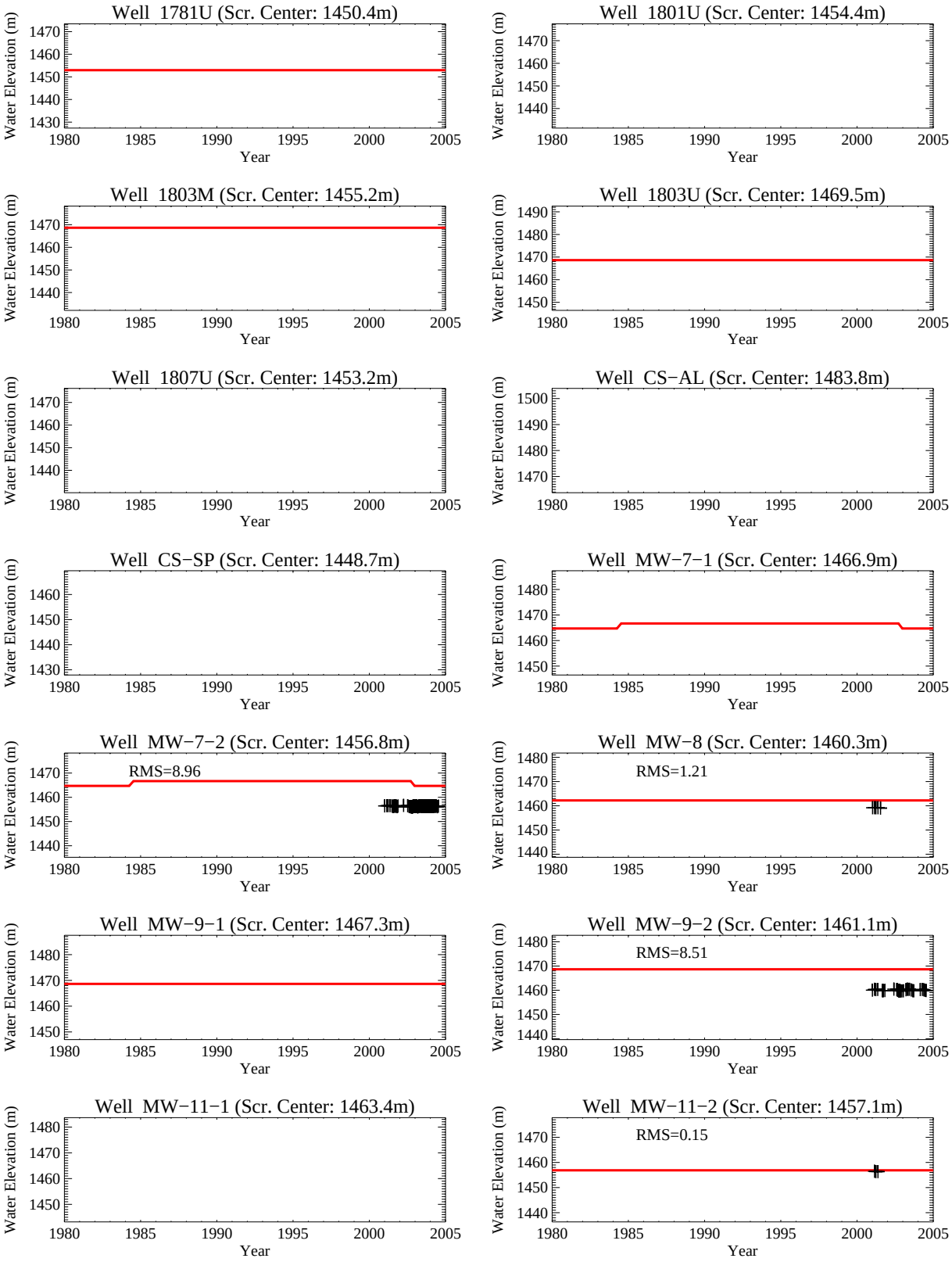

Figure A-7-11. Time series water elevation plots for the southern shallow perched water (red line = predicted elevation of 0.95 saturation, back crosses = measured data).

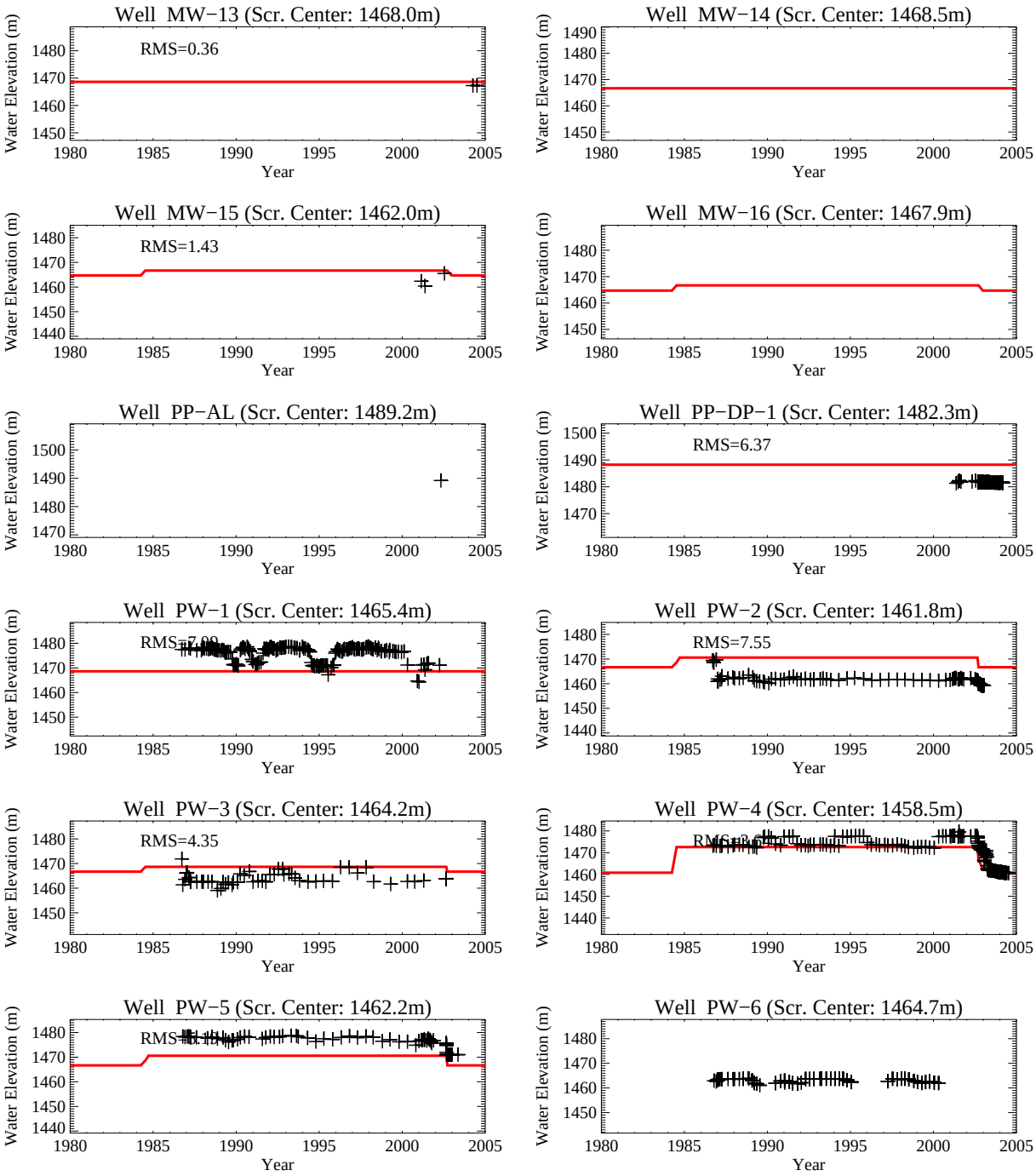

Figure A-7-12. Time series water elevation plots for the southern shallow perched water, continued (dashed blue line = well screen top and bottom, red line = predicted elevation of 0.95 saturation, black crosses = measured data).